Max-Planck-Institut
für Meteorologie

MAX-PLANCK-GESELLSCHAFT

International Max Planck Research School
on Earth System Modelling

Holocene and Eemian Climate Variability

Nils Fischer

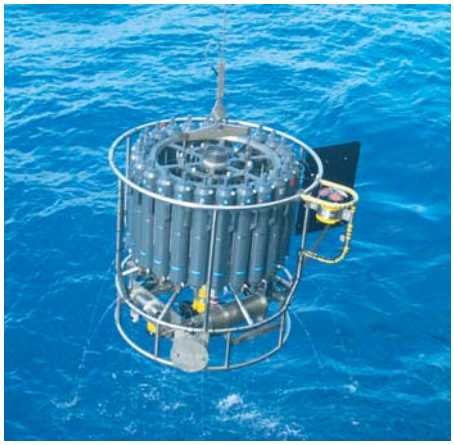

Berichte zur Erdsystemforschung 91/2011

Reports on Earth System Science

Hinweis

Die Berichte zur Erdsystemforschung werden vom Max-Planck-Institut für Meteorologie in Hamburg in unregelmäßiger Abfolge herausgegeben.

Sie enthalten wissenschaftliche und technische Beiträge, inklusive Dissertationen.

Die Beiträge geben nicht notwendigerweise die Auffassung des Instituts wieder.

Die "Berichte zur Erdsystemforschung" führen die vorherigen Reihen "Reports" und "Examensarbeiten" weiter.

Notice

The Reports on Earth System Science are published by the Max Planck Institute for Meteorology in Hamburg. They appear in irregular intervals.

They contain scientific and technical contributions, including Ph. D. theses.

The Reports do not necessarily reflect the opinion of the Institute.

The "Reports on Earth System Science" continue the former "Reports" and "Examensarbeiten" of the Max Planck Institute.

Anschrift / Address

Max-Planck-Institut für Meteorologie
Bundesstrasse 53
20146 Hamburg
Deutschland

Tel.: +49-(0)40-4 11 73-0
Fax: +49-(0)40-4 11 73-298
Web: www.mpimet.mpg.de

Layout:

Bettina Diallo, PR & Grafik

Titelfotos:
vorne:
Christian Klepp - Jochem Marotzke - Christian Klepp
hinten:
Clotilde Dubois - Christian Klepp - Katsumasa Tanaka

Berichte zur Erdsystemforschung 91/2011

Holocene and Eemian Climate Variability

Nils Fischer

aus Berlin

Hamburg 2010

Reports on Earth System Science 91/2011

ISSN 1614-1199

Nils Fischer
Max-Planck-Institut für Meteorologie
Bundesstrasse 53
20146 Hamburg
Germany

Als Dissertation angenommen
vom Department Geowissenschaften der Universität Hamburg

auf Grund der Gutachten von
Prof. Dr. Jochem Marotzke
und
Dr. Johann H. Jungclaus

Hamburg, den 29. November 2010
Prof. Dr. Jürgen Oßenbrügge
Leiter des Departments für Geowissenschaften

ISSN 1614-1199

Holocene and Eemian Climate Variability

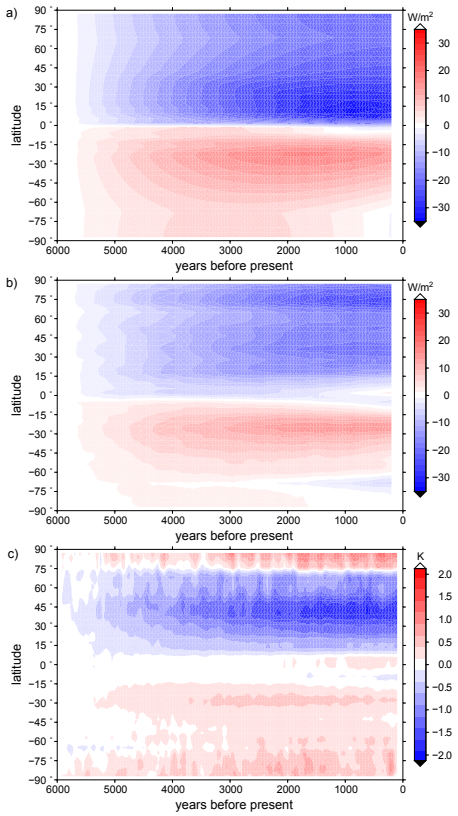

Nils Fischer

Hamburg 2010

Abstract

Using a coupled atmosphere-ocean general circulation model (AOGCM) with applied orbital forcing, we investigate the climate evolution and variability of the last two interglacial periods, the mid-Holocene (6,000 years before present) and the Eemian (125,000 years before present). Earth's orbital parameters in these two periods lead to an increase in the Northern Hemisphere's seasonal insolation cycle which is stronger in the Eemian than in the Holocene. We focus on ocean circulation changes, its evolution and variability, and the seasonal temperature cycle.

Time-slice simulations of the two paleo periods reveal that the induced changes in annual mean temperature are regionally enhanced through atmosphere-ocean feedbacks. In high northern latitudes, an insolation induced temperature increase is enhanced by increased ocean heat transport and reduced sea-ice cover, resulting in an intensified ocean heat release. Orbital forcing has similar effects proportional to the forcing strength on climate and climate variability in the Holocene and the Eemian simulation.

In a transient simulation from the mid-Holocene to today, we find that the orbital forcing strengthens the Atlantic meridional overturning circulation (AMOC) due to a density increase of the North Atlantic deep water produced in the northern ocean's convection regions. In the Labrador Sea, this results from the advection of more saline water from the eastern North Atlantic. In the Nordic Seas, decreasing temperatures cause a substantial increase in water mass density and result in enhanced overflows.

The AMOC exhibits variability on interannual and multi-centennial time-scales. The interannual variability is connected to atmospheric forcing, dominated by the North Atlantic Oscillation. The multi-centennial AMOC variability results from accumulating salinity anomalies in the sub-tropical gyre which, at some threshold, spread to the sub-polar gyre and trigger a change in AMOC strength. The irregular period and amplitude of the low-frequency variability indicates that it is an accumulated response of the coupled system to small scale perturbations.

Investigating the evolution of the seasonal temperature cycle, we find that its amplitude is determined by seasonal insolation changes in the low- and mid latitudes, and by sea-ice cover in the high latitudes. The sea-ice effect impacts the temperature response over the continents adjacent to the Arctic as is also visible in paleo temperature reconstructions.

In a first unaccelerated transient simulation of the mid- to late Holocene with a comprehensive AOGCM, we were able to investigate changes in the ocean state due to slowly varying forcing. We identified and attributed an AMOC increase and AMOC variability on time-scales from interannual to multi-centennial and found that the strength of the seasonal cycle is not only insolation dependent.

Contents

Chapter 1

Introduction

In the discussion on the magnitude of the anthropogenic contribution to observed and future climate change, the amplitudes and time-scales of natural climate variability are a major source of uncertainty (Jansen et al. 2007; Hegerl et al. 2007). Instrumental records that allow for an assessment of natural variability, however, exist only for the last 100 years. Also, instrumental records of the ocean component of the climate system are spatially not as well resolved as for the atmosphere. The time-scales of interest regarding future climate change are on the order of 100 years. Investigation of the role of natural climate variability thus requires data series longer than 100 years. In addition, variability of the ocean plays a major role on these time-scales (e.g., Mitchell 1976; Stocker and Mysak 1992; Bindoff et al. 2007).

The recent interglacial climate periods, the mid-Holocene (6,000 years before present, 6 ka) and the Eemian (125 ka) are thought of as analogs of future climate change, e.g., regarding changes in high northern latitudes (Miller et al. 2006). Interglacial climates and climate variability are studied intensively in terms of paleo-proxy reconstruction of climate variables and in terms of climate modelling. In modelling studies of interglacial climate, the focus until now has mainly been on changes in the atmosphere component of the climate system. In the present study, we attempt to add to the physical understanding of natural climate variability with a thorough investigation of changes in the ocean part and its circulation under interglacial boundary conditions.

Using a state-of-the-art coupled atmosphere-ocean general circulation model (AOGCM) and applying orbital forcing, we perform three time-slice simulations of Holocene, Eemian and pre-industrial climate and a 6,000 year-long transient simulation from the mid-Holocene to today. We assess the impact of orbital forcing on mean climate and investigate mechanisms responsible for the change in and between the components of the climate system. Furthermore, we explore the time-scales and amplitudes of natural climate variability and what mechanisms may account for them. These mechanisms can be insolation-induced direct effects, e.g., changes in the latitudinal temperature gradient and changes in the seasonal temperature cycle, and also indirect effects, e.g., changes in sea-ice cover and changes in the meridional atmospheric and oceanic heat transports.

1.1 Holocene and Eemian Boundary Conditions

The climatic periods we investigate are the current interglacial, which is called the Holocene and which started around 11 ka, and the last interglacial, called the Eemian, which lasted from 127 ka to 115 ka. In the aftermath of the preceding glacial periods, disintegrating continental ice sheets were the major influence on climate change at the beginning of the interglacial periods (e.g., Davis and Brewer 2009). Since we are mainly interested in the influence of orbital parameters, we choose - also according to previous paleo modeling studies - time-slices at 6 ka for the Holocene and 125 ka for the Eemian, respectively. In those two times, continental ice sheets and sea-level were both stable and comparable to today's configuration (Fairbanks 1989; Overpeck et al. 2006).

Apart from greenhouse gas concentrations, the main difference in climate forcing between the two paleo time-slices and the present climate are the parameters of the Earth's orbit around the Sun which influence the total, spatial, and temporal distribution of incoming solar radiation. These parameters are the eccentricity, the obliquity and the precession of the vernal equinox and can be calculated from celestial mechanics (Berger 1978). The orbital parameters vary on periods of approximately 20,000 years for the precession of the vernal equinox, 40,000 years for the obliquity, and 100,000 years for the eccentricity. The eccentricity modulates the amplitude of the precessional effect, which depends on the difference in the Earth's distance to the Sun between perihelion and the opposite aphelion. In both the Holocene and the Eemian time-slices, obliquity is enhanced and, concurrently, summer solstice is close to perihelion, which leads to asymmetric seasonal insolation changes in the Northern and Southern Hemisphere. Higher insolation in the boreal summer and less in the boreal winter leads to an increase in the amplitude of the seasonal insolation cycle in the Northern Hemisphere. In the Southern Hemisphere, the effect is reversed and smaller in amplitude, resulting in a decrease of the amplitude of the seasonal insolation cycle. The two hemispherically opposite effects are further enhanced in the Eemian time-slice where, additionally, the eccentricity was larger than in the Holocene and the present day.

Although the latitudinal changes in annual mean insolation do not exceed $4\,\mathrm{W/m^2}$, paleo reconstructions and previous modeling studies have shown that the increase in the amplitude of the seasonal insolation cycle is not only visible on seasonal timescales, but also affects the annual mean climate response (e.g., Braconnot et al. 2007b; Wanner et al. 2008). These annual mean changes cannot solely be explained by orbitally induced changes in insolation, but rather they have to be caused by indirect effects in the climate system such as feedbacks between the atmosphere, ocean, and sea-ice (e.g., Claussen et al. 1999; Otto et al. 2009).

1.2 State of the Art and Research Questions

Previous studies of Holocene and Eemian climate with AOGCMs mainly focussed on changes in the atmosphere component of the climate system, e.g., changes in the low latitude monsoon systems (Braconnot et al. 2008) and the Northern Hemisphere's winter storm tracks (Kaspar et al. 2007). The state of the ocean component in AOGCM studies was only investigated in terms of changes in surface variables (Braconnot et al. 2007b) and changes of the temperature at the thermocline (Liu et al. 2003). Using a more simplified Earth system model of intermediate complexity (EMIC), changes in ocean circulation in the Holocene were the subject of two studies by Renssen et al. (2005, 2006).

Comparing changes in the mean state of three time-slice simulations of Holocene, Eemian and pre-industrial climate with applied orbital forcing, we add a new aspect to previous modeling studies with AOGCMs and focus also on ocean dynamics. In particular, we pose the following reseach questions in chapter 2:

(1) How do changes in orbital parameters alter atmospheric and oceanic circulation and the associated heat transports, and how do these changes in circulation and heat transports influence regional climate?

(2) Are there differences in the simulated climate under Eemian and Holocene boundary conditions disproportionate to the forcing thus implying irregular responses to the induced insolation changes?

Ocean circulation contributes significantly to the climatic mean state and to climate variability. This is especially true for the ocean circulation in the Atlantic Ocean, which transports large amounts of heat from the tropics to the high northern latitudes, resulting in comparably mild climate conditions in large parts of northern Europe (e.g., Keith 1995; Ganachaud and Wunsch 2000; Trenberth and Caron 2001). Due to its ability to integrate climate variations on short timescales with relatively small amplitudes (Hasselmann 1976), the ocean exhibits variability on time-scales up to many centuries. This low-frequency variability and the corresponding mechanisms have been subject of recent AOGCM modeling studies (e.g., Vellinga and Wu 2004; Jungclaus et al. 2005; Park and Latif 2008). These studies were performed under quasi-equilibrium or idealized periodic forcing.

By contrast we perform a transient simulation of the last 6,000 years from the mid-Holocene to today with orbital forcing. If the climate changes induced by orbital forcing in the time-slice simulations do not show irregular responses, this indicates that the results we infer from our Holocene simulation are also valid for the Eemian interglacial. Climate model studies applying Holocene boundary conditions can be evaluated against climate reconstructions from paleo-proxy archives, and allow for an investigation of

climate variability on long time-scales driven by long-term forcing. So far, however, few transient Holocene climate simulations have been performed and most have been concerned with the analysis of atmosphere and upper ocean changes (e.g. Lorenz et al. 2006). There are a few exceptions already mentioned above: a study by Liu et al. (2003) that discussed the oceanic state in different, relatively short Holocene time-slice experiments using a coupled AOGCM, and studies with an EMIC by Renssen et al. (2005, 2006) that also analyzed evolution of dynamic processes involved with ocean circulation changes on orbital time-scales in the Holocene.

Since variability of the ocean ranges from seasonal to multi-centennial time-scales that are superimposed on each other, it is difficult to disentangle the respective processes. We analyze ocean circulation in the transient Holocene simulation and address two main research questions in chapter 3:

(3) How does the ocean circulation evolve in the long-term under Holocene orbital forcing?

(4) On what time-scales does the ocean circulation show variability and what are the responsible mechanisms?

Several studies of Holocene climate have shown the importance of the seasonal cycle amplitude on mean climate (e.g., Braconnot et al. 2007b). Nevertheless, how the seasonal temperature cycle actually evolves, taking into account internal processes in the climate system that potentially alter the direct response to the changes in insolation, has so far not been investigated.

Reconstructing seasonal temperatures for Greenland during the Dansgaard-Oschger events in the last deglaciation, Denton et al. (2005) found that the annual mean temperature changes were mainly dominated by the winter signal. The authors attributed the strong decline in winter temperatures to an expansion of sea ice in the Arctic Ocean and the North Atlantic that leads to continental climate conditions over a large area in the Northern Hemisphere.

We analyze the transient Holocene simulation of the last 6,000 years and quantify the effect of insolation changes on the amplitude of the seasonal temperature cycle and test if the sea-ice effect proposed by Denton et al. (2005) is also acting in the mid- to late Holocene.

We have stated earlier that paleo model simulations can be evaluated against climate reconstructions from proxy archives. These are increasing in availability and in temporal and spacial resolution in the form of compilations, which allow for a comparison to modelled climate data. Using one such compilation of reconstructed European summer and winter temperatures (Davis et al. 2003), we investigate the correspondence between model and data. On the one hand, this will help us to assess on what spatial and temporal scales the model results are reliable and to detect features and processes

missing in the model. On the other hand, the model results are not limited spatially or to certain climate variables and thus allow for a more comprehensive analysis that may help to interpret the proxy data. In chapter 4, we address the following research questions:

(5) How does the seasonal temperature cycle in the Holocene evolve towards present day orbital conditions and what processes determine the amplitude of the seasonal temperature cycle?

(6) How do the modelled seasonal temperatures compare to reconstructed temperatures from paleo proxies?

1.3 Thesis Outline

The thesis consists of three chapters written in the style of journal publications. Each of these chapters can be read individually. They are self-contained with individual introductions, model and experimental setup descriptions, and conclusions.

In chapter 2 we compare changes in atmospheric and oceanic heat transports in time-slice simulations of Holocene, Eemian, and pre-industrial climate. This chapter has been published in *Climate of the Past*[1] and is included here with editorial adjustments. Chapters 3 and 4 address different research questions using results from a 6,000 year-long transient simulation from the mid-Holocene to today with the same model setup as in chapter 2. Changes in ocean circulation under Holocene orbital forcing and the causative processes are the subject of chapter 3, in which we also examine the time-scales and amplitudes of ocean circulation variability. Chapter 4 addresses the evolution of the seasonal temperature cycle and the relevant processes determining its amplitude. The results are compared to paleo temperature reconstructions.

We conclude the thesis with a summary of the main findings in chapter 5, in which we furthermore propose possible directions of future research.

[1] Fischer, N. and Jungclaus, J.H., 2010: Effects of orbital forcing on atmosphere and ocean heat transport in Holocene and Eemian climate simulations with a comprehensive Earth System model, *Climate of the Past*, **6 (2)**, 155-168

Chapter 2

Effects of Orbital Forcing on Atmosphere and Ocean Heat Transports in Holocene and Eemian Climate Simulations

Orbital forcing exerts direct insolation effects and also alters climate indirectly through feedback mechanisms that modify atmosphere and ocean dynamics and meridional heat and moisture transports. We investigate the regional effects of these changes by detailed analysis of atmosphere and ocean circulation and heat transports in a coupled atmosphere-ocean general circulation model with an integrated land surface model (ECHAM5/JSBACH /MPIOM). We perform long-term quasi-equilibrium simulations under pre-industrial, mid-Holocene (6,000 years before present), and Eemian (125,000 years before present) orbital boundary conditions.
Compared to pre-industrial climate, Eemian and Holocene temperatures are generally warmer at higher and cooler at lower latitudes. Changes in sea-ice cover, ocean heat transports, and atmospheric circulation patterns enhance the insolation induced warming signal in the high northern latitudes and lead to pronounced regional heterogeneity. Over Europe, the warming signal is most pronounced over the northeastern part, in accordance with recent reconstructions for the Holocene. We attribute this warming to enhanced northward ocean heat transport in the Nordic Seas and enhanced ocean-to-atmosphere heat flux over the Barents Shelf in connection with a retreat of sea ice and intensified winter storm tracks over northern Europe.

2.1 Introduction

Changes of insolation distribution due to variations in the Earth's orbit around the sun are considered the dominant external forcing of glacial-interglacial cycles throughout the Quaternary (the last 2.5 million years) (Milankovic 1941; Hays et al. 1976;

Imbrie et al. 1992). Their impact on the climate of interglacial periods has been studied in previous coupled atmosphere-ocean modeling work, mainly focussing on the atmosphere component of the climate system (e.g., Braconnot et al. 2007a,b). Notable exceptions were transient simulations of the Holocene with a coupled Earth system model of intermediate complexity (EMIC) by Renssen et al. (2005, 2006) and a Holocene time-slice study with 120-year-long simulations with a coupled atmosphere-ocean GCM by Liu et al. (2003), who analyzed ocean dynamics. Subject of the present study are effects of orbital forcing on regional climate and the role of orbitally induced changes in atmospheric and oceanic circulation and the associated heat transports in the Holocene (6,000 years before present - yBP) and the last interglacial period, the Eemian (125,000 yBP), compared to pre-industrial climate in a fully coupled atmosphere-ocean-sea ice-biosphere general circulation model (GCM).

Glacial-interglacial cycles in the Quaternary had a periodicity of approximately 100,000 years for the last 500,000 years and the interglacial periods lasted for 7,000 to 17,000 years. The main driver of the cycles is assumed to be summer insolation at high northern latitudes. It increases when the eccentricity of the Earth's orbit around the sun is high, the obliquity of the Earth's axis of rotation is increased and, concurrently, perihelion is close to summer solstice. For the last two interglacial periods insolation maxima at high northern latitudes occurred 9,000 yBP in the Holocene and 127,000 yBP in the Eemian. Due to the global climate system's inertia, e.g., continental ice sheets and ocean heat content, there is a delay up to several millennia in climate response, thus the climate optimum of the present interglacial, the Holocene, as well as that of the Eemian occurred several millennia after the insolation maximum. During the Eemian, the eccentricity of the Earth's orbit around the sun was larger than in the Holocene and, in consequence, insolation changes were more pronounced.

The paleo model intercomparison project PMIP2 (Braconnot et al. 2007a) compared the Holocene climate to pre-industrial climate using data obtained from different GCMs and EMICs. For the Holocene simulations the models showed an increased seasonal cycle in the Northern Hemisphere with annual mean temperatures increasing in the higher latitudes and decreasing in the tropics. Their study concluded that the sea ice-albedo-feedback strengthens the seasonal cycle in the Northern Hemisphere. The study showed that the ocean played a major role in the evolution of past climates, since the results matched proxy reconstructions better than those obtained from the atmosphere only study PMIP (Joussaume and Taylor 1995) performed earlier. Nevertheless, PMIP2 related publications did not discuss ocean dynamics in detail.

Using an atmosphere-ocean GCM, Kaspar et al. (2007) found an increase of Eemian winter storm tracks over the North Atlantic and a decrease over the Pacific. The Atlantic storm tracks experienced a significant northward shift. The changes were attributed to orbitally induced changes in the meridional temperature gradient. With a similar model setup, Groll et al. (2005) investigated the relationship between regional

temperatures and large-scale circulation for the Eemian compared to the pre-industrial climate. Their simulations showed a decrease in the Arctic Oscillation temperature signal (the correlation between sea-level pressure anomalies and near surface temperature) due to lower simulated winter temperature in the Northern Hemisphere in the Eemian but similar circulation variability.

An analysis of ocean dynamics in the Holocene was performed by Renssen et al. (2005, 2006) in a transient simulation of the Holocene from 9,000 yBP to today in a coupled atmosphere-sea ice-ocean-vegetation EMIC. The large-scale features of the differences in Holocene climate compared to pre-industrial were similar to those in PMIP2 and the authors proposed geophysical mechanisms concerning changes in the ocean. Deep water formation in the Atlantic changed due to changed sea-ice cover and ocean-sea ice interaction. In their model study on Holocene climate, Liu et al. (2003) found a symmetric annual mean temperature response of the ocean surface to orbital forcing in both hemispheres, a cooling at low and a warming at high latitudes. By contrast, the thermocline response was dominated by an asymmetric pattern with cooling in the Northern and warming in the Southern Hemisphere mid-latitudes determined mainly by local winter insolation through surface water subduction.

Three of the five coupled GCM studies however, had to apply heat and/or freshwater flux adjustment between the atmosphere and ocean model in order to obtain a stable climate. The EMIC applied in Renssen et al. (2005) that applied fresh water flux adjustment only and the model used by Liu et al. (2003) did not use flux adjustment, but analyzed comparably short simulations (120 years). The flux adjustment fields were obtained under pre-industrial boundary conditions and for the heat flux exceed changes induced by orbital forcing. Therefore, the ocean state is "biased" to a pre-industrial state and thus the effects of orbital forcing on the state of the ocean are superimposed.

Reconstructions from paleo proxies revealed differing surface temperature trends in northern Europe and the Nordic Seas on regional scales over the ocean (Hald et al. 2007) as well as over land (Davis et al. 2003) and showed that the warming over northeastern Europe and Scandinavia is the most pronounced signal.

In a study applying the same model setup as in the present one, Otto et al. (2009) investigated the contributions of the different components of the climate system, atmosphere, ocean and vegetation, to changes in surface temperature in the Holocene. They find that the ocean, the atmosphere and interactions between the two are the main contributors and that vegetation related feedbacks only play a minor role.

In this study, we apply a GCM setup without flux adjustment to perform climate simulations integrated sufficiently long to obtain quasi-equilibrated climate states. We are thus able to explain the regional patterns of climate change under full consideration of the oceanic changes induced by insolation forcing. We perform detailed analyses of changes in the ocean circulation and heat transports and investigate their effects on regional climate in conjunction with changes in the state of the atmosphere. We present

results obtained from two time-slice simulations with a comprehensive GCM compared to a control run under pre-industrial conditions: one of Holocene climate, 6,000 yBP, and one of Eemian climate, 125,000 yBP.

2.2 Model and Experimental Setup

2.2.1 Model Setup

The climate simulations are performed using the Max-Planck-Institute for Meteorology's coupled climate model. The model consists of the spectral atmosphere model ECHAM5 (Roeckner et al. 2003) run at truncation T31, corresponding to a horizontal resolution of a $3.75^\circ \times 3.75^\circ$ longitude-latitude grid with 19 vertical hybrid sigma pressure levels with the highest level at 10 hPa. Integrated in the atmosphere model is the land surface model JSBACH (Raddatz et al. 2007) with a dynamic vegetation module (Brovkin et al. 2009). ECHAM5 is coupled to the general circulation ocean model MPI-OM (Marsland et al. 2003) run in resolution GR30 with 40 vertical levels (30 levels are within the top 2000 meters) and an included Hibler-type zero-layer dynamic-thermodynamic sea-ice model with viscous-plastic rheology (Semtner 1976; Hibler 1979).

The ocean model uses a bipolar orthogonal spherical coordinate system and is based on an Arakawa C-grid and allows for an arbitrary placement of the poles. In the setup applied here, the North Pole is shifted over Greenland to avoid numerical singularities combined with the advantage of relatively high resolution in the deep water formation regions, around Greenland maintaining isotropic conditions. The model's South Pole is located at the center of Antarctica also resulting in increased resolution of the deep water formation regions around Antarctica. The horizontal grid spacing varies between 30 km around Greenland to 368 km in the tropical Pacific.

The coupling between the atmosphere and the ocean model is performed by the OASIS coupler (Valcke et al. 2003). Fluxes of momentum, heat, and freshwater from the atmosphere to the ocean are transfered and interpolated onto the ocean grid. From the ocean to the atmosphere sea surface temperature, sea ice thickness and fraction, snow cover on sea ice, and surface velocities are transmitted.

The model includes a river run-off scheme (Hagemann and Dumenil 1998; Hagemann and Gates 2003) where river run-off is transferred to the ocean together with the difference in precipitation and evaporation. Mass balance for glaciers and ice-sheets is not accounted for, since snow falling on Antarctica and Greenland is transferred to the nearest ocean grid cell instantaneously.

The coupled model (Jungclaus et al. 2006) runs without flux adjustment and consequently allows for a more realistic representation of oceanic heat transports than flux-adjusted models. The time-step is 20 minutes for the atmosphere and 2.4 hours

for the ocean model components. The coupling time-step between the atmosphere and ocean model is 24 hours.

2.2.2 Experimental Setup

We run three time-slice simulations for each climatic period under investigation. The respective orbital parameters of the Earth are calculated after Berger (1978) for the Eemian (125,000 yBP), the Holocene (6,000 yBP) and a pre-industrial control climate (1,200 yBP). The latter is chosen such that no anthropogenic influences such as changes in greenhouse gas concentration, etc. need to be considered. Greenhouse gas concentrations are set to pre-industrial values in all three simulations (CO_2 to 280 ppm, CH_4 to 700 ppb, N_2O to 265 ppb). The solar constant is also unaltered in all three experiments since corresponding changes in insolation are small compared to changes induced by changing orbital parameters. In the Holocene simulation, the continental ice sheets and sea level are assumed to be similar to today's. Due to sparse information and better comparability the same continental ice sheets are prescribed in the Eemian simulation. Land surface changes are accounted for by the dynamic vegetation module. Changes in atmospheric dust loads due to volcanic eruptions are not taken into account. The pre-industrial control simulation was initialized by Levitus and Isayev (1992) climatology for the ocean.

The Holocene and the Eemian simulations start after 2,500 years of integration of the pre-industrial control run by changing the orbital parameters accordingly. The control run was assumed to be in equilibrium with the pre-industrial boundary conditions. Both paleo-simulations are integrated for further 1,800 years without acceleration or asynchronous coupling of the atmosphere and ocean component. Only the last 1,000 years are taken into account in the following analysis assuming that the atmosphere, vegetation and the upper and middle ocean are in equilibrium with the new boundary conditions. In all three experiments, the drift of global ocean temperature at 2200 m over the investigated simulation period is 0.05 K, global salinity at 2200 m does not show a trend.

2.3 Results

Altered insolation distribution due to changes in orbital boundary conditions leads to an enhanced seasonal cycle in both the Holocene and the Eemian simulation because the obliquity is increased and summer solstice is closer to perihelion than under pre-industrial conditions. Hence, the qualitative changes with respect to pre-industrial climate are similar in both simulations. Since eccentricity is increased and summer solstice is closer to perihelion in the Eemian simulation, the changes in the seasonal cycle are more pronounced than in the Holocene simulation.

2.3.1 Large Scale Features of Mean Climate

During the Holocene and the Eemian, reduced insolation in the summer months compared to pre-industrial conditions at low latitudes leads to lower temperatures in the tropics and sub-tropics especially over the Sahel region, India, and southeast Asia (Fig. 2.1 a). Higher temperatures occur at high latitudes, where summer insolation is increased. The largest increase occurs in the Arctic region (Fig. 2.2) over the Barents Shelf (3 K in the Holocene, 7 K in the Eemian) and along the east coast of Greenland (3 K in the Holocene, 4 K in the Eemian). The Southern Ocean experiences an increase in temperature of 1-2 K (2-3 K in the Eemian) and Antarctica of about 0.5 K in the Holocene (1 K in the Eemian). In the North Atlantic, temperatures south of Iceland are decreasing by up to 1 K in the Eemian simulation.

We attribute the temperature decrease in the tropics to an intensification of the African monsoon system, with increased cloud cover over the Sahel region shielding the land surface from direct insolation. Sensible heat flux from the land surface to the atmosphere is thus reduced by up to 30 W/m^2 and 60 W/m^2 in the Holocene and Eemian, respectively, whereas latent heat flux increases by similar amounts. The hydrological cycle is further increased by an increase in vegetation cover. The subsequent decrease in surface albedo (see below) however, is not counterbalancing the cooling effect. The temperature increase in the Arctic is due to a reduction in sea-ice cover in the Arctic and changes in atmospheric and oceanic circulations and heat transports which will be discussed in further detail in the following sub-sections.

Changes in precipitation in the Holocene and the Eemian (Fig. 2.1 b) are qualitatively similar but more enhanced in the Eemian simulation, with the strongest increase of up to 2.5 mm per day over the Sahel region and the western Indian ocean. Over the Sahel this increase is due to similar increases in advective and convective precipitation whereas over the Indian ocean the increase is only seen in convective precipitation. The latitudinal precipitation maximum over the region between 10°S and the Equator reduces in the Eemian simulation (though not significantly) by 0.2 mm/day to 6.0 mm/day. The latitudinal band between 15°N and 30°N with no precipitation (over the Sahel region) narrows in the Holocene simulation to 20°N and 30°N and has almost vanished to a small band around 30°N in the Eemian simulation. The strongest decrease of 2.5 mm/day occurs over the eastern equatorial Atlantic and over the eastern Indian Ocean near Indochina and south of Indonesia.

Over the Northern Hemisphere's continents at low latitudes, there is a slight increase in precipitation whereas Southern Hemisphere's continents experience a slight decrease. Although a thorough investigation of the monsoon systems is beyond the scope of this study, this could be an indication of a shift in the inter-tropical convergence zone, ITCZ. Following the definition of the ITCZ location given in Braconnot et al. (2008) we detect a northward shift over Africa of 1.5°(3°) over western and central Africa to 9°(10°) over

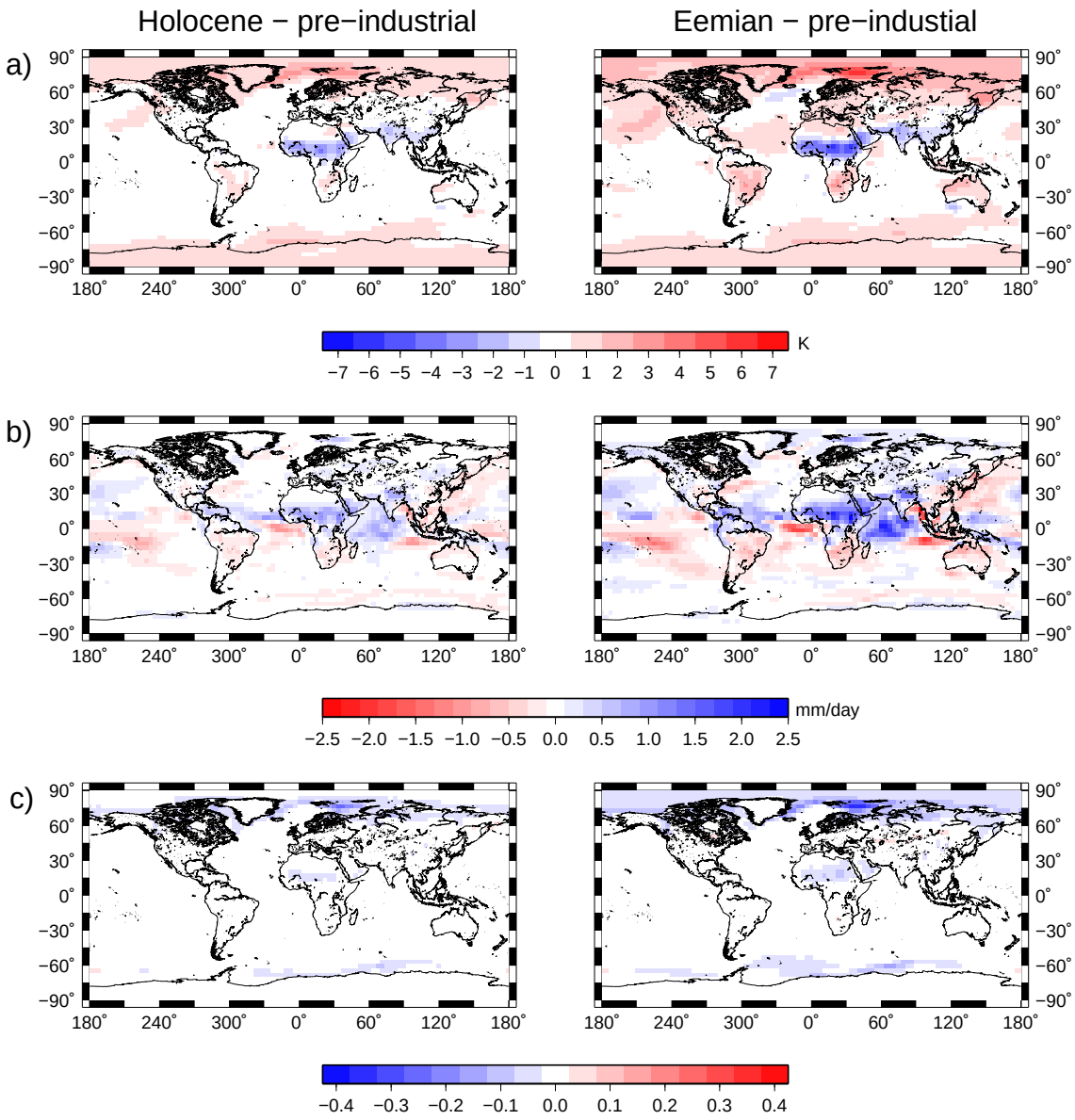

Figure 2.1: 1,000 year mean differences of Holocene (left) and Eemian (right) minus pre-industrial: **a)** near surface temperature (2m-temperature) in K, **b)** precipitation in mm/day **c)** surface albedo.

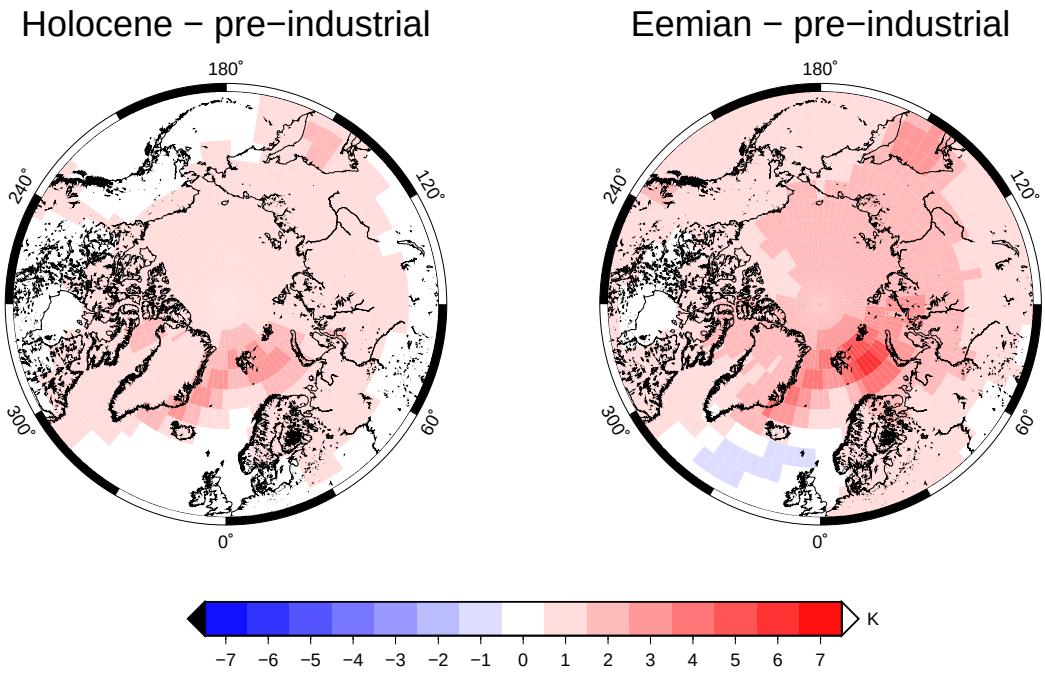

Figure 2.2: Temperature changes (in K) in the Arctic region for the Holocene and the Eemian compared to pre-industrial climate.

eastern Africa in the Holocene (Eemian) simulation compared to the pre-industrial one (not shown). Precipitation is increasing in the Arctic with the strongest signal over the Barents Shelf (1 mm/day). Over the Pacific Ocean, precipitation is decreasing in the eastern part of the Northern Hemisphere and over the central part of the Southern Hemisphere. In the southwestern Pacific, there is an increase in precipitation east of the Philipines and southeast of New Guinea. Most parts of Antarctica experience changes in precipitation below 10%. Albeit the increase of 1 K in temperature, very dry conditions with precipitation well below 1 mm/day prevail.

Surface albedo (Fig. 2.1 c) is reduced in the Sahel in the Holocene and the Eemian owing to an increase in vegetation cover and in the Arctic due to reduction in sea ice cover especially over the Barents Shelf and on the east coast of Greenland. Because of a decrease in snow cover and a northward shift in the boreal tree line, surface albedo is reduced in most parts of northern Siberia, Scandinavia and northern North America.

2.3.2 Atmospheric Circulation and Heat Transports

We calculate components of meridional advective atmospheric heat transport after Keith (1995). Total advective meridional atmospheric heat transport (htra) is defined as:

$$\text{htra} = \int (c_p T + gz + Lq) v \frac{\mathrm{d}p}{g} \mathrm{d}x \mathrm{d}z$$

with c_p the specific heat capacity of dry air, T temperature, L latent heat of condensation, q water vapor content, g gravitational acceleration, v wind velocity, p pressure and x and z the zonal and vertical coordinate, respectively. The integration is performed in the vertical and zonal dimension. The sum of the first two terms is the dry static energy and the third the moist energy. The dry and moist contributions are then split up in three components each: 1) a mean meridional component, i.e., time and zonal mean velocity and mean energy, 2) a transient eddies component, i.e., time anomalies of velocity and energy from the zonal mean, and 3) a stationary eddies component, i.e., spatial anomalies of velocity and energy from the time and zonal mean.

The zonal integral of heat transport over a hundred year mean of pre-industrial climate shows a similar distribution as the ECMWF analysis from present day data in Keith (1995) (not shown). Total advective heat transport is nearly symmetric in both hemispheres with maxima of 5 PW at 45°N and 35°S respectively. Mean meridional circulation and stationary eddies contribute about 2 PW each at low latitudes (up to 25°N /25°S), at latitudes from 30° to 60° transient eddies contribute 4 PW in the Northern Hemisphere and 6 PW in the Southern Hemisphere of which 2 PW are compensated for by mean meridional circulation transport associated with the Ferrel Cell.

Comparing the heat transports in the pre-industrial simulation and the Holocene and Eemian simulation (Fig. 2.3), the total advective heat transport to the Northern Hemisphere decreases up to 0.15 PW (5%) and 0.35 PW (12%) for the Holocene and the Eemian respectively at 20°N . The differences in dry and moist components of the heat transport tend to compensate each other since they are both related to the Hadley circulation, where the upper branch transports dry static energy to the poles (positive sign) and the lower branch transports latent heat to lower latitudes (negative sign). Thus, a reduction in the strength of the Hadley Cell in the Holocene and the Eemian simulation leads to a decrease in sensible heat transport to the poles and an effective increase in latent heat transport to the poles.

From 30°N to 45°N , there is a slight increase of 0.05 PW (Holocene) and 0.1 PW (Eemian) compared to the total of around 5 PW due to increasing mean meridional circulation. At mid- to high-northern latitudes there is a reduction in atmospheric heat transport due to reduced heat transport contribution by transient eddies, which cannot be completely compensated for by an increase in stationary eddy heat transport at the same latitude region. Significance has been tested by comparing the changes computed

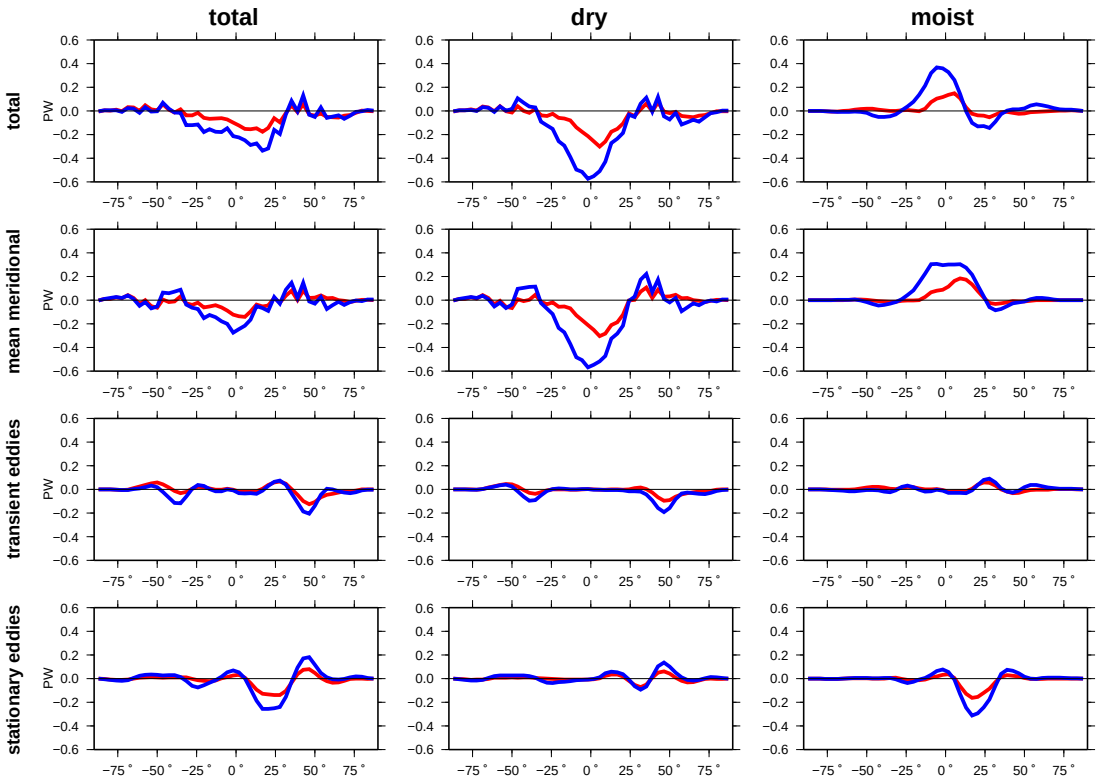

Figure 2.3: Differences in zonally integrated atmospheric heat transports (in PW - 10^{15} W) averaged over 100 years (red line: Holocene - preindustrial; blue line - Eemian - pre-industrial) total (left column), dry or sensible heat (middle column) and moist or latent heat (right column) contributions. In the horizontal the rows show total, mean meridional, transient eddy and stationary eddy contributions from top to bottom.

from the total advective heat transport to changes computed from the total implied heat transports of the 1000 year investigation period divided in 100-year-periods. The changes discussed exceed two standard deviations.

To check whether the decrease in transient eddy heat transport is associated with cyclone activity we analyzed Northern Hemisphere winter storm tracks by investigating anomalies in geopotential height at 500 hPa on the synoptic scale, 2.5-6 days, (Blackmon 1976) in the three simulations. Fig. 2.4 shows mean geopotential height differences and differences of the calculated storm tracks in the Northern Hemisphere.

The Holocene and the Eemian simulations again show qualitatively similar results with the stronger amplitude in the Eemian simulation. Cyclone activity is reduced over the north Pacific, large parts of Siberia, and the Mediterranean region, whereas it is increased from northwestern North America over the North Atlantic through northern and central Europe.

The changes in storm tracks are in accordance with changes in the North-Atlantic-Oscillation (NAO) pattern we derived from empirical orthogonal function analysis of North Atlantic sea level pressure anomalies (Hurrell 1995). There we find an expansion of the high pressure region around the Azores Islands into the Bay of Biscay and parts of western France in the Holocene and more pronounced in the Eemian. The low pressure region that is centered over the southern tip of Greenland in our model remains constant in all three simulations. The increase of the high pressure region leads to a northward shift of the zero-line in the pressure dipole of the high and the low pressure regions. Assuming that most storm tracks pass the dipole along the zero line, this shift corresponds to the northward shift of the North Atlantic storm tracks. The time-series of the NAO-index (not shown) exhibits decreasing amplitudes of the negative NAO-phases which is connected to the decrease in storm track activity in southern Europe and the Mediterranean region.

2.3.3 Sea Ice

In the Holocene and the Eemian simulation, sea-ice cover in the Arctic is reduced compared to pre-industrial (Fig. 2.5) especially in the summer months where the insolation in high northern latitudes increases by up to $40\,\mathrm{W/m^2}$ in the Holocene and $65\,\mathrm{W/m^2}$ in the Eemian.

In the winter months, where in both the Holocene and the Eemian insolation is lower compared to pre-industrial, sea ice is not building up to compensate for the reduction. This leads to an almost ice-free Barents Shelf troughout the year and a retreat of the ice margin along the east coast of Greenland. The corresponding reduction in surface albedo (Fig. 2.1 c) leads to increased ocean heat uptake in summer that reduces sea-ice growth in winter and thus leads to a positive sea ice-albedo feedback. Additionally, the lack of sea-ice cover in winter increases the heat flux from the ocean to the atmosphere.

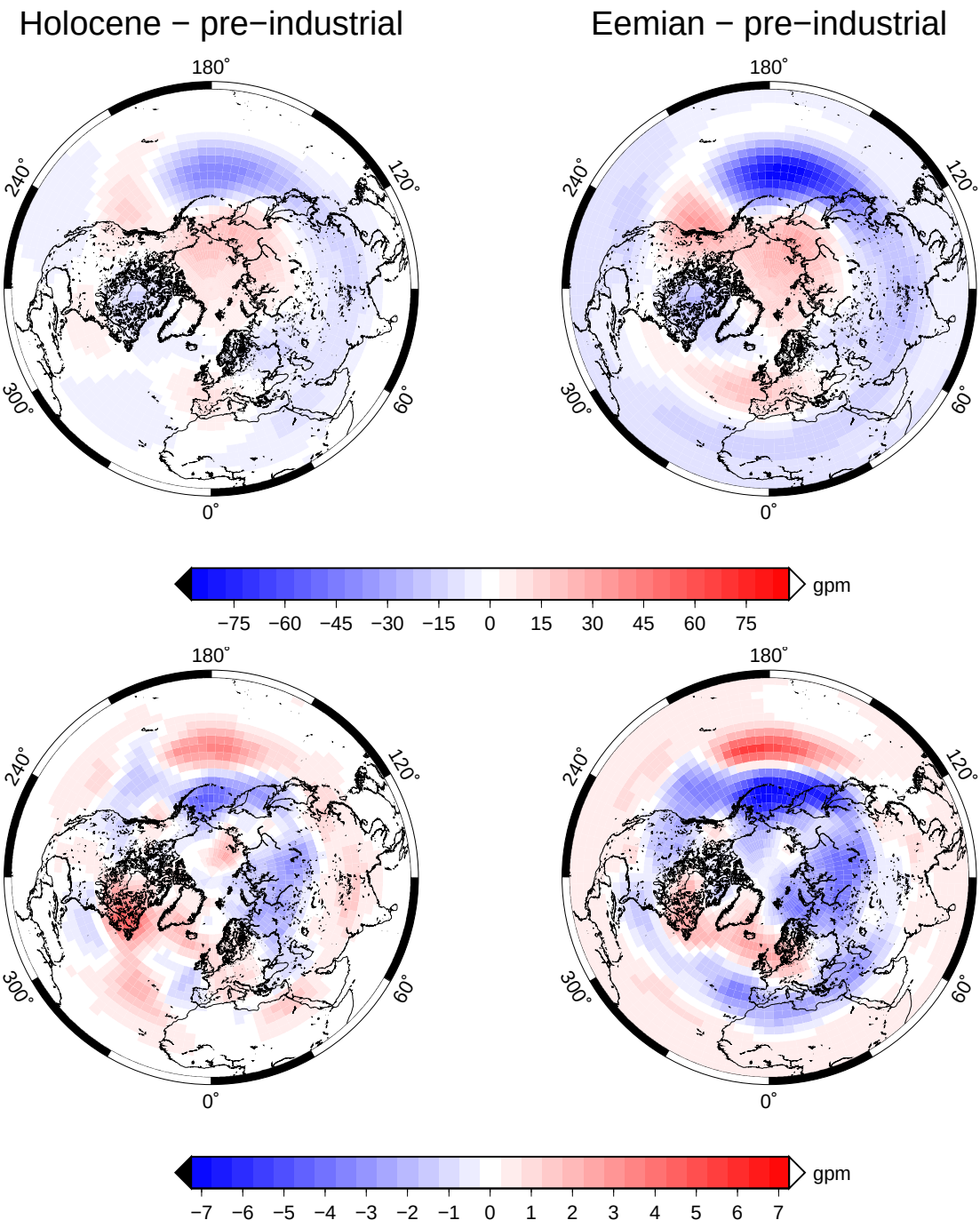

Figure 2.4: Northern Hemisphere differences in mean winter geopotential height in gpm (upper row) and winter storm tracks, defined as synoptic-scale geopotential height anomalies at 500 hPa in gpm (lower row).

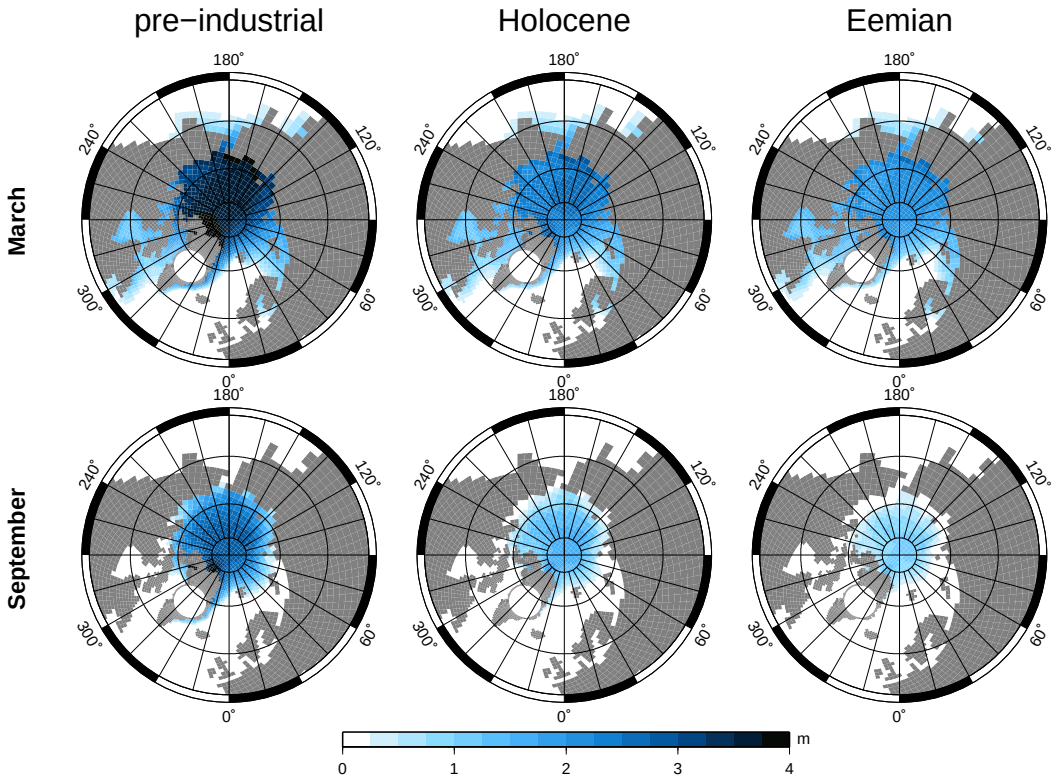

Figure 2.5: Sea ice thickness in m in the Arctic Ocean in pre-industrial, Holocene, and Eemian conditions in March (upper row) and September (lower row).

Around Antarctica sea-ice thickness is reduced especially in the Wedell Sea up to 1 m except for an increase in the western Ross Sea up to 0.4 m (not shown).

2.3.4 Oceanic Circulation and Heat Transports

We define the Atlantic meridional overturning circulation (AMOC) as the zonally integrated stream function over the Atlantic basin. In the pre-industrial control run, it has a maximum of 16 Sv (1 Sv = 10^6 m^3/s) at 30°N at 1000 m depth. Antarctic bottom water reaches up to 30°N below 3000 m depth with a strength of 2 Sv. In the Nordic Seas, the clockwise circulation cell reaches up to 80°N with an intensity of 2 Sv.

In the Holocene and the Eemian simulation, the AMOC at latitudes up to 75°N reduces to 14 Sv and 12 Sv, respectively, at its maximum compared to the pre-industrial simulation (Fig. 2.6). The reduction in AMOC is accompanied by an intensification of Antarctic Bottom Water in the deep ocean of up to 1 Sv in the Eemian simulation. Both the Eemian and the Holocene simulations show an increase in overturning of up to 1 Sv compared to the pre-industrial simulation north of 75°N .

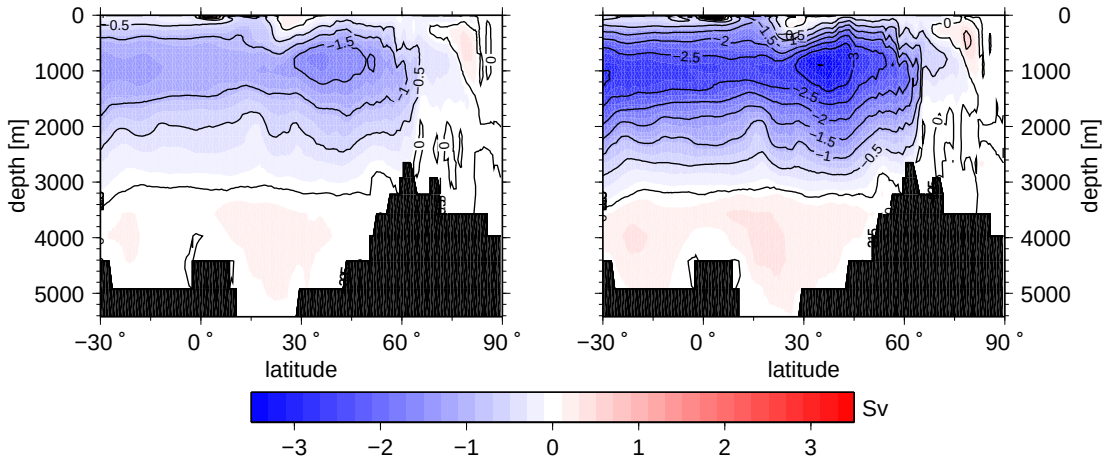

Figure 2.6: Differences of the zonally integrated vertical stream function in the North Atlantic in Sv ($10^6\,\mathrm{m}^2/\mathrm{s}$) for **a)** Holocene - pre-industrial and **b)** Eemian - pre-industrial.

Large scale horizontal circulation in the North Atlantic is expressed in terms of the vertically integrated horizontal barotropic stream function ($\psi(x,y) = \iint v\,dx\,dz$, with v meridional velocity, x and z the zonal and vertical coordinates). The Nordic Seas gyre maximum intensity increases by up to 1 Sv in the Holocene simulation and by 1.5 Sv in the Eemian (pre-industrial maximum: 16 Sv) and it expands further north due to the retreat of sea ice and an increasing density gradient, with relatively dense water in the center and less dense water at the margins.

An investigation of wind stress over the Nordic Seas basin does not show a clear influence on the gyre circulation. Wind stress curl slightly increases along the Norwegian coast, but decreases along the Greenland coast.

The sub-polar gyre shows a more diverse signal: the volume transport on the western side of the Reykjanes Ridge southwest of Iceland, which is 35 Sv in the pre-industrial simulation, reduces by 2 Sv in the Holocene and 4 Sv in the Eemian. Whereas in the deep water formation region south of the southern tip of Greenland, it is remaining at its pre-industrial maximum (48 Sv) in both the Holocene and the Eemian simulation.

The sub-tropical gyre weakens by up to 3 Sv in the southwestern part east of the Carribbean in the Holocene and 6 Sv in the Eemian. The reduction is also affecting the North Atlantic Current which reduces by 2 Sv in the Holocene and 6 Sv in the Eemian (pre-industrial maximum at 30°W: 48 Sv).

We analyze poleward Atlantic heat transport (htro) defined similarly to atmospheric heat transports:

$$\text{htro} = c_p \int v\,\theta\,\mathrm{d}x\mathrm{d}z$$

(Bryan 1962) where c_p is specific heat capacity of water, v meridional velocity, θ the potential temperature, and x, z the zonal and vertical coordinates. The integration is performed in the vertical and the zonal direction in the margins of the Atlantic basin assuming it to be closed with no net volume transport (with a net volume transport the absolute heat transport value would depend on a reference temperature, set to 0°C here). It has been shown in Hall and Bryden (1982) that the transport occurring through Bering Strait (approx. 0.4 Sv in all three model simulations) is negligible and the heat flux estimate thus meaningful. Velocity and potential temperature are split up into a zonal mean and deviations from the zonal mean. Heat transport via AMOC is then defined as the integral of the product of the zonal mean temperature and velocity and heat transport via ocean gyres as the integral of the product of the deviations from zonal mean temperature and velocity.

The poleward oceanic meridional heat transport in the Atlantic at 30°N decreases by up to 0.08 PW (-10%) in the Holocene and 0.12 PW (-16%) in the Eemian compared to the pre-industrial simulation (Fig. 2.7). From 60°N to 75°N heat transport increases by up to 0.02 PW (+10%) and 0.03 PW (+15%) for the Holocene and the Eemian respectively. Analysis of the contributions of oceanic heat transport from meridional overturning circulation (MOC) and ocean gyres reveals that at 30°N MOC (gyre) heat transport changes contribute 0.05 PW (0.03 PW) to the total heat transport decrease in the Holocene and 0.07 PW (0.05 PW) in the Eemian. At high northern latitudes the increase in oceanic heat transport is only due to increased gyre heat transport.

This transport is analyzed in further detail by calculating the volume and heat transports into and out of the Nordic Seas (see Table 2.1 and Fig. 2.8 for passages). The total values of the heat transport budget depend on the reference temperature which we choose as the mean temperature of the Nordic Seas basin in the three simulations ($\mathrm{T_{ref}} = 3.64°\mathrm{C}$) and subtracted it from the potential temperature ($\theta \rightarrow \theta - \mathrm{T_{ref}}$). Water is transported into the Nordic Seas from the North Atlantic through the Iceland-Scotland-Ridge (ISR) and from the Arctic through the Fram Strait (FRA) and out of the basin through the Denmark Strait (DEN) and through the passage between Svalbard and Norway onto the Barents Shelf (BAR). The heat transport is directed as the volume transport in case of ISR and BAR, whereas it has opposite sign for DEN and FRA. This is due to the fact that the water masses that enter the Nordic Seas through FRA and leave the basin through DEN have lower temperature than the chosen reference temperature so that the effective heat transport is negative in case of FRAM and positive in case of DEN.

In the Holocene and more enhanced in the Eemian simulation, the volume transports

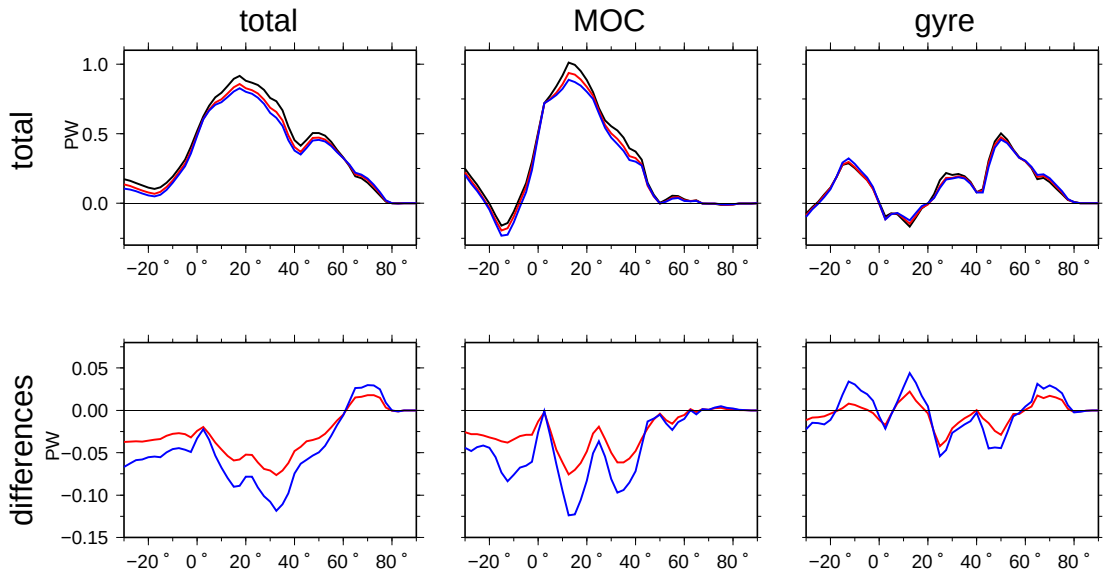

Figure 2.7: Upper row: heat transports in PW (10^{15} W) in the Atlantic basin in pre-industrial (black), Holocene (red), and Eemian (blue) simulations, total and contributions to heat transport from meridional overturning circulation and via gyre transport. Lower row: heat transport differences for Holocene - pre-industrial (red) and Eemian - pre-industrial (blue).

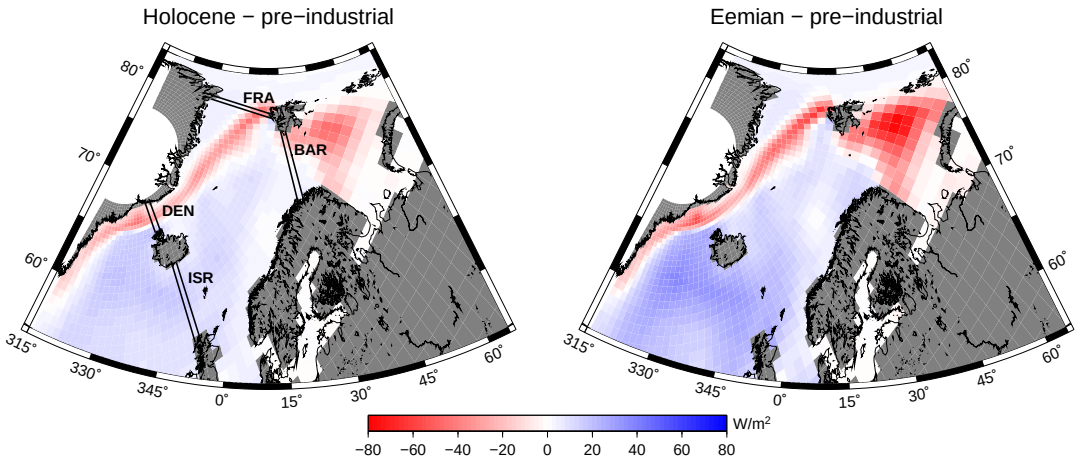

Figure 2.8: Ocean-atmosphere heat flux differences in W/m^2 over the Nordic Seas and Barents Shelf. Increases in heat flux from the ocean to the atmosphere (negative sign) occur mainly in regions where sea ice cover is decreased, over the Barents Shelf and on the east coast of Greenland. South of Iceland and in the eastern part of the Nordic Seas ocean-to-atmosphere heat flux is reduced. The black lines denote the passages used for the calculation of the heat transport in and out of the basin: ISR - Iceland-Scottland-Ridge, DEN - Denmark Strait, BAR - Barents Shelf, FRA - Fram Strait.

through all passages increase due to enhanced circulation. Nevertheless, this increase in volume transport is not sufficient to explain the changes in heat transport. In case of ISR and BAR, the increase in volume transport has the same sign as the increase in heat transport. In case of the BAR, the relative increase in heat transport is larger then the increase in volume transport. The heat transport increase is also due to an increase of 5% in heat content of the Nordic Seas basin for the Holocene and the Eemian simulation compared to the pre-industrial. This increase in heat content also contributes to the increase of effective heat transport to the Arctic through FRA due to the increased temperature difference between the two basins. The temperature difference between the Nordic Seas and the North Atlantic on the other hand decreases and so, despite the increase in volume transport, the effective heat transport into the Nordic Seas via DEN decreases.

The ocean-atmosphere heat flux over the Nordic Seas which is directed from the ocean to the atmosphere in the three simulations reduces only slightly from 178.9 TW ($67.5\,W/m^2$) in the pre-industrial to 176.5 TW ($66.6\,W/m^2$) in the Holocene and 171.5 ($64.7\,W/m^2$) in the Eemian simulation. Over the Barents Shelf, ocean-atmosphere heat flux increases significantly from 29.4 TW ($21.0\,W/m^2$) in the pre-industrial to 43.0 TW ($30.6\,W/m^2$) in the Holocene and 58.8 TW ($41.9\,W/m^2$) in the Eemian simulation. Over the Nordic Seas, the spatial distribution of ocean-atmosphere heat flux changes such

Table 2.1: Heat transports (in TW), volume transports (in Sv), and changes in volume transport with respect to the pre-industrial transports (in %) into (positive) and out of (negative) the Nordic Seas through the passages depicted in Fig. 2.8. Increasing negative values for BAR and FRA indicate increased heat transports into the Arctic.

Section	Transport	PRI	HOL	EEM
ISR	heat	183.8 TW	199.8 TW	213.9 TW
	volume	5.65 Sv	6.22 Sv (+10%)	6.88 Sv (+21%)
DEN	heat	55.3 TW	44.2 TW	38.9 TW
	volume	-6.11 Sv	-6.75 Sv (+10%)	-7.14 Sv (+16%)
BAR	heat	-11.0 TW	-19.1 TW	-27.0 TW
	volume	-2.25 Sv	-2.68 Sv (+19%)	-3.10 Sv (+38%)
FRA	heat	-47.8 TW	-53.0 TW	-61.2 TW
	volume	2.65 Sv	2.98 Sv (+12%)	3.30 Sv (+25%)

that it increases along the east coast of Greenland where the ice margin has shifted north and decreases over the rest of the basin especially east of Iceland (Fig. 2.8). In the northern part, where the sea ice along the coast of east Greenland has retracted there is an increase in ocean-atmosphere heat flux of up to $70\,\mathrm{W/m^2}$ (Fig. 2.8) accompanied by an increase in deep water formation north of 75°N (Fig. 2.6).

2.4 Discussion

Globally, we detect higher temperatures at high latitudes and lower temperatures in the tropics and northern sub-tropics in the Holocene and the Eemian simulation compared to temperatures in the pre-industrial simulation. This is in accordance with the changes in orbital forcing, i.e. the differences are directly related to differences in insolation. For the Holocene these results agree reasonably well with reconstructions obtained from marine alkenone proxies (Rimbu et al. 2003) as well as with results from the PMIP2 exercise (Braconnot et al. 2007a,b) and qualitatively with the results of Liu et al. (2003). Enlarged eccentricity and summer solstice being closer to perihelion in the Eemian simulation lead to more enhanced changes compared to the Holocene simulation. Besides these zonally averaged effects of the orbital forcing, feedback mechanisms between the ocean and the atmosphere manifest themselves in particularly enhanced temperature signals in the tropical African monsoon region and in the Nordic Seas.

The intensification of precipitation over the African monsoon region in the Holocene and the Eemian simulation is accompanied by a decrease in mean temperature over land leading to a decrease in land-sea-contrast. Increased precipitation in the northern subtropics, related to a northward shift of the intertropical convergence zone, ITCZ, also

leads to a northward expansion of the Sahel region at the expense of the desert. This increase in vegetation then again enhances the hydrological cycle through increased evaporation (Braconnot et al. 2008, 1999) thus creating a feedback loop. The effect is present in our paleo model simulations but might be underestimated since the dynamic vegetation module is not capable of changing the soil type. In the setup used in this study, the vegetation is shifting but the soil and its albedo is fixed to pre-industrial conditions. A thorough analysis of African and also Indian monsoon dynamics in the atmosphere-ocean GCMs used in PMIP2 has been performed by Zhao et al. (2005). They conclude that the intensification of the African monsoon is mainly due to advective moisture transport from the oceans, probably owing to the fact that the models investigated do not include dynamic vegetation.

In high northern latitudes, the increase in summer insolation influences the sea ice coverage in the Arctic. The sea-ice melt in the summer months due to the increased insolation is enhanced by the sea ice-albedo feedback (e.g., Harvey 1988) and cannot be counterbalanced by sea-ice built-up in winter. In the absence of sea ice over the Barents Shelf and along the east coast of Greenland, sea-ice cover cannot act as an insulator between the ocean and the atmosphere. The heat flux from the ocean to the atmosphere increases over the Barents Shelf and shifts further north over the Nordic Seas in the Holocene and the Eemian simulation. This enhances the overall warming signal in high northern latitudes, counterbalancing the decrease in winter insolation due to the prolonged winter season. The heat is transported by the relatively warm and saline waters coming from the North Atlantic over the Iceland-Scotland-Ridge into the Nordic Seas. The volume transport and thus the heat transport consists of vertical overturning circulation and horizontal gyre circulation contributions. The increase in heat transport to high northern latitudes is mainly due to a strengthened gyre circulation in the Nordic Seas that is caused baroclinically, by an increase in the density gradient and to some extent, by an increase in wind stress at the eastern margin of the basin along the Norwegian coast. The strengthening of the gyre is favored by increased convection at its center, which is visible in the local increase in meridional overturning circulation at 75°N in the Holocene and the Eemian simulation.

Bitz et al. (2006) investigate changes in the ocean in a coupled AOGCM (CCSM3) under increasing CO_2 forcing. They also find increased circulation and thus heat transport in the Arctic region comparable to the changes we find in our paleo-simulations. They attribute this increase to increased convection along the Siberian Shelf. Our findings concerning the enhanced temperature increase in the Barents Shelf region agree with paleo reconstructions of SST (e.g., Hald et al. 2007; Duplessy et al. 2001) for that area in the mid-Holocene, although temperature increase in Duplessy et al. (2001) is dated to around 8,000 - 7,000 yBP. Reconstructions of surface temperature in Europe (Cheddadi et al. 1996; Davis et al. 2003; Hald et al. 2007) reveal higher temperatures especially in northeastern Europe that could be explained by the heat release from the

Barents Sea, but a lower temperature increase in central and western Europe where the eastern Atlantic is not considerably warmer than for pre-industrial conditions. The model simulations however, do not show a significant decrease in precipitation especially over Scandinavia as suggested by several paleo studies (e.g., Cheddadi et al. 1996; Barnekow 2000; Antonsson et al. 2008). The coarse spatial resolution might not be able to resolve the heterogeneous pattern seen for example in Wanner et al. (2008).

The surface temperature for the Holocene obtained from multi-model ensemble means in PMIP2 (Braconnot et al. 2007a) does not show regional amplifications in the high northern latitude band (70°N to 90°N), but rather a homogeneous signal over the whole Arctic domain with regional differences below 0.5 K. For the Eemian, the temporal and spatial resolution of reconstructions of the Barents sea region is too coarse to compare them to our model results. Since the forcing is similar to the Holocene one, but more enhanced and the effects are also similar, but more enhanced, the proposed mechanism seems to apply too.

The increased winter storm tracks over the North Atlantic and into northern and central Europe and decreased winter storm tracks in the southern North Atlantic and the Mediterranean region in the Holocene and the Eemian simulation agree with results presented by Kaspar et al. (2007). Although changes in temperature for winter over North America in their simulations are lower than the ones found in our simulations.

In their study on Eemian European winter temperatures, Kaspar et al. (2005) show that reduced sea ice cover in winter over the Barents Sea in conjunction with lower average sea level pressure over the North Atlantic and a subsequent expansion of Icelandic low leads to stronger westerlies at 60°N and increased heat transport from the Atlantic into northern Europe. The results on westerlies and heat transport obtained from our experiments are similar, except for the expansion of the Icelandic low. A difference is the west-to-east temperature gradient over Europe that changes sign in their simulation, as opposed to our experiment where temperatures over western Europe do not experience strong changes in the Holocene and the Eemian simulations.

The global temperature, precipitation and albedo changes shown in transient experiments of the Eemian performed with an earlier generation of the model setup used in this study (Schurgers et al. 2007) are in good agreement with the results presented here. The changes in their study of the Eemian period from 127,000 yBP - 125,000 yBP are larger than in this study where we only consider a timeslice at 125,000 yBP conditions. This is because the initial conditions of their transient experiment that were obtained from a equilibrium experiment run under orbital forcing corresponding to the insolation maximum in the Eemian which was at 128,000 yBP and declined thereafter. They did not take into account the melting of continental ice sheets of the preceding glacial period.

The results obtained in this study using a general circulation Earth system model agree with climate data reconstructed from paleo proxies in the Nordic Seas (e.g.,

Rimbu et al. 2003). But they disagree with proxy data in the eastern North Atlantic that show lower temperatures on the western coast of Europe off Portugal and northern Africa off Morocco (Rimbu et al. 2004; Lorenz et al. 2006). This might be related to the model's representation of the North Atlantic current that is flowing in a east-west direction rather than a southwest to northeast direction thus transporting heat to the eastern North Atlantic.

For the Eemian simulation the comparison with proxy data is even more complicated, since the distribution of continental ice sheets in the Northern Hemisphere and their deglaciation is still under debate (e.g., Bauch and Erlenkeuser 2008). The subsequent freshwater inputs into the ocean which alter the ocean circulation and the climatic response are not considered in this study. The results presented here are rather an account of changes induced by orbital forcing only.

2.5 Conclusion

We have analyzed the influence of changing orbital parameters in time-slice simulations of the mid-Holocene and the Eemian with a fully coupled atmosphere-ocean general circulation model. The main results are:

- Changes in mean temperature induced by changed orbital parameters are regionally enhanced through feedback mechanisms in the climate system.
- In the Holocene and the Eemian simulations, the temperature in the Arctic is higher not only in summer but throughout the whole year. This is due to increased oceanic heat transport in the high northern latitudes and reduced sea-ice cover leading to enhanced heat release to the atmosphere over the Nordic Seas and the Barents Sea.
- The increase in temperature over Europe is more enhanced in the northeastern part of the continent than in the central and western part.
- Changes in atmospheric circulation in the Northern Hemisphere lead to a reduction of storm tracks over the Mediterranean region especially in the Eemian simulation and an increase of storm tracks over the northern North Atlantic over Iceland into northern and central Europe.
- Changes in mean climate, atmospheric, and oceanic circulation are qualitatively similar in the Holocene and Eemian simulations. We did not find a non-linear response of the climate system to changing orbital parameters for interglacial periods.

Chapter 3

Evolution and Variability of Ocean Circulation in a Transient Holocene Simulation

Applying orbital forcing to a coupled atmosphere-ocean general circulation model (AO-GCM) including a land surface model (ECHAM5/JSBACH/MPI-OM), we perform a transient simulation from the mid-Holocene to today and study changes in ocean circulation and its variability.

On top of a long-term increase in the Atlantic meridional overturning circulation (AMOC), the dominant temporal modes of variability in ocean circulation appear on interannual and multi-centennial time-scales.

The long-term AMOC increase results from water mass property changes in the deep water formation regions. In the Labrador Sea, a density increase of the convected deep water is due to increased salinity advection from the eastern North Atlantic. In the Nordic Seas, lower temperatures cause a substantial density increase and result in enhanced overflows.

The interannual AMOC variability is connected to atmospheric forcing dominated by the North Atlantic Oscillation (NAO). The multi-centennial variability results from salinity anomalies that accumulate in the sub-tropical gyre and, after reaching a threshold, penetrate into the convection regions in the North Atlantic, where they trigger the oscillation. The amplitude and period of the oscillations is dependent on the phasing of the effects altering salinity in the tropical Atlantic, the Southern Ocean and also on the conditions prevailing in the Arctic Ocean and the Nordic Seas.

In a first transient AO-GCM study of mid-Holocene, we are able to assess AMOC evolution and AMOC variability and identify the corresponding mechanisms. Our findings add to the understanding of ocean circulation obtained from simpler model set-ups and are supported by paleo-reconstructions of AMOC strength and variability.

3.1 Introduction

In the Atlantic, ocean circulation transports large amounts of heat from low- and mid latitudes to high latitudes and leads to comparably high temperatures in northern Europe (e.g., Jung 1952; Bryan 1962; Vonder Haar and Oort 1973; Keith 1995; Ganachaud and Wunsch 2000; Trenberth and Caron 2001). This heat transport is connected to the strength of the Atlantic meridional overturning circulation (AMOC), which brings warm and saline water from the tropical Atlantic to mid- and high latitudes. The main drivers of AMOC strength are believed to be buoyancy forcing in the tropical and northern Atlantic and wind forcing over the Southern Ocean (see review by Kuhlbrodt et al. 2007). In a transient simulation from the mid-Holocene to today, the last 6,000 years, with a coupled atmosphere-ocean general circulation model (AOGCM) we investigate how changes in insolation forcing affect the overall AMOC strength and on what time-scales and amplitudes ocean circulation variability occurs. Also, we study how changes in the mean state might alter this variability and what mechanisms are responsible for AMOC variability.

The main natural climate forcing in the last 6,000 years are changing orbital parameters (Wanner et al. 2008; Renssen et al. 2009) that alter the Earth's obliquity, its movement around the Sun, and thus the seasonal and meridional distribution of incoming solar short-wave radiation (Milankovic 1941; Berger 1978). In the mid-Holocene, obliquity was larger than today and perihelion was close to summer solstice, resulting in an enhanced seasonal insolation cycle in the Northern Hemisphere. Although annual changes in insolation are smaller than 4 W/m^2, seasonal effects are amplified or dampend by feedbacks between different components of the Earth system and cause responses in the climate system on time-scales longer than seasonal (e.g., Braconnot et al. 2007a,b; Otto et al. 2009). A review of climate evolution from the mid- to the late Holocene is given in Wanner et al. (2008).

The effects of Holocene orbital boundary conditions on the AMOC have so far only been studied in simulations with climate models of intermediate complexity (EMICs). In a transient simulation of Holocene climate starting 9,000 years before present, Renssen et al. (2005) found a Holocene increase in deep water formation in the Labrador Sea due to surface cooling. In the Nordic Seas, they found a decrease in deep water formation due to increased freshwater influx from the Arctic Ocean, in which larger sea-ice cover increased sea-ice export, which, in turn, increased freshwater export to the sinking region. Both effects, the increase in deep water formation in the Labrador Sea and the derease in the Nordic Seas, balanced each other, leaving the overall AMOC strength constant in their experiment. Centennial scale variability was found in a study with the same model setup and additional decadal-to-centennial scale total solar irradiance forcing (Renssen et al. 2006).

Variability of the AMOC has been the subject of many previous studies using AO-

GCMs (e.g., Delworth et al. 1993; Latif et al. 2004). On interannual time-scales, it has been attributed mainly to atmospheric processes, in particular to the North Atlantic Oscillation (NAO), the dominant atmospheric mode in the North Atlantic region (Hurrell 1995). In an NAO-positive phase, enhanced surface westerlies over the North Atlantic strengthen the North Atlantic Current and zonally displace the position of the sub-polar front - the border between the sub-tropical and the sub-polar gyre (Marshall et al. 2001). Additionally, ocean heat loss to the atmosphere is enhanced over the Labrador Sea, favoring deep convective events. In the Nordic Seas, on the other hand, temperatures and freshwater influx are increased (Furevik and Nilsen 2005) and deep water formation is reduced (Dickson et al. 1996). Although the atmospheric forcing varies on very short time-scales, influencing surface temperatures and wind-driven currents within days, basin-scale ocean circulation takes up to a decade to adjust to changed atmospheric conditions (e.g., Eden and Willebrand 2001).

Pronounced multi-centennial variability with a period of 320 years has been found in an ocean-only general circulation model driven by spatially correlated white-noise freshwater fluxes superimposed on climatological fluxes (Mikolajewicz and Maier-Reimer 1990). The centers of action of the oscillation were the Southern and the Atlantic Ocean connected by the thermohaline circulation. A similar so called "loop" oscillation was found by Winton and Sarachik (1993). In more recent studies, Vellinga and Wu (2004) and Park and Latif (2008) found centennial-scale variability in coupled AOGCM simulations applying equilibrium or idealized insolation forcing. The responsible mechanisms the authors proposed involved advection of salinity anomalies to the convection regions from the tropical Atlantic (Vellinga and Wu 2004) and the Southern Ocean (Park and Latif 2008).

The investigation of the evolution of ocean circulation and its variability in a transient simulation of the mid to late Holocene offers several advantages: First, the more realistic setting gives the opportunity to compare the model results to reconstructions obtained from paleo-proxies. Second, the evolution of well studied patterns of climate variability under slowly evolving boundary conditions can be assessed. Third, the length of the simulation allows us to expand the range of time-scales over which we can investigate climate variability to the multi-centennial band.

The chapter is organized as follows. We introduce the model and experimental setup in section 3.2, and present the results on the evolution and the variability of AMOC and the evolution and variability of the NAO and its influence on European climate in section 3.3. The discussion of the results in relation to existing literature in section 3.4 is followed by the conclusions in the final section 3.5.

3.2 Model and Experimental Setup

The transient Holocene simulation is performed using the Max-Planck-Institute for Meteorology's coupled climate model. The model consists of the spectral atmosphere model ECHAM5 (Roeckner et al. 2003) run at truncation T31, corresponding to a horizontal resolution of a $3.75° \times 3.75°$ longitude-latitude grid, with 19 vertical hybrid sigma pressure levels and the highest level at 10 hPa. Integrated in the atmosphere model is the land surface model JSBACH (Raddatz et al. 2007) with a dynamic vegetation module (Brovkin et al. 2009). ECHAM5 is coupled to the ocean general circulation model MPI-OM (Marsland et al. 2003) run in resolution GR30 with 40 vertical levels (30 levels are within the top 2000 meters). It includes a zero-layer dynamic-thermodynamic sea-ice model with viscous-plastic rheology (Semtner 1976; Hibler 1979).

The ocean model uses a bipolar orthogonal spherical coordinate system on an Arakawa C-grid with the North Pole shifted over Greenland and the South Pole located at the center of Antarctica. This avoids numerical singularities and yields the advantage of relatively high resolution in the deep water formation regions around Greenland and Antarctica. The horizontal grid spacing varies between 30 km around Greenland to 368 km in the tropical Pacific.

The coupling between the atmosphere and the ocean model is performed by the OASIS coupler (Valcke et al. 2003). Fluxes of momentum, heat, and freshwater from the atmosphere to the ocean are transferred and interpolated onto the ocean grid. From the ocean to the atmosphere sea surface temperature, sea ice thickness and fraction, snow cover on sea ice, and surface velocities are transmitted.
The model includes a river run-off scheme (Hagemann and Dumenil 1998; Hagemann and Gates 2003) where river run-off is transferred to the ocean together with the difference in precipitation and evaporation. Mass balance for glaciers and ice-sheets is not accounted for, since snow falling on Antarctica and Greenland is transferred to the nearest ocean grid cell instantaneously.
The coupled model (Jungclaus et al. 2006) represents oceanic heat transports realistically and therefore runs without flux adjustment. The time-step is 20 minutes for the atmosphere and 2.4 hours for the ocean model. The coupling time-step between the atmosphere and ocean model is 24 hours.

We initialize the transient experiment from the 3,500-year-long mid-Holocene (6,000 years before present) time-slice simulation with orbital forcing presented in chapter 2. The orbital forcing is applied on a yearly basis following VSOP87 (Bretagnon and Francou 1988). No further external forcing such as solar, volcanic, or greenhouse gases is applied and greenhouse gases are set to pre-industrial values (CO_2 to 280 ppm, CH_4 to 700 ppb, N_2O to 265 ppb). No acceleration technique is applied.

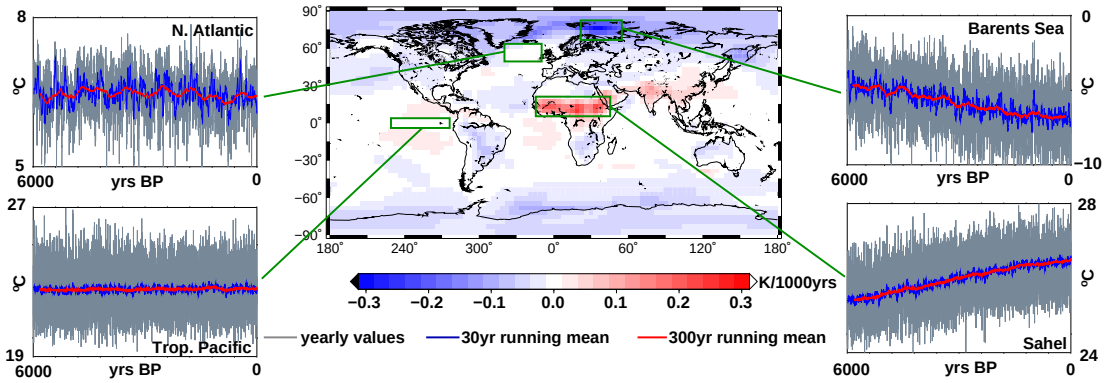

Figure 3.1: Linear trend in annual mean surface temperature over the simulation period in K/ka - Kelvin per 1,000 years, with time-series of surface temperature for the North Atlantic, the Barents Shelf, the Sahel region, and the tropical Pacific.

3.3 Results

The results section is structured as follows. In subsection 3.3.1, we very briefly describe the changes in mean climate in the transient Holocene simulation, followed by a detailed analysis of long-term changes in the Atlantic meridional overturning circulation in subsection 3.3.2. In subsection 3.3.3 we discuss variability in overturning circulation on interannual time-scales. Subsection 3.3.4 deals with the evolution and variability of the NAO and its influence on climate in Europe. In subsection 3.3.5 we investigate variability in overturning circulation on multi-centennial time-scales.

3.3.1 Mean Climate Changes in the Transient Holocene Simulation

Orbitally induced changes in the meridional and temporal distribution of incoming solar radiation are mostly visible on the seasonal time-scale, whereas changes in the annual mean do not exceed $4\,\mathrm{W/m^2}$. The changes in seasonal surface temperature do not always reflect the insolation changes directly, but correspond to changes induced by processes that act on longer time-scales as we discuss in chapter 4. The long-term changes in surface temperature and precipitation in the course of the transient experiment are similar to the differences between the mid-Holocene and pre-industrial climate we have described in chapter 2 in section 2.3.1. There is a significant change in the annual mean surface temperature (Fig. 3.1) with increasing temperatures at low latitudes and decreasing temperatures at high latitudes.

Over northern Africa, in the Sahel region, there is a pronounced warming signal due to a reduction in cloud-cover and precipitation (Fig. 3.2), enhanced by an increase in desert area. The surface temperatures over the North Atlantic and the Barents Shelf

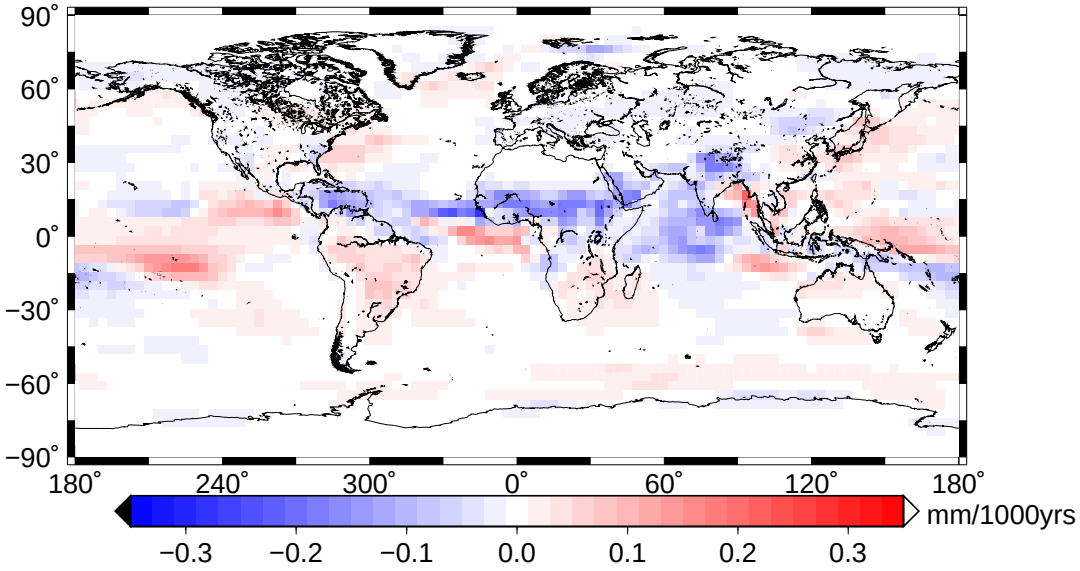

Figure 3.2: Linear trend in annual mean precipitation over the simulation period in mm per 1,000 years

show long-term variability likely influenced by variability in ocean circulation. The temperature over the tropical Pacific does not show a trend or any long-term variability. The increase in temperature over the Sahel region is stronger in the beginning of the simulation than towards the end indicating that it is related to the changes in low latitude winter insolation that shows a stronger gradient in the beginning than in the end of the Holocene. The regional surface climate variables (e.g., temperature, precipitation, albedo) in the end of the transient Holocene simulation match those from the time-slice simulation under pre-industrial orbital boundary conditions.

3.3.2 Long-Term Evolution of Atlantic Meridional Overturning Circulation

We infer the long-term evolution of the ocean circulation from linear trends and differences in the mean state of the climate system in the beginning and the end of the experiment. Time-series of some quantities are introduced in the current section already to show their connection to ocean circulation and to substantiate the arguments we put forward. A more detailed discussion of the time-series will follow in sections 3.3.3 and 3.3.5 that deal with ocean circulation variability.

We define the Atlantic meridional overturning circulation (AMOC) as the zonally integrated stream function over the Atlantic Ocean basin (Fig. 3.3 a). At the start of the experiment under mid-Holocene orbital boundary conditions, the AMOC has a maximum of 15 Sv ($1\,\mathrm{Sv} = 10^6 \mathrm{m}^3/\mathrm{s}$) at around 30°N at 1,000 m depth. The Antarctic

bottom water cell has a maximum of about 3 Sv and reaches as far north as 40°N at 3,500 m depth. In the Nordic Seas, the AMOC has a strength of 2 Sv at latitudes up to 75°N. The linear trend over the simulation period (Fig. 3.3 b) shows an overall increase of the AMOC up to 65° with the largest increase of 0.3 Sv per 1,000 years just north of the maximum. In the Nordic Seas, the stream function has a negative trend over the simulation period and decreases by 0.05 Sv per 1,000 years. Similar to the surface climate variables, the AMOC values at the end of the transient experiment are also similar to those obtained from the pre-industrial time-slice simulation.

A possible explanation for the AMOC increase could be increased formation of North Atlantic Deep Water (NADW) via deep convection in the North Atlantic and the Nordic Seas. The mixed layer depth in March, defined as the depth above which the water masses are well mixed, is a measure of where deep convection occurs in the model and indicates that NADW is formed in the Nordic Seas and in a region at the mouth of the Labrador Sea south of Greenland which we will refer to as Labrador Sea in the following (Fig. 3.4 a). The linear trend in the March mixed layer depth (Fig. 3.4 b) indicates a northward shift and an expansion of the convection region in the eastern Nordic Seas and decreases along the sea-ice margins east of Greenland. The expansion of the convection region, however, does not directly lead to increased overturning in the Nordic Seas - on the contrary, there is a decrease in AMOC (Fig. 3.3 b). The positive trend in AMOC at latitudes of the Greenland-Scotland-Ridge indicates that the overflows, and therefore the Nordic Seas contribution to the lower branch of the AMOC, are increasing thorughout the simulation period. In the second region where deep convection occurs, the Labrador Sea, the mixed layer depth exhibits a negative trend over the simulation period. Thus, the evolution of the March mixed layer depth alone does not answer the question why the AMOC increases.

For this reason, we investigate the water mass properties of three basins in the NADW formation regions - the Nordic Seas, the Labrador Sea, and the North Atlantic.

The Nordic Seas

A measure for the amount of deep water formed in the Nordic Seas contributing to NADW is the overflow from the Nordic Seas to the North Atlantic over the shallow sills of the Denmark Strait (DEN), between Greenland and Iceland, and the Iceland Scotland Ridge (ISR) (see Fig. 2.8 for a map). In case of the latter, the overflows pass the sill mainly through the Faroer-Bank-Channel that is represented in the model's orography. To discriminate these overflow waters from southward flowing surface waters that constitute the East Greenland Current in DEN, we introduce a lower density boundary of 1027.8 kg/m^3. The water flux from the Nordic Seas into the North Atlantic fulfilling the density criterion increases by 1 Sv for ISR and by 2 Sv for DEN (Fig. 3.5), increasing the total overflow from 3 to 5.5 Sv. If the overflow strength would directly

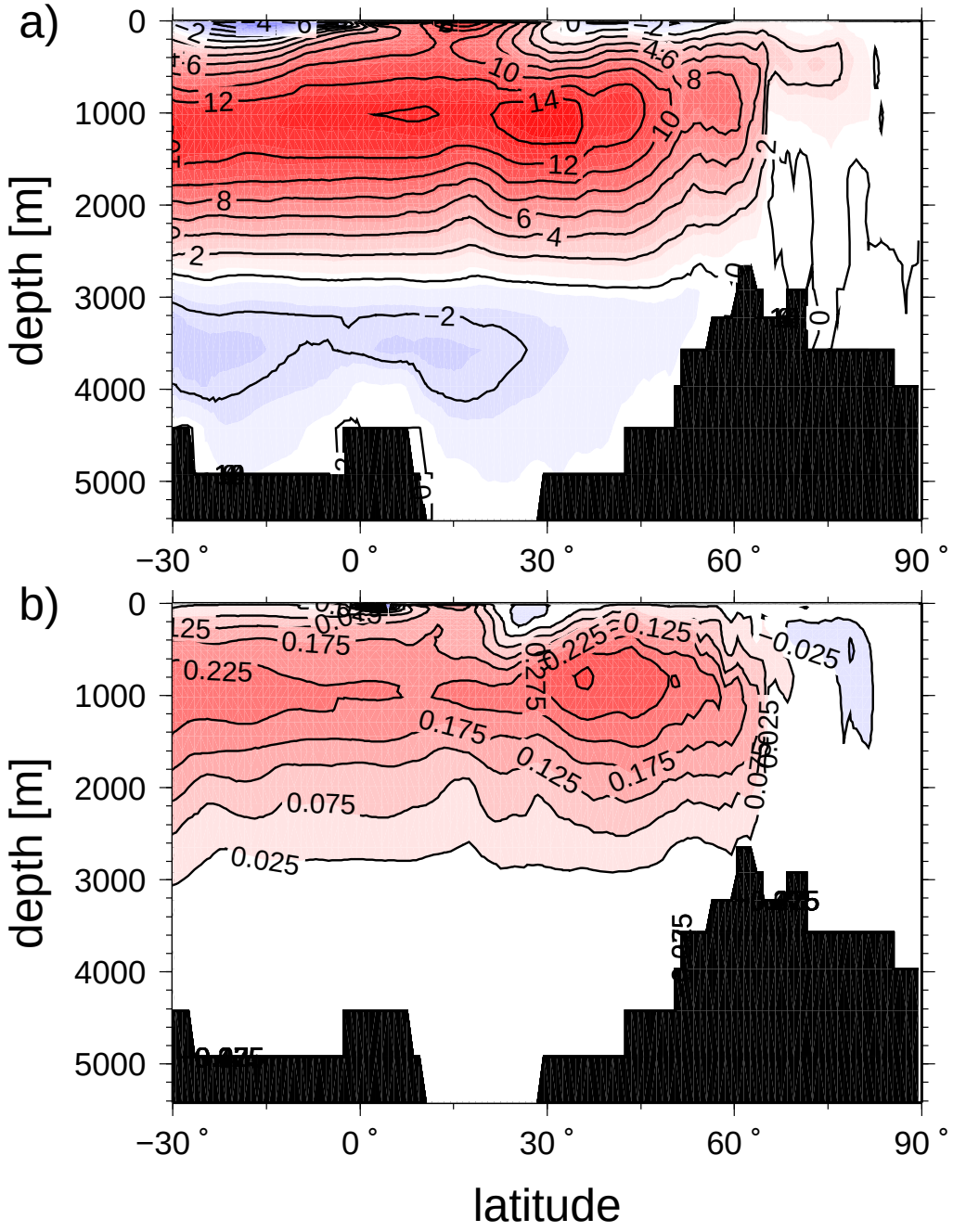

Figure 3.3: **a)** Zonally integrated stream function over the Atlantic basin representing Atlantic meridional overturning circulation (AMOC), time-mean of the first 1,000 years of the simulation (in Sv = $10^6 m^3/s$). **b)** Linear trend in AMOC over the simulation period (in Sv/ka = $10^6 m^3/s$ per 1000 years). The black surface represents zonal minimum topography.

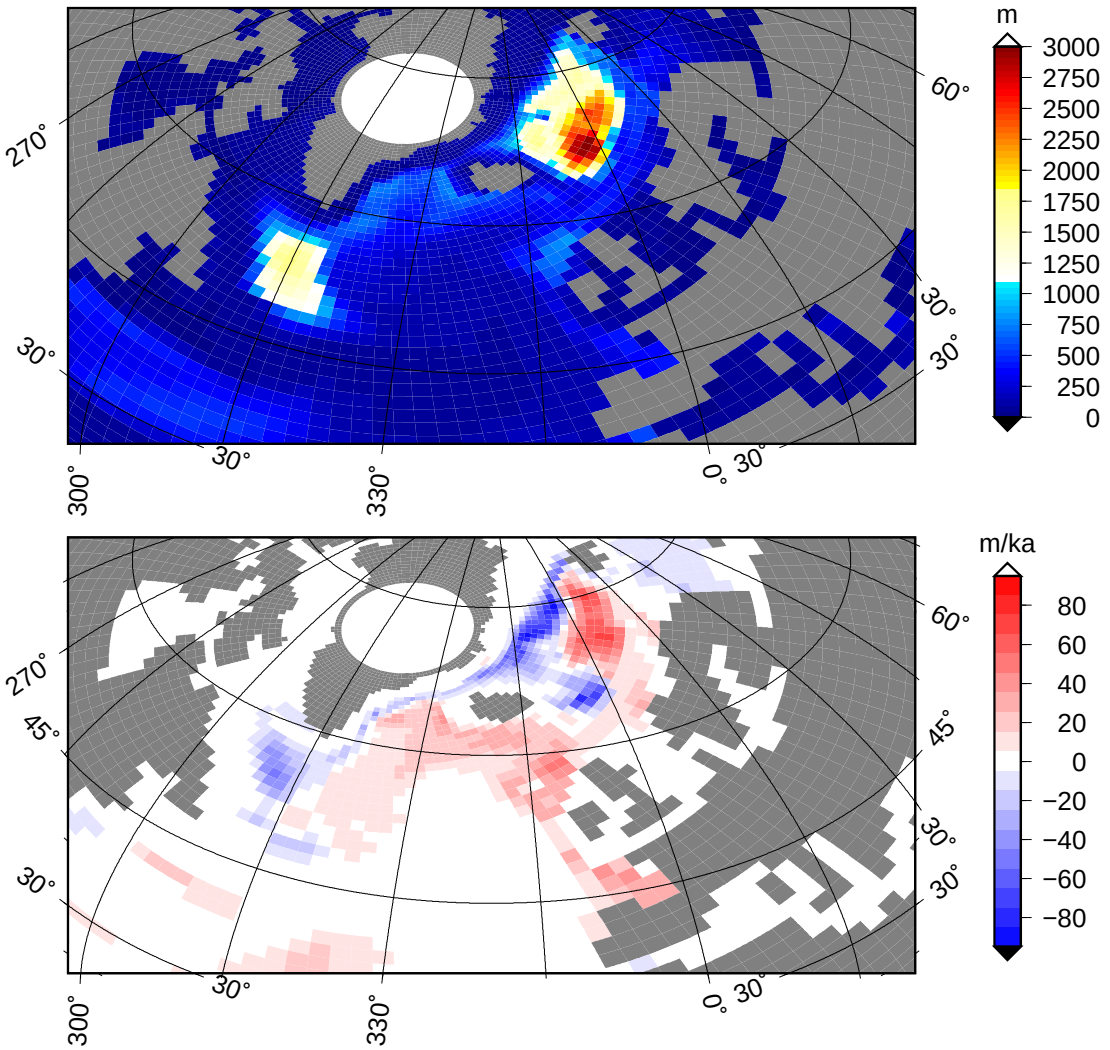

Figure 3.4: **a)** Mixed layer depth in the North Atlantic, time-mean over the first 1,000 years of the simulation (in m). **b)** Linear trend in mixed layer depth (in m/ka = m per 1000 years).

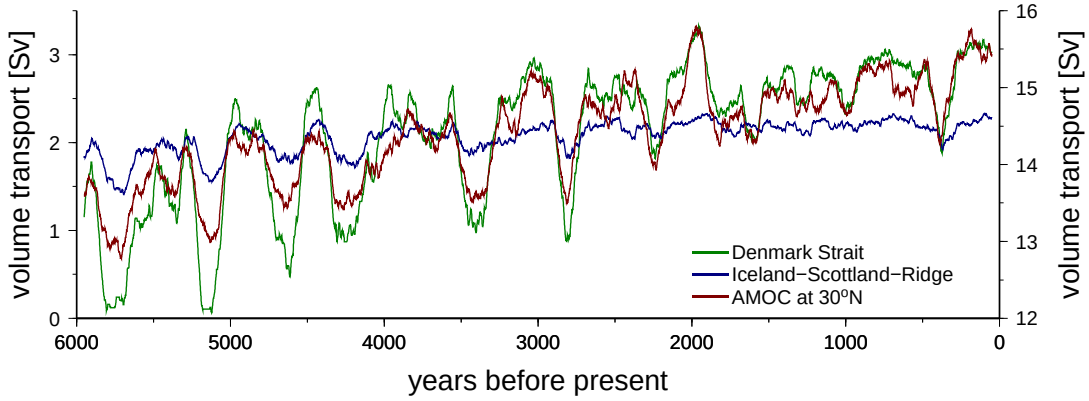

Figure 3.5: Time-series of overflow water entering the North Atlantic from the Nordic Seas via Denmark Strait (green) and the Iceland-Scotland-Ridge (blue) and the AMOC at 30°N (red, right y-axis) - in Sv = $10^6 m^3/s$.

depend on the convection in the Nordic Seas, this would result in an increase of the zonally integrated stream function north of the ISR (Fig. 3.3 b). North of the ISR however, the trend in AMOC is negative, hence the overflow formation cannot only be conducted during the transformation of surface water to deep water during local deep convection events.

Alternatively, we propose that the overall increase in density by 0.1 kg/m^3 of the water masses in the Nordic Seas, which is about four times the increase in density in the North Atlantic (Fig. 3.6 a and c), causes an increase in the hydraulic pressure between the Nordic Seas and the North Atlantic and leads to an increase in overflows.

In addition to this main effect, the horizontal cyclonic circulation persisting in the Nordic Seas contributes to the increased formation of overflows as follows: In the course of the simulation, water entering the Nordic Seas through ISR is getting more saline, since freshwater influx over the North Atlantic decreases (Fig. 3.13 b). As a result, water mass density in the upper ocean increases on the eastern side of the Nordic Seas basin (Fig. 3.7). Increased sea-ice cover in the Arctic Ocean leads to enhanced sea-ice export via Fram Strait. Sea ice melting along the western side of the Nordic Seas basin decreases the near surface salinity, and the water masses following the cyclonic circulation in the Nordic Seas are subducted below the fresh surface waters. This explains the horizontal density gradient in the Nordic Seas (Fig. 3.7), with relatively high density in the center and lower density at the basin margins that forms a "doming" structure. The increase in water mass density at the basin's margins results in a decrease of the horizontal density gradient. The subsequent reduction in baroclinicity weakens the cyclonic circulation at the margins of the Nordic Seas and at the southern gateways to the North Atlantic (Fig. 3.8). Also, the stratification of the water column

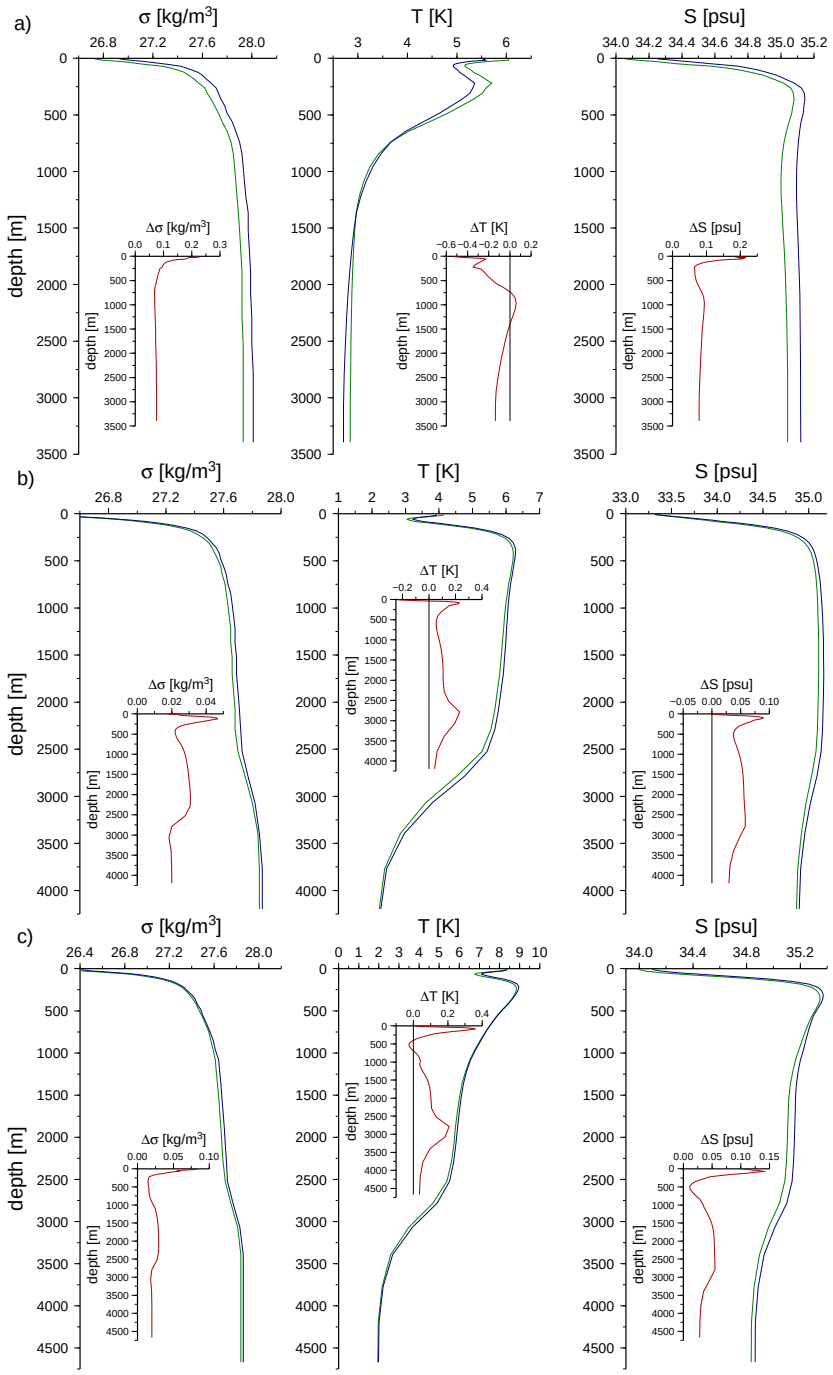

Figure 3.6: Vertical profiles of density (in kg-1000/m^3 - left), temperature (in K - middle), and salinity (in psu - right) in the first 1,000 years of the experiment (green) and the last 1,000 years (blue). The insets show the difference between the two time-periods (red). **a)** Nordic Seas, **b)** Labrador Sea, and **c)** the North Atlantic.

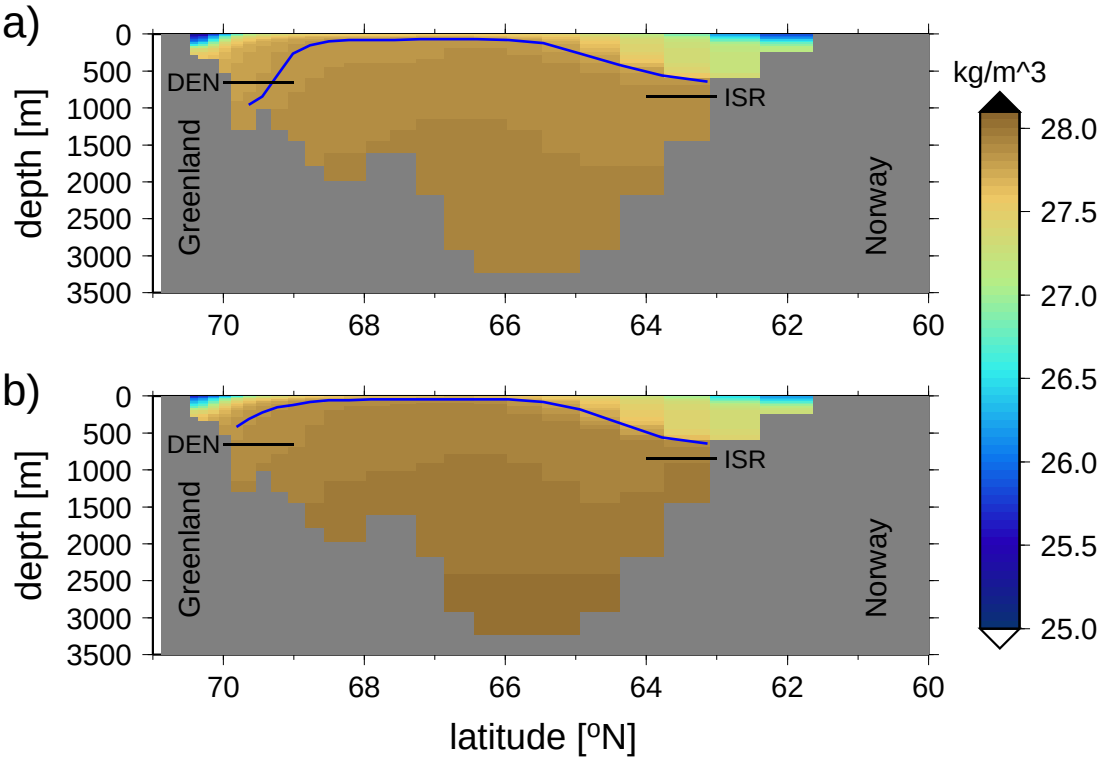

Figure 3.7: Density profile at a cross-section of the Nordic Seas: a) time-mean of the first 1,000 years the of the transient simulation and b) of the last 1,000 years. The blue line depicts the depth of the lightest overflow water (ρ_c=27.8) the vertical black lines the sill depths of the Denmark Strait (DEN) and the Iceland-Scotland-Ridge (ISR). For convenience, 1000 kg are subtracted from the density value.

in the western Nordic Seas increases and explains the decrease in mixed layer depth (Fig. 3.4 b). The increase in overall density in the Nordic Seas basin and the enhanced lifting of the pycnoclines at the margins, outweigh the decrease in cyclonic circulation at the southern boundary and result in increasing overflows over both sills, the ISR and DEN, in the course of the experiment.

A prominent feature in Fig. 3.8 is an increase in cyclonic circulation in the northeastern Nordic Seas. Here, the increase in water mass density and the subsequent lift of the pycnoclines decreases the stratification of the watercolumn, by displacing the less dense surface water masses. This local increase in the "doming" structure results in enhanced baroclinicity and strengthens cyclonic circulation and also favors deep convection as can be inferred from the increase in mixed layer depth in that region (Fig. 3.4 b).

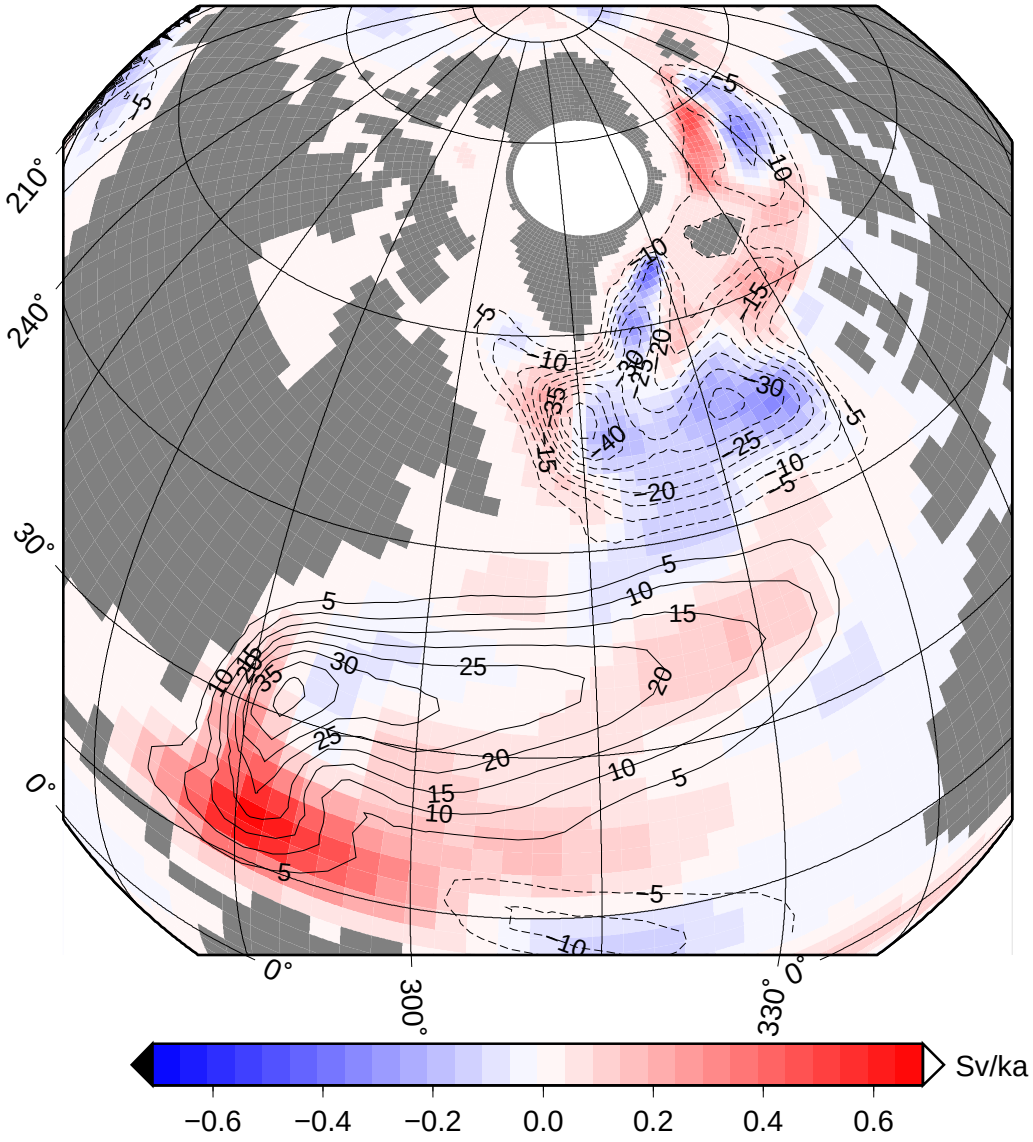

Figure 3.8: Long-term evolution of the gyre circulation, represented by the barotropic stream function, in the North Atlantic Ocean. Contour lines denote the mean state at mid-Holocene conditions (in Sv = $10^6 m^3/s$) and color tiles the linear trend (in Sv/ka - $10^6 m^3/s$ per 1,000 years). Note that for positive values of the mean state (continuous contour lines - anti-cyclonic circulation) of the stream function, a positive trend means an increase and a negative trend a decrease, and vice versa for negative values of the mean state (dashed contour lines - cyclonic circulation).

The Labrador Sea

The second main contribution to NADW is formed in the Labrador Sea. Since there are no orographic constraints that allow us to calculate a volume transport as in the case of the overflows from the Nordic Seas, we introduce a different measure: We define the Labrador Sea sinking region as the ocean model gridboxes in the area south of Greenland where the mixed layer depth has exceeded 800 m at least once during the simulation. As a measure for NADW formation in the Labrador Sea we introduce Labrador Sea water (LSW) thickness as the mean vertical distance between two density boundaries over the individual water columns. The upper density boundary is the density below the mean near-surface temperature maximum in the Labrador Sea and deeper density boundary at the thermocline (Fig. 3.6 b). The upper boundary is chosen to exclude the low salinity surface waters advected from the boundary currents (Labrador and East Greenland Current). These dominate the density stratification of the upper water column throughout the year, except in winter, when increased heat loss weakens the stratification and enables deep convection events. The qualitative results on the evolution of the LSW thickness are robust against different choices of the upper density boundary.

There is a close correspondence to the time-series of the AMOC maximum at 30°N (Fig.3.10). Under the assumption that deep water formation in the Labrador Sea contributes to the AMOC strength, the definition of the LSW thickness is a reasonable measure for the relative amount of that contribution. The LSW thickness increases from 1250 m to 1400 m throughout the experiment. Additionally, the LSW is getting denser as can be seen in the relatively strong density increase in the Labrador Sea between 600 and 2750 m depth (Fig. 3.6 b). This also projects onto the density profile of the whole North Atlantic basin (Fig. 3.6 c). As a result, although convection in the Labrador Sea is not getting deeper throughout the simulation (Fig. 3.4 b), the AMOC gets stronger because the density of the convected deep water increases.

Figure 3.9 shows 100-year low pass filtered time-series of the LSW thickness, sea surface temperature (SST), sea surface salinity (SSS), and heat and freshwater flux between the atmosphere and the ocean. All quantities are correlated to the LSW thickness. A vigorous AMOC leads to enhanced meridional heat transport and eventually to higher SST in the Labrador Sea and an increased heat flux from the ocean to the atmosphere. Enhanced SSS is also contributing to enhanced convection which, in turn, enhances the AMOC.

To identify a cause and effect relationship, we calculate at which lag the maximum correlation occurs between LSW thickness and the different surface properties. For this we use the linearly detrended unfiltered time-series to avoid the introduction of artificial averaging effects. For the SSS the maximal correlation coefficient appears at lag zero. The LSW thickness leads the SST (maximal correlation at lag 7 years) and

therefore also the ocean-atmosphere heat flux and, because of enhanced evaporation above warm surface waters, also the freshwater flux. Furthermore, the surface quantities are correlated to the LWS thickness, but do not show a trend in the simulation period. This suggests that in the long-term the properties of the sub-surface water masses advected to the Labrador Sea are more decisive than the atmospheric conditions above the region. Subsequently, an explanation for the long-term positive trend in the LSW thickness is likely to be found below the surface.

As can be seen in the mean vertical profile of properties of the water column in the Labrador Sea, the density increase is stronger in the near-surface layers than directly at the surface, with the maximum increase being at 110 m (Fig. 3.6 b). This decreases the stratification of the water column, leading to stronger convection events triggered by surface water conditions. The increase in salinity and also in temperature of the sub-surface layers suggests that the corresponding water masses are advected from the eastern side of the North Atlantic via the sub-polar gyre (Fig. 3.11). Similarly to what happens in the Nordic Seas, these advected water masses are subducted below the relatively fresh surface waters from the East Greenland Current.

A second mechanism with a possible impact on the decrease in water stratification, and hence, increase in LSW, is less ocean heat uptake from the atmosphere over the Labrador Sea in the summer months. In the winter season, when convection usually occurs, SST, SSS, and ocean-atmosphere heat flux stay constant over the whole experiment and correspond closely to AMOC variations on shorter time-scales as explained above. In summer, ocean-atmosphere heat flux shows a decreasing trend, along with decreasing SST. This could possibly lead to a pre-conditioning of the water masses in summer that favors convection in the winter time.

The North Atlantic

Changes in water mass properties in the Labrador Sea and the Nordic Seas are induced by advection of warmer and more saline water from the eastern North Atlantic (Fig. 3.12). Near surface salinity in the eastern North Atlantic increases as well as temperature. The increase in upper ocean temperature is visible all along the Gulf Stream and the North Atlantic Current whereas upper ocean salinity stays constant in the Gulf Stream region off the east coast of North America. The differences in the ocean-atmosphere heat and freshwater fluxes (Fig. 3.13) correspond to changes in temperature and salinity qualitatively. The difference between the two is, however, that changes in upper ocean temperature influence ocean-atmosphere heat flux, whereas salinity does only react to changes in surface freshwater fluxes. To a certain degree warmer upper ocean waters enhance evaporation, and hence, the freshwater flux.

The strong temperature and salinity signals along the latitude band between 40 and 50°N are due to a shift in the position of the boundary between the sub-polar

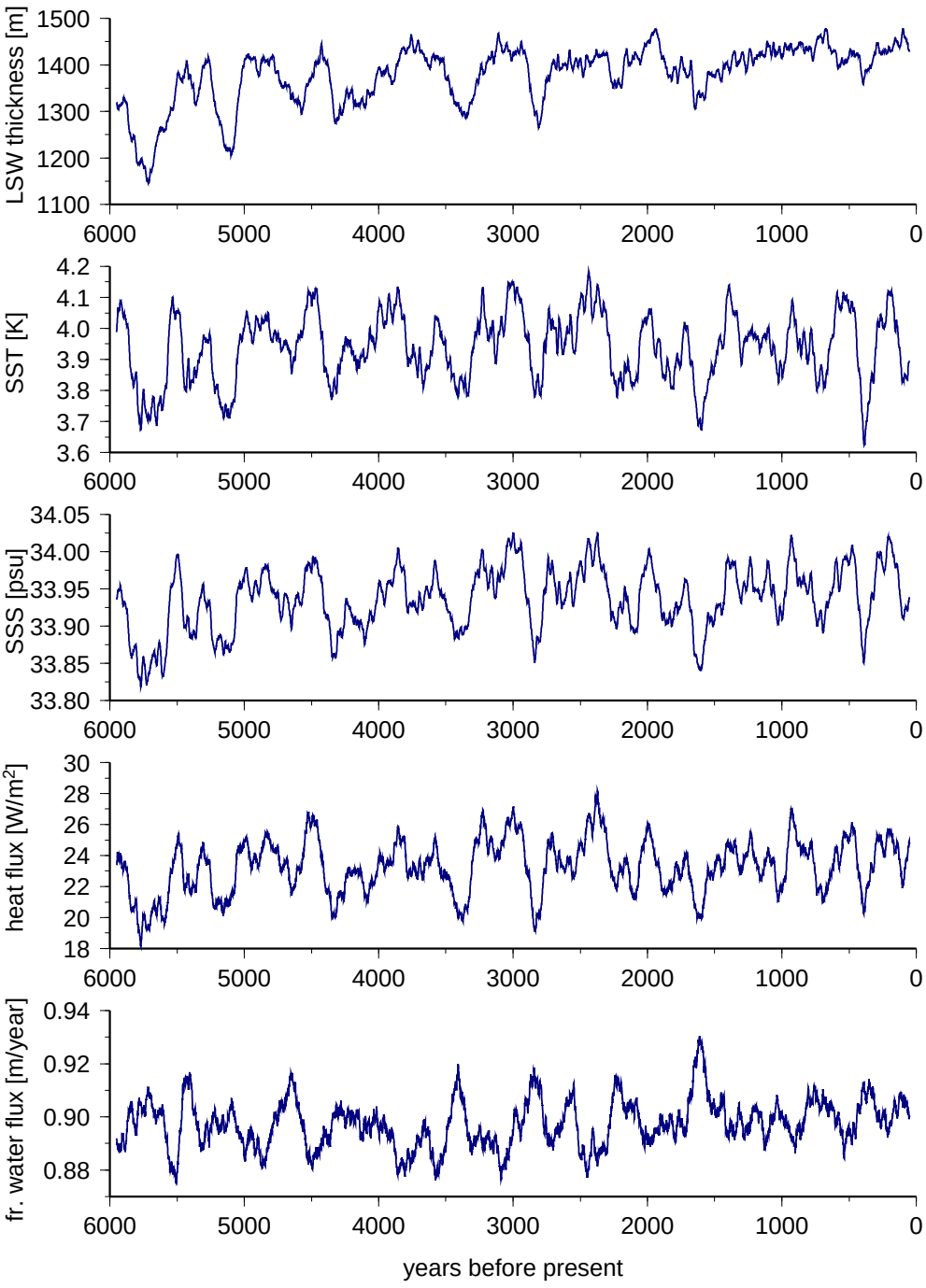

Figure 3.9: Time-series of (from top to bottom) LSW thickness (in m), Labrador Sea near surface (upper 200 m) temperature (in K) and salinity (in psu), atmosphere-ocean heat flux (in W/m^2), and atmosphere-ocean freshwater flux (in m/year) - for both fluxes positive sign means flux from the the atmosphere to the ocean. All time-series are filtered with a 100-year running mean.

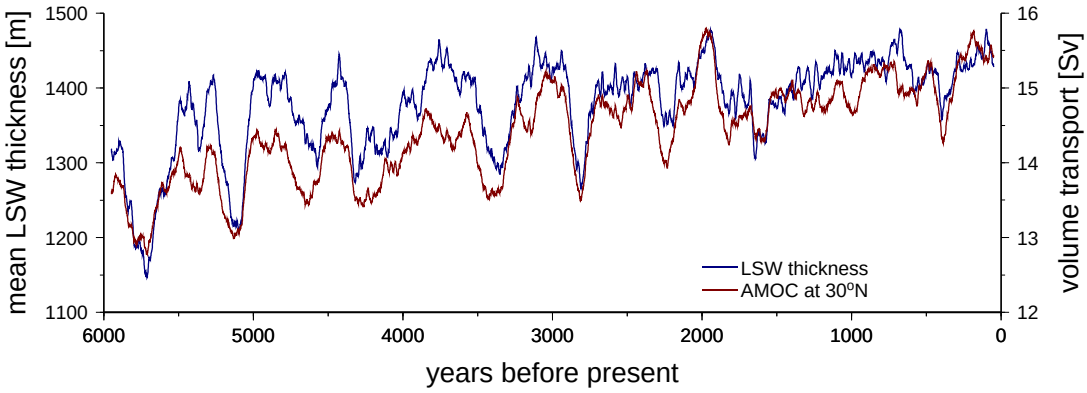

Figure 3.10: Time-series of mean Labrador Sea water (LSW) thickness (blue, in m) and Atlantic meridional overturning circulation at 30°N (red, in Sv = $10^6 m^3/s$). Both time-series are filtered with a 100-year running mean.

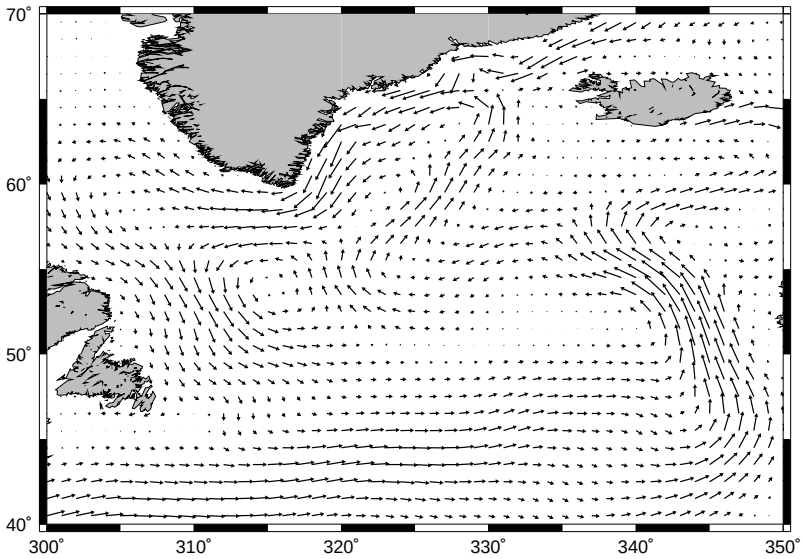

Figure 3.11: Horizontal velocities for the sub-polar gyre region at 110 m depth (time-mean of the first 1,000 years, MPI-OM grid interpolated on a regular 360x180 grid).

gyre (SPG) and the sub-tropical gyre (STG) (Fig. 3.8). The strength of the western SPG decreases, which results in less transport of relatively cold and fresh water to the area east of New Foundland. Thus, in this region, the inflow of the warm and saline water masses from the western STG increases. The North Atlantic Current then transports warmer and more saline water by the strengthend southwestern SPG to the northeastern Atlantic. Here, the effect is amplified by decreased freshwater influx from the atmosphere.

A strong decrease in freshwater influx is also visible in the Northern Hemisphere's tropical Atlantic. An increase in air pressure over the sub-tropical and northern tropical Atlantic leads to an increase in easterly winds over the northern tropical Atlantic. This hinders the development of convective precipitation, because the specific humidity in the atmospheric layers where convective precipitation develops decreases substantially by approximately 10% (Fig. 3.14). Since, on the other hand, evaporation over the northern tropical Atlantic stays constant, the moisture is most likely transported to the tropical Pacific, where air pressure decreases and convective precipitation increases. An influence of these changes in ocean-atmosphere interaction on the ocean state at higher latitudes via advection of water of increasing salinity is nevertheless unlikely as the northward salinity transport along a transect across the Atlantic Ocean from Cape Hatteras to Iberian Peninsula does not exhibit a trend throughout the simulation.

3.3.3 Interannual Variability of Atlantic Meridional Overturning Circulation

The long-term trend in the AMOC is superposed by variability on various time-scales (Fig. 3.15). A variance spectrum and a wavelet analysis (Torrence and Compo 1998) of the time-series of the maximum AMOC at 30°N show significant variability on interannual time-scales and also reveal nearly continuous significant variability on multicentennial time-scales. The amplitude of variability on both time-scales is of the same order of magnitude as the linear increase over the simulation period. We will investigate how these different AMOC variabilities interact with other climate quantities in the ocean and the atmosphere and find out what mechanisms may account for them.

A correlation map of the unfiltered and detrended AMOC time-series with surface temperature reveals negative correlation in the Labrador Sea and North Africa and positive correlation in the eastern Atlantic, the Nordic Seas, and western North America (Fig. 3.16). This is very similar to the surface temperature response to the North Atlantic Oscillation (NAO). The correlation map of AMOC at 30°N with sea level pressure (SLP) is also in agreement with the first EOF of winter SLP anomalies (see also section 3.3.4 below), or leading mode of variability in SLP, generally attributed to the NAO (Fig. 3.16). The similarity between the AMOC- and the NAO correlation to surface temperature and SLP indicates that on annual to interannual time-scales

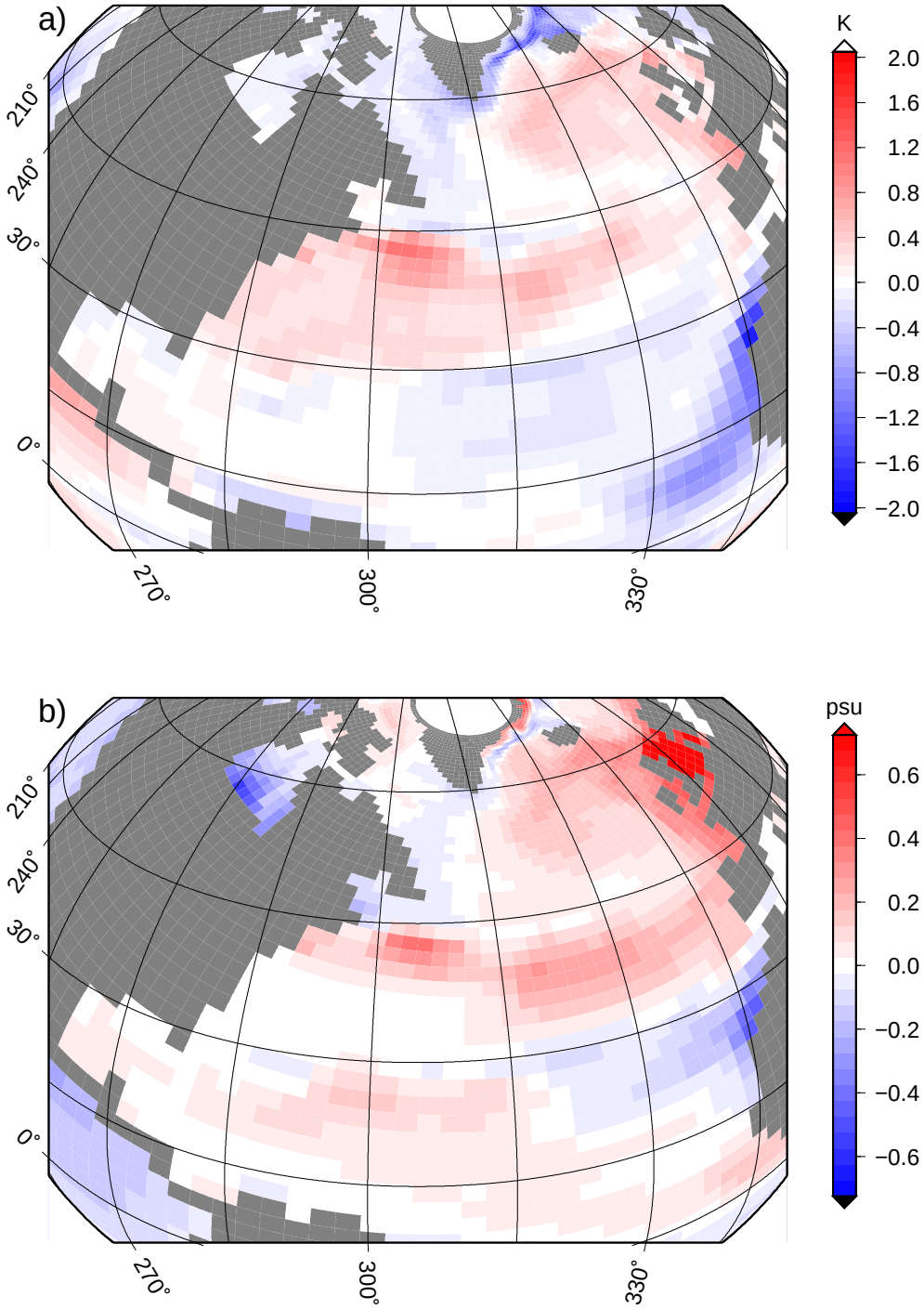

Figure 3.12: Differences between the last 1,000 and the first 1,000 years of the experiment in the upper ocean (upper 60m) **a)** temperature (in K) and **b)** salinity (in psu) in the tropical and northern Atlantic ocean.

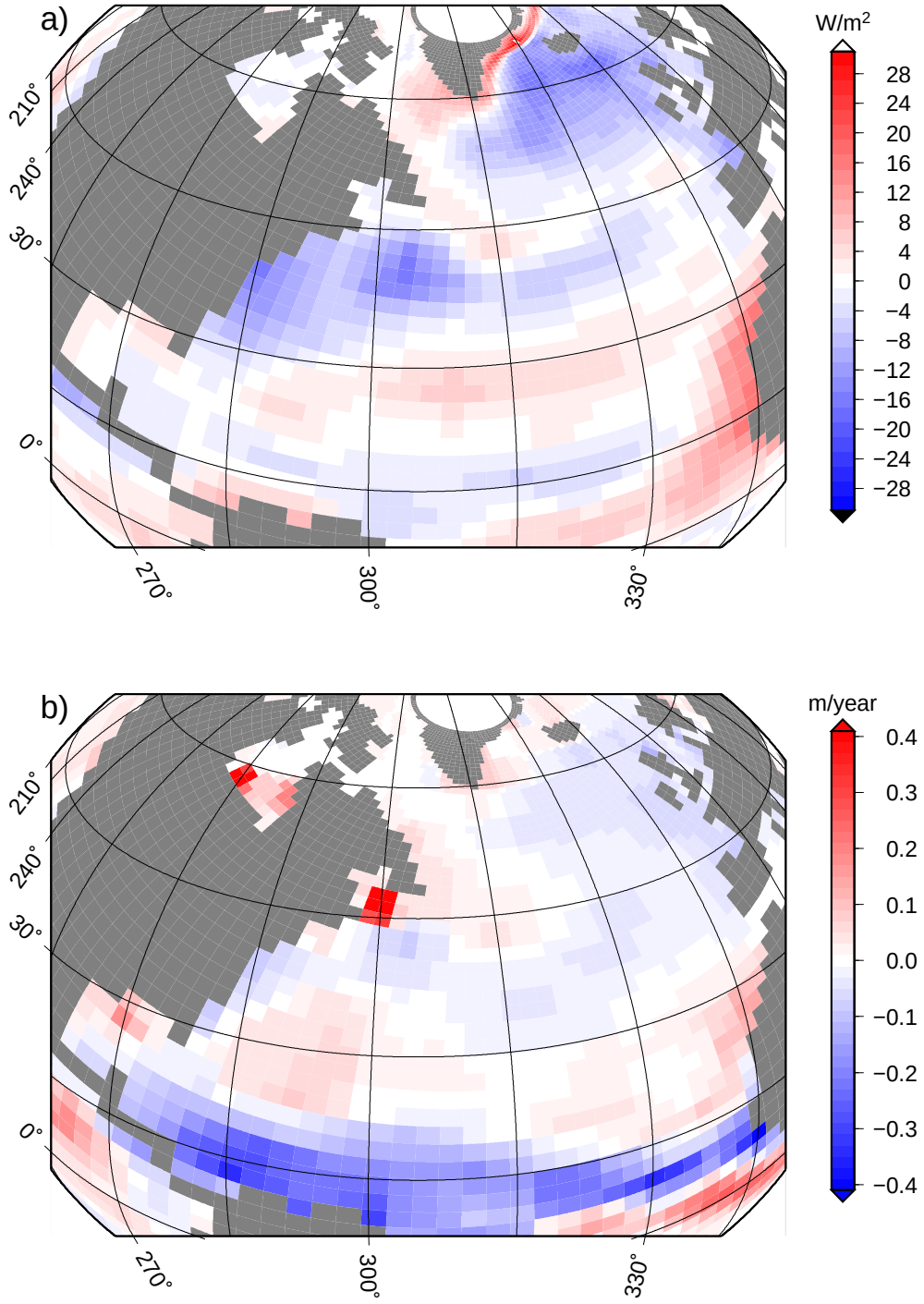

Figure 3.13: Differences between the last 1,000 and the first 1,000 years of the experiment in **a)** atmosphere-ocean heat flux (in W/m^2) and **b)** atmosphere-ocean freshwater flux (in m/year) in the tropical and northern Atlantic ocean. Positive values represent fluxes from the atmosphere into the ocean.

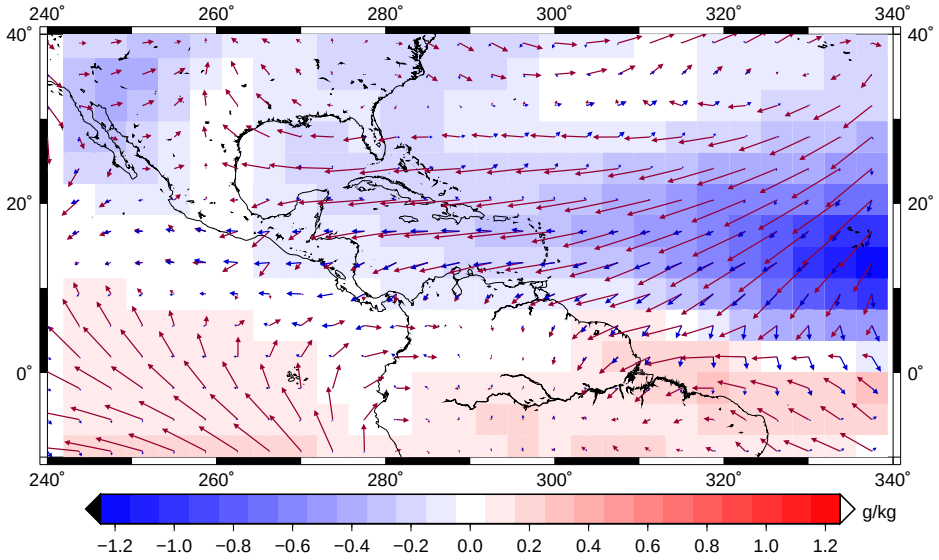

Figure 3.14: Mean wind in the first 1,000 years of the simulation (red arrows) and change in wind direction and speed (blue arrows, difference between first and last 1,000 years, scaled-up by factor 4). Tiles represent change in specific humidity from the first 1,000 years of the experiment compared to the last 1,000 years (in g/kg).

ocean circulation responds to the atmospheric state. During an NAO positive state the wind stress is enhanced over the North Atlantic leading to enhanced wind driven circulation in the upper branch of the AMOC. At the same time, enhanced low pressure over Greenland leads to the advection of cold air from the Arctic to the Labrador Sea, where relatively low temperatures enhance convection and the formation of Labrador Sea water, strengthening the lower AMOC branch. The wind effect is visible in the response of the barotropic stream function on NAO (Fig. 3.17). The increase in wind stress over the North Atlantic leads to the generation of a gyre anomaly, the "intergyre" (Marshall et al. 2001), which strengthens the STG and weakens the southeastern part of the SPG and strengthens its northwestern part.

To test if the NAO influences the AMOC in the whole Atlantic basin, or if the influence is confined locally, we perform a correlation analysis between the NAO-index and the two-dimensional zonally integrated streamfunction. The correlation map shows a positive correlation along the latitude band between 25 and 45°N and a negative correlation from 50 to 65°N (Fig. 3.18 a). At the surface, the correlation pattern can be attributed to NAO-related changes in wind stress that enhances along the North Atlantic Current (25 and 45°N) and the northern part of the SPG (50 to 65°N - note that the mean AMOC is negative, i.e., directed southward, at the surface at these latitudes (Fig. 3.3 a)). In the deeper ocean, the correlation pattern can be attributed

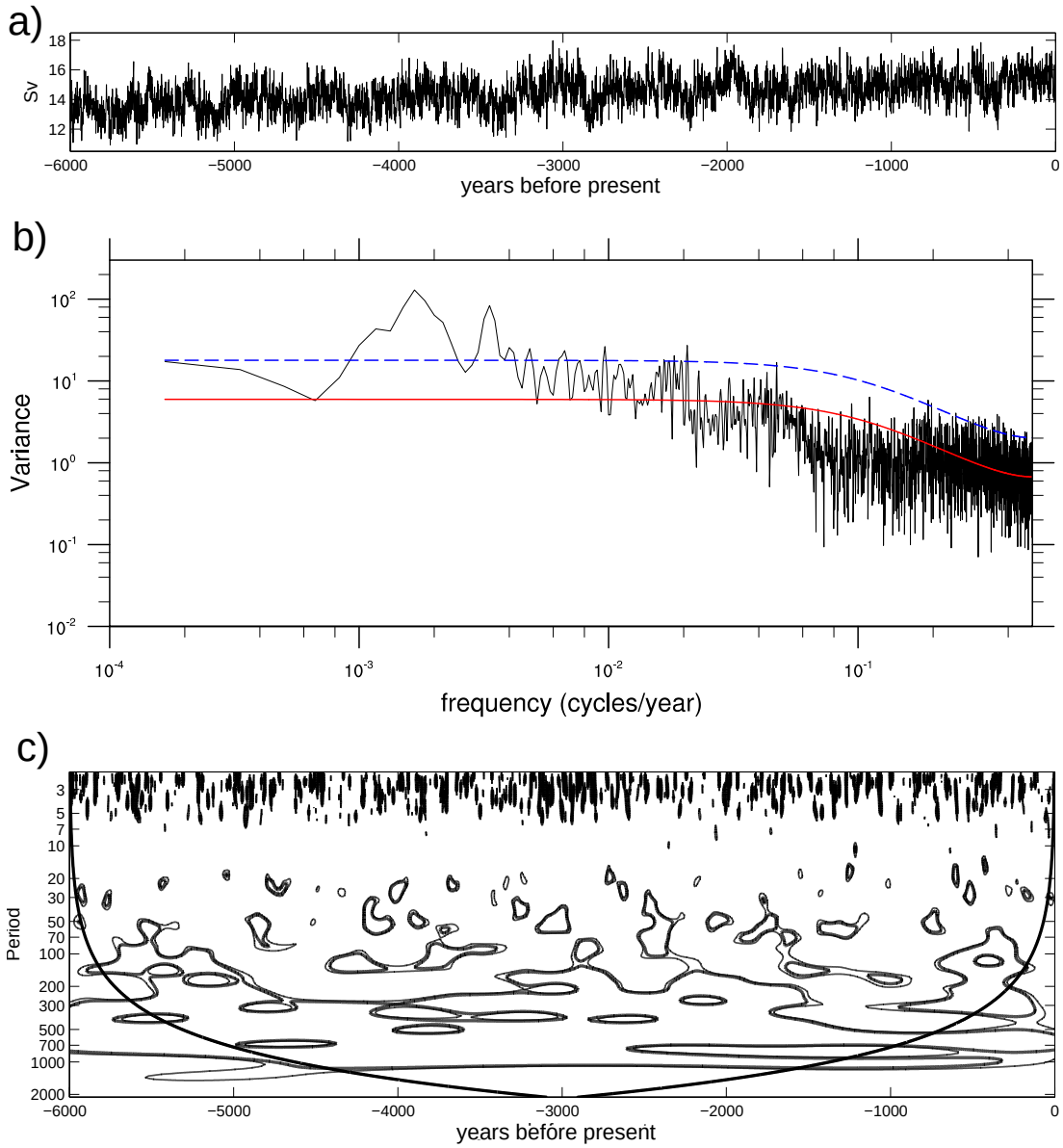

Figure 3.15: **a)** Time-series of the AMOC at 30°N at 1000 m depth. **b)** Variance spectrum of the detrended and normalized AMOC time-series. The red line denotes the spectrum of a fitted "red-noise"-process. Values above the blue line are significant on the 95% confidence level. **c)** Wavelet spectrum of the detrended and normalized AMOC time-series. The thick (thin) contour lines show variability at the 95% (90%) significance level. The bowl shaped line denotes the cone of influence below which the wavelet analysis is not valid.

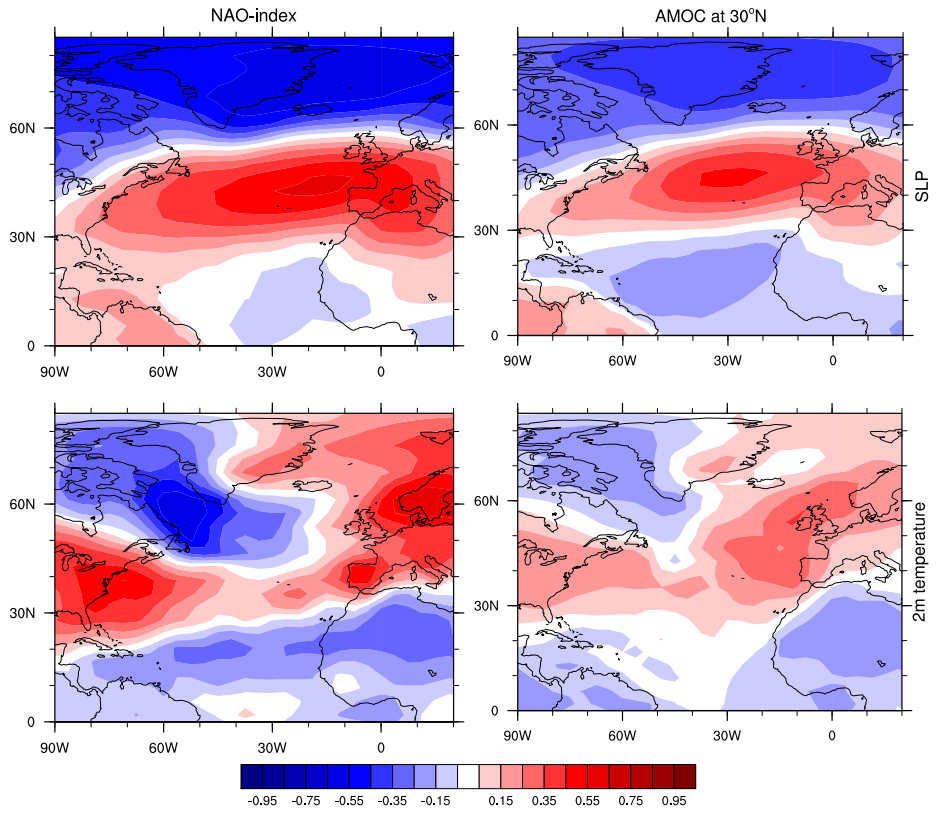

Figure 3.16: Two-dimensional correlation maps of the NAO-index time-series (left column) and of the AMOC at 30°N (right column) with sea level pressure (SLP, upper row) and 2m temperature (lower row) over the North Atlantic.

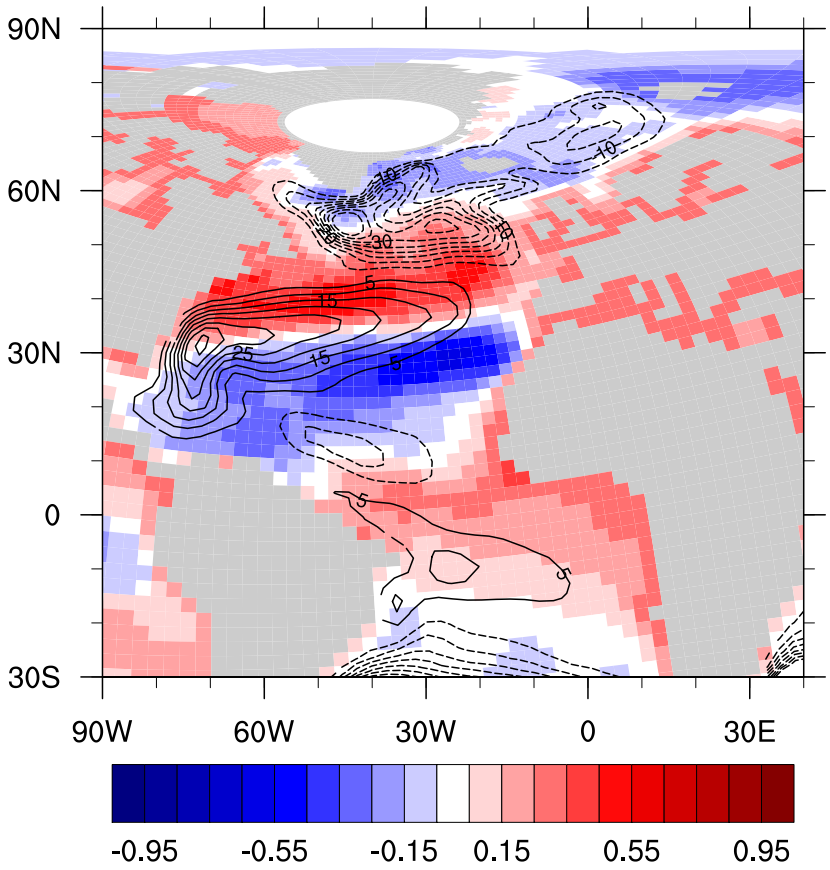

Figure 3.17: Correlation map of the NAO-index with the barotropic stream function in the North Atlantic. Contour lines denote the mean values of the barotropic stream function over the whole transient simulation (in Sv = $10^6 m^3/s$). For anti-cyclonic gyres positive correlations mean an increase with positive NAO and negative correlations a decrease with positive NAO, and vice versa for cyclonic gyres.

to the influence of the NAO on the formation of NADW in the Labrador Sea and the Nordic Seas. The correlation between the AMOC and the LSW thickness is most pronounced at 40 to 50°N (Fig. 3.18 b) and the correlation between the AMOC and overflows at 60 to 70°N (Fig. 3.18 c). This indicates that changes in LSW thickness and overflow strength will most likely influence the AMOC at these latitudes. Taking into account atmosphere-ocean freshwater and heat fluxes, this suggests that during an NAO positive phase NADW formation in the Labrador Sea, coincident with the western SPG, is strengthend because of enhanced heat loss and decreased freshwater influx. In the Nordic Seas, the opposite, decreased heat loss and enhanced freshwater influx, leads to a reduction in NADW formation.

Because of the ocean's inertia, the responses at greater depth are not at their maximum amplitude instantly. Diffusion and advection of the surface induced signals lead to delayed responses. Lagged correlation maps (Fig. 3.19) reveal that the heat loss effect over the Labrador Sea has maximal amplitude after two years, the freshwater anomaly in the Nordic Seas takes seven years until it has maximal impact on the overflow strength and another five until it leads to a maximal reduction in the AMOC at 30°N. The freshwater anomaly in the Nordic Seas is also partly advected to the Labrador Sea by the East Greenland Current and results in a basin wide negative correlation between the NAO and the AMOC after twelve years.

3.3.4 Evolution and Variability of the North Atlantic Oscillation and its Impact on European Temperatures

Since the NAO is the dominant mode of climate variability in the North Atlantic region and has a major influence on the AMOC on interannual time-scales, we take a closer look at the representation of the NAO in the current model setup and its evolution in the Holocene simulation.

We compute the NAO-index from the first empirical orthogonal function (EOF) of winter SLP anomalies (November to February) over the North Atlantic region (Hurrell 1995). Over the simulation period, the first EOF pattern exhibits the typical dipole pattern, with poles over Greenland and west of the Bay of Biscay and it explains 54% of the variability in winter SLP (Fig. 3.16). The first EOF pattern is temporarily stable as we also infer from calculations of winter SLP anomaly sub-sets of the simulation that show some variability in position of the dipole, but no clear trend. A time-series of the NAO-index, however, shows a trend: from prevailing positive values at the beginning of the experiment to prevailing negative values towards the end. The variance spectrum of the NAO-index is white and shows significant variability only up to interannual time-scales. The implications of the long-term change in NAO variability on Atlantic Ocean circulation are resulting from the accumulation of the short-term influence discussed above. During more NAO negative phases, the northwestern part of the SPG weakens

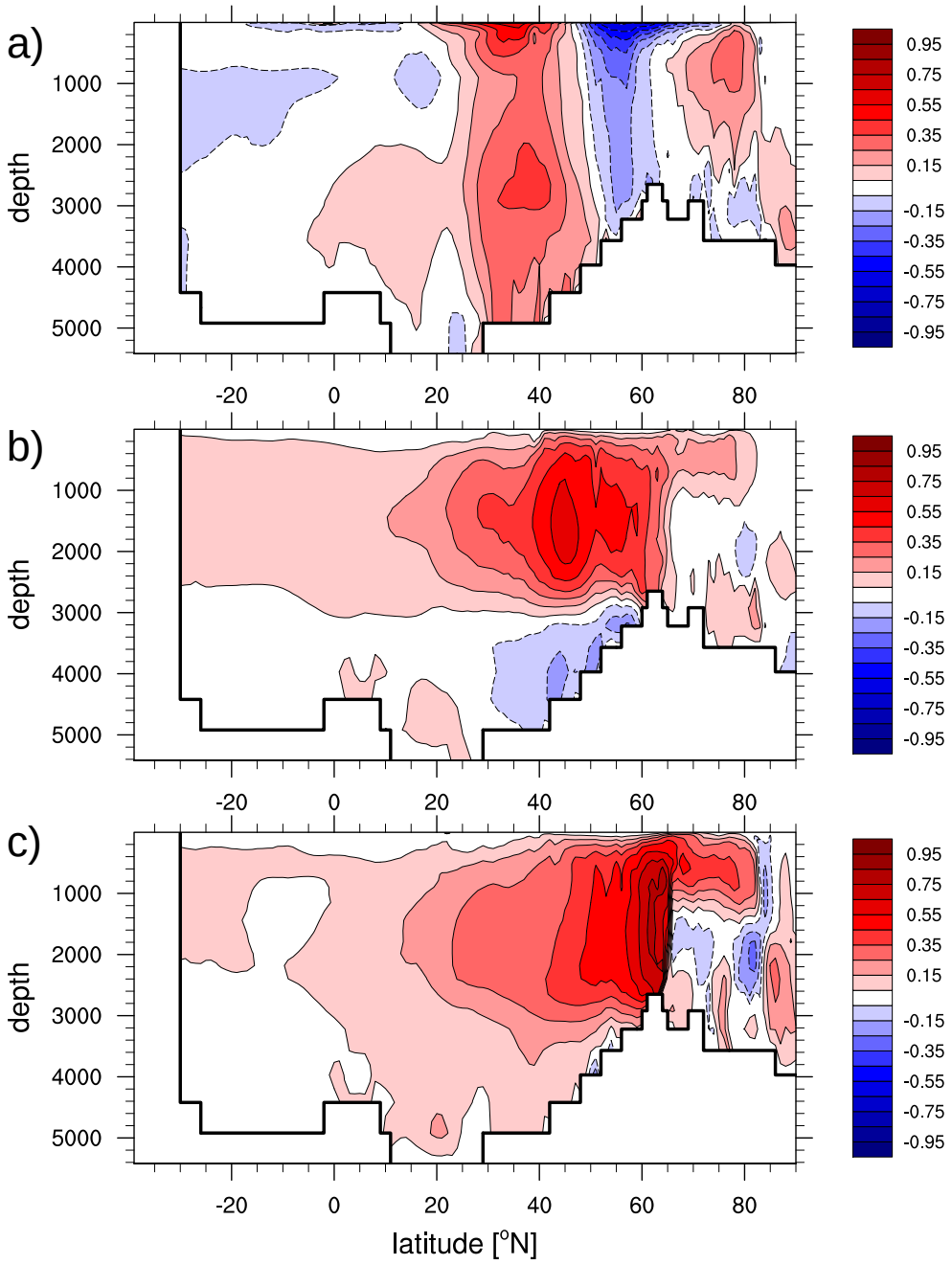

Figure 3.18: Correlation maps of the two-dimensional AMOC and **a)** the NAO-index, **b)** the LSW thickness, and **c)** the overflow strength.

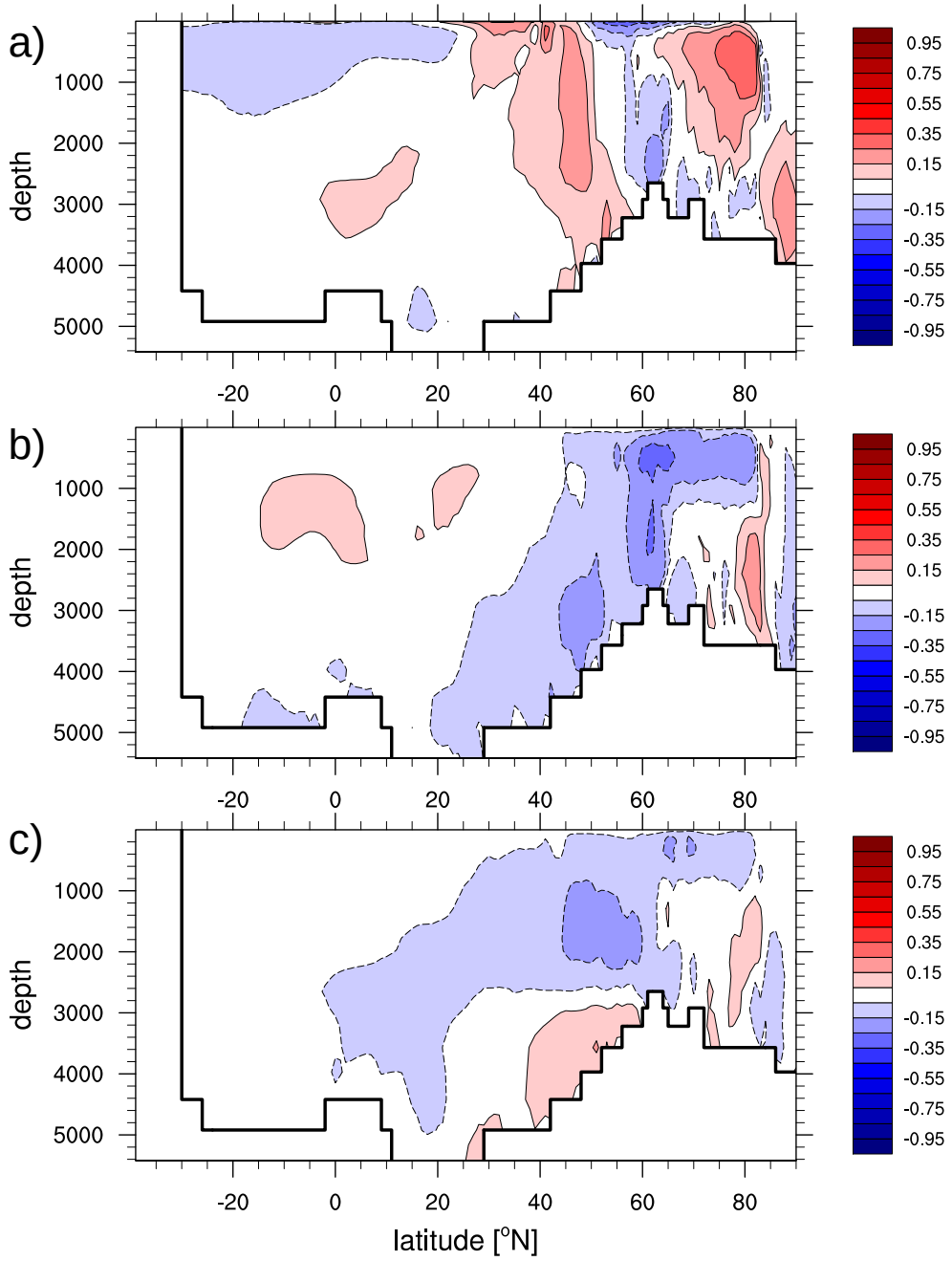

Figure 3.19: Correlation maps of the two-dimensional AMOC and the NAO-index at **a)** lag 2 years, **b)** lag 7 years, and **c)** lag 12 years. The NAO-time-series and the AMOC-field are smoothed with a 5-year running mean.

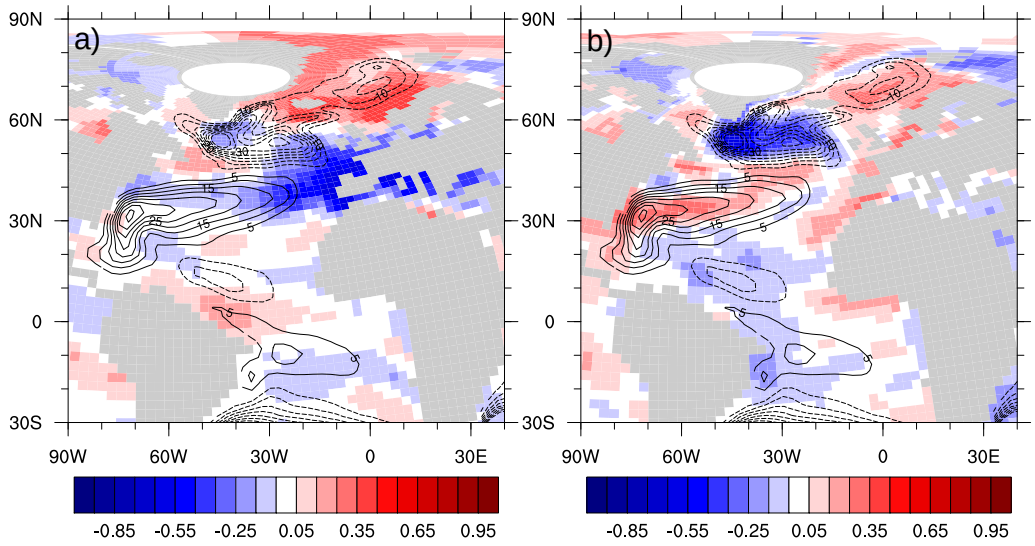

Figure 3.20: Correlation maps of the NAO-index with **a)** atmosphere-ocean freshwater flux and **b)** atmosphere-ocean heat flux. Both fluxes are defined positive from the atmosphere to the ocean.

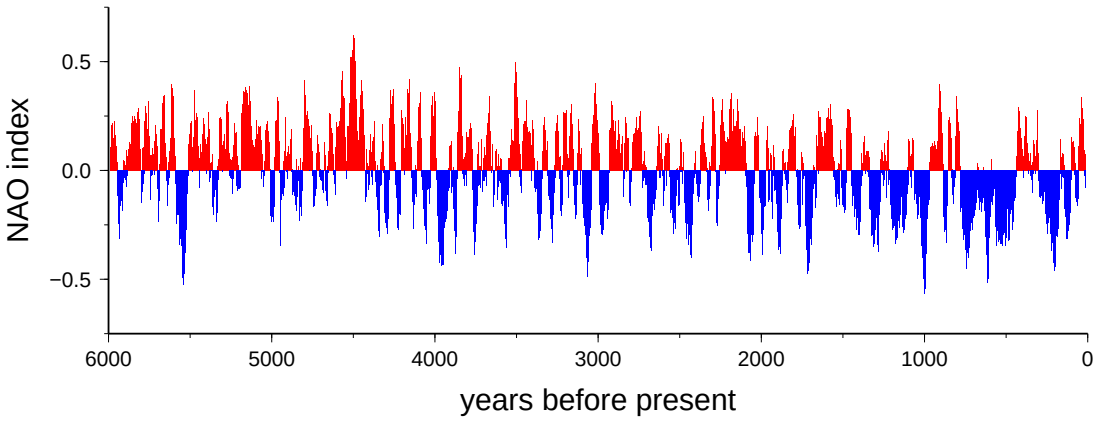

Figure 3.21: Time-series of North Atlantic Oscillation index calculated from the first EOF of winter mean sea level pressure over the North Atlantic region (30-year running mean).

as well as the "intergyre" anomaly. The latter leads to a stronger southeastern SPG and a weaker northern STG (Fig. 3.8). The strengthening in the southern part of the STG is consistent with an increase in easterly winds in that region (Fig. 3.14).

In the Nordic Seas, fewer NAO positive phases over a long period of time lead to reduced temperatures and freshwater influx. This results in increasing density in the upper ocean layers. In combination with the advection of more saline water masses from the North Atlantic, the increase in sea-ice cover in the Arctic Ocean, and the downward propagation of the water mass changes via convection and diffusion, the NAO shift contributes to the long-term change in water mass properties in the Nordic Seas (Section 3.3.1). Based on the correlation pattern (Fig. 3.20), an increase in NAO negative phases would also lead to an increase in freshwater influx in the eastern North Atlantic. This increase, however, is not apparent in the long-term as can be seen from the freshwater flux difference (Fig. 3.13). This discrepancy indicates that although NAO plays an important role in the variability and long-term evolution of ocean circulation in the North Atlantic, responses of other processes are superposed on the NAO response and can either amplify, balance, or outweigh it.

Besides the effect of the NAO on ocean circulation in the North Atlantic, it also impacts temperatures over the European continent (Fig. 3.16). The correlation between the NAO-index and annual mean surface temperature in Europe is positive with the strongest signals over southern Scandinavia and the Iberian Peninsula. This homogeneous response over the European continent is not in line with the common picture of the influence of the NAO that usually displays a dipole in the temperature response over northern and southern Europe.

This seeming contradiction is due to the fact that the correlation map (Fig. 3.16) is derived from annual mean values of temperature and not only winter temperatures - in which case also our model shows the dipole pattern. We discuss the different seasonal responses of European surface temperature to the NAO in the following: To test the influence of the NAO on temperatures and temperature variability in northern and southern Europe (defined as the regions 10°W, 40°E, 55°N, 75°N and 10°W, 40°E, 35°N, 50°N, respectively) we calculate histograms of winter and summer mean temperatures during NAO positive and NAO negative phases over northern and southern Europe (Fig. 3.22 a and b). We define NAO positive/negative years as years where the NAO-index exceeds 1/-1.

The strongest response to changes in NAO appears in the northern European winter, when temperatures are high during NAO positive phases and low during negative NAO phases. In the southern European winter, the surface temperature response is reversed. In the subsequent summer months, however, surface temperatures over southern Europe are lower after preceding NAO negative phases during the winter. A direct influence of atmospheric winter conditions on summer temperatures is, however, questionable due to the long delay time. An intermediary process such as the summer NAO, or heat

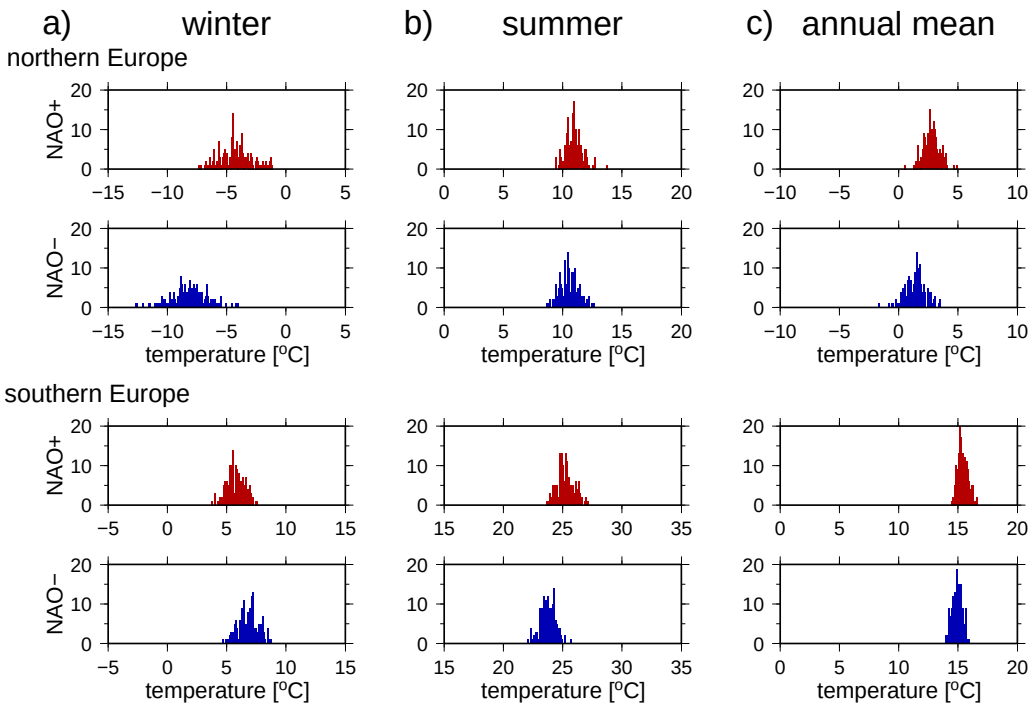

Figure 3.22: Histograms of mean **a)** winter, **b)** summer, and **c)** annual temperatures during NAO positive and NAO negative phases for northern (10°W, 40°E, 55°N, 75°N) and southern (10°W, 40°E, 35°N, 50°N) Europe.

uptake in the Mediterranean Sea is likely involved. Furthermore, increased advection of moisture from the Atlantic Ocean that leads to enhanced cloud cover and precipitation over southern Europe in summers succeeding NAO negative phases could be responsible. In total, the annual mean temperature response to NAO positive phases is - although not as strong as on the seasonal scale - positive over northern and southern Europe (Fig. 3.22 c).

Another interesting feature of the NAO time-series is that positive and negative phases dominate continuously over periods as long as 300 years (Fig. 3.21). Since the NAO has been proposed to play a role in climate periods over Europe where temperatures were unusually high or low for time-intervals of many decades to centuries, i.e., the Medieval Warm Period and the Little Ice Age, these prolonged periods of one dominating NAO phase could be realized by internal variability only.

3.3.5 Multi-centennial Variability of Ocean Circulation

In addition to the interannual AMOC variability, AMOC variability on multi-centennial timescales is significant (at the 95% level) over the simulation period (Fig. 3.15). This is

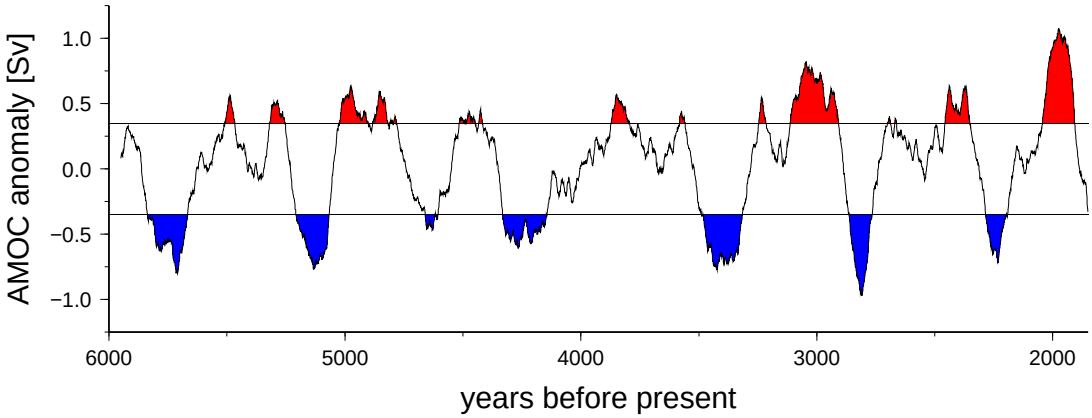

Figure 3.23: Detrended time-series of the AMOC at 30°N (100 year running-mean, in Sv = $10^6 m^3/s$). Red contours indicate years with a positive long-term AMOC anomaly, blue contours denote years with a negative AMOC anomaly that were selected to calculate the composites.

also expressed in long-term oscillations in the time-series of ocean quantities connected to the AMOC (Section 3.3.1). The remarkably close correlation on these time-scales between the AMOC maximum at 30°N and both measures of corresponding contributions from the two deep water formation regions, the overflows for the Nordic Seas (Fig. 3.5) and the LSW thickness for the Labrador Sea (Fig. 3.10), indicates that the water mass properties in the convection regions play an important role in the long-term variability.

There are seven realizations of the oscillation in the first 4,200 years of the simulation and its shape is reminiscent of a rectangular function with prevailing states with a length of more than 100 years where the AMOC is strong or weak and relatively rapid transitions shorter than 100 years between the two. The transition from the strong state to the weak state is steady, whereas the transition from the weak state to the strong state is interrupted at times. The periodicity of the oscillation is varying between 400 and 700 years and its amplitude decreases strongly after the first 4,200 years of the simulation (Fig. 3.15, Fig. 3.10, and Fig. 3.5).

Since the length of this time-period is relatively short compared to the 400 to 700 year periods, and the period is varying strongly within the cycles, the statistics we applied for the interannual variability to calculate lead and lag relationships are not very robust in the case of the multi-centennial variability. Thus, instead of calculating correlations we perform a composite analysis of different climate variables potentially connected with the AMOC restricted to these 4,200 years of the simulation. We detrend the time-series of the AMOC at 30°N, apply a 100-year running-mean filter and define positive anomaly-periods when the long-term variability exceeds 0.35 Sv and negative

anomaly-periods when it is below -0.35 Sv (Fig. 3.23).

To exclude the possibility that the resulting composite maps show a response of the model to the long-term changes due to the external orbital forcing, rather than to the long-term variability, we perform a "mini-ensemble" analysis by applying shorter time-windows of 1,500 years length and compare the resulting composite maps (three each) with the 4,200-year composite maps. All features apparent in the long composite and on the three shorter ones are restricted to the Atlantic Ocean basin north of the equator and the Arctic Ocean. There are no significant and at the same time coherent signals visible in the other ocean basins.

The temperature composite map (Fig. 3.24 a) shows increased temperatures in the North Atlantic and decreased temperatures in the Nordic Seas. The change in sign of the temperature signal along the Greenland-Scotland-Ridge, that constitutes the topographic border between the North Atlantic and the Nordic Seas, suggests that it is related to changes in the gyre component of the ocean heat transport that is dominating the meridional heat transport at latitudes higher than 45°N (Fig.3.25 a).

The composite of gyre-circulation-related northward heat transport (Fig. 3.25 b) shows that heat transport is enhanced in the region south of the Greenland-Scotland-Ridge and decreased north of it (heat transport contributions are calculated from the zonal mean velocities over the Atlantic basin for the meridional overturning circulation contribution and spatial deviations from the zonal mean velocities for the gyre contribution, see section 2.7 in chapter 2). The differences in the gyre circulation show a weakening of the cyclonic ocean circulation in the Nordic Seas and an increase in the southeastern part of the sub-polar gyre (Fig. 3.24 d). This enhances the transport of warm and saline water by the northern part of the SPG from the eastern side of the North Atlantic to the western side. The increase in meridional heat transport during strong AMOC phases is thus only spread in the North Atlantic basin and not to the Nordic Seas.

The decrease in cyclonic circulation in the Nordic Seas furthermore reduces the export of relatively fresh water into the North Atlantic via the East Greenland Current. Taking into account the atmosphere-ocean heat flux changes between strong and weak AMOC phases (Fig. 3.24 c) this contributes to advantageous water mass properties, cold at the surface and saline below the surface, in the Labrador Sea that enhance the formation of LSW.

Since on multi-centennial time-scales, the overflow strength is correlated with the AMOC strength as well as with LSW thickness, but the temperature, gyre circulation and to that end the ocean heat transport signal in the composites are of opposite sign in the Nordic Seas compared to the Labrador Sea, other processes must be involved. The decoupling between the temperature and salinity changes, that have opposite signs in the North Atlantic, but both positive sign in the Nordic Seas, supports the notion that the properties of North Atlantic inflow into the Nordic Seas are not as relevant for the

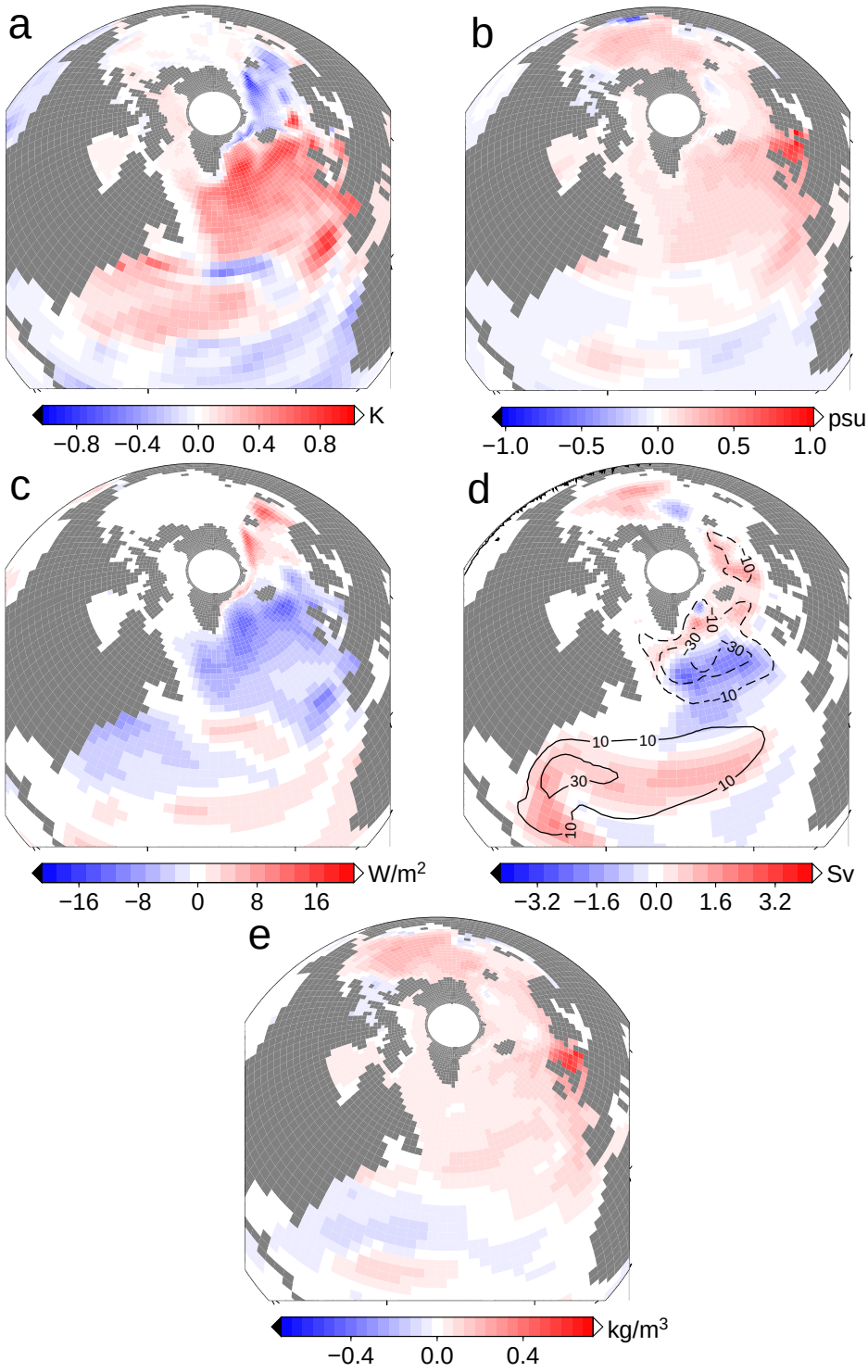

Figure 3.24: Composite maps of the North Atlantic and Arctic Ocean (difference in the corresponding fields between periods of strong and weak AMOC states - see Fig. 3.23): **a)** upper ocean temperature (in K), **b)** upper ocean salinity (in psu), **c)** atmosphere-ocean heat flux (in W/m^2), **d)** gyre circulation (in Sv = 10^6m^3/s, contour lines depict mean state of the gyre circulation), and **e)** upper ocean density (in kg/m^3).

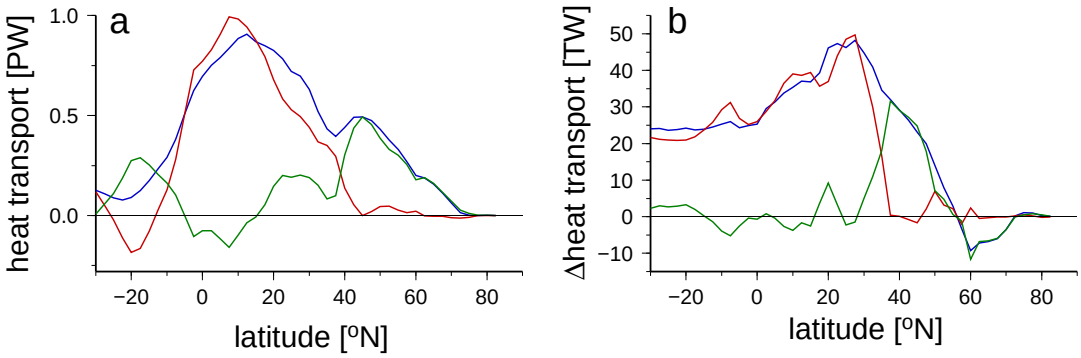

Figure 3.25: **a)** Time-mean over the simulation period of advective heat transport in the North Atlantic (in PW = 10^{15}W) and **b)** differences in the composites where weak AMOC periods are subtracted from strong AMOC periods (in TW = 10^{12}W). The total advective heat transport (blue) can be split in contributions from meridional overturning circulation (red) and gyre circulation (green).

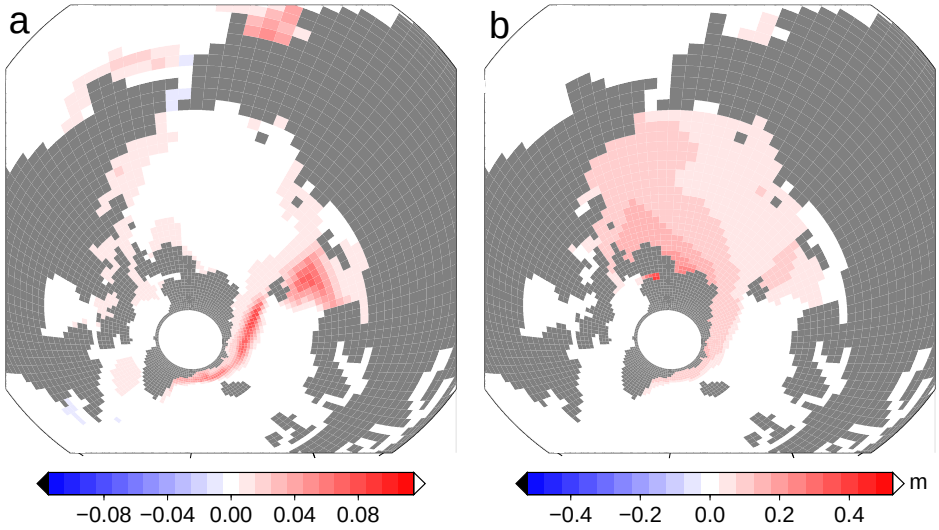

Figure 3.26: Composite maps of Arctic Ocean sea ice **a)** extent (in cell area fraction) and **b)** thickness (in m).

correlation as for the Labrador Sea. Atmosphere-ocean heat flux in the northwestern Nordic Seas and over the Barents Shelf is markedly reduced due to increased sea-ice cover (Fig. 3.26 a). In combination with increased sea ice volume and concurrent brine rejection in the Arctic Ocean (Fig. 3.26 b), especially in the western part north of Greenland and Canada, this causes an increase in salinity in the Arctic Ocean and the Nordic Seas (Fig.3.24 b).

Overall, the density in both deep water formation regions increases during phases of a strong AMOC (Fig.3.24 e): Over the Labrador Sea, mainly through enhanced advection of saline waters from lower latitudes and also due to increased ocean heat loss to the atmosphere; over the Nordic Seas, the main reason is a decrease in surface temperature amplified by an increase in salinity, due to in turn increased sea-ice volume. Deep water formation in both basins is thus favored, explaining the positive correlation between the AMOC strength and both measures for deep water formation, LSW thickness and overflows on multi-centennial time-scales.

So far, we have analyzed the differences between the strong and the weak state of the AMOC in the upper ocean properties and atmosphere-ocean fluxes involved, but do not yet know why the multi-centennial oscillations between the two states occur. Again, since we have only few realizations of the oscillation and the period is varying strongly a lead/lag correlation analysis is not applicable. The composite analysis showed that the main driver of the AMOC at the multi-centennial time-scale is salinity in the convection regions in the North Atlantic.

Salinity anomalies in the Atlantic Ocean basin including the Arctic Ocean show what process is responsible for the oscillatory behavior: Figure 3.27 shows zonally averaged salinity anomalies of the Atlantic Ocean at different instants of a single multi-centennial AMOC cycle. During a strong AMOC phase (a), convection in the North Atlantic is enhanced and positive salinity anomalies at latitudes where convetion occurs reach from the surface to the deep ocean. The lower branch of the AMOC transports these anomalies southwards, where they leave the Atlantic Ocean basin for the Southern Ocean. In the latitude regions of the STG (10 to 40°N), negative salinity anomalies accumulate from the surface to 1,000 m depth. After reaching a critical threshold the negative salinity anomalies propagate into the SPG region and thus the convection regions, initiating the transition to the weak AMOC state (b). As negative salinity anomalies prevail in the sinking regions during the transition, positive salinity anomalies accumulate in the STG region (c). The low AMOC state (d) is the reverse of the strong AMOC state (a) with strong positive salinity anomalies in the STG region. At a critical threshold, the positive salinity anomalies in the STG region again propagate into the SPG region (e). The cycle is completed by reaching the strong AMOC state again (f).

All of the seven multi-centennial oscillations in the simulation have the six stages described above in common. The salinity anomalies in the STG region are generated by evaporation in the low- and precipitation in high latitudes and advection of water

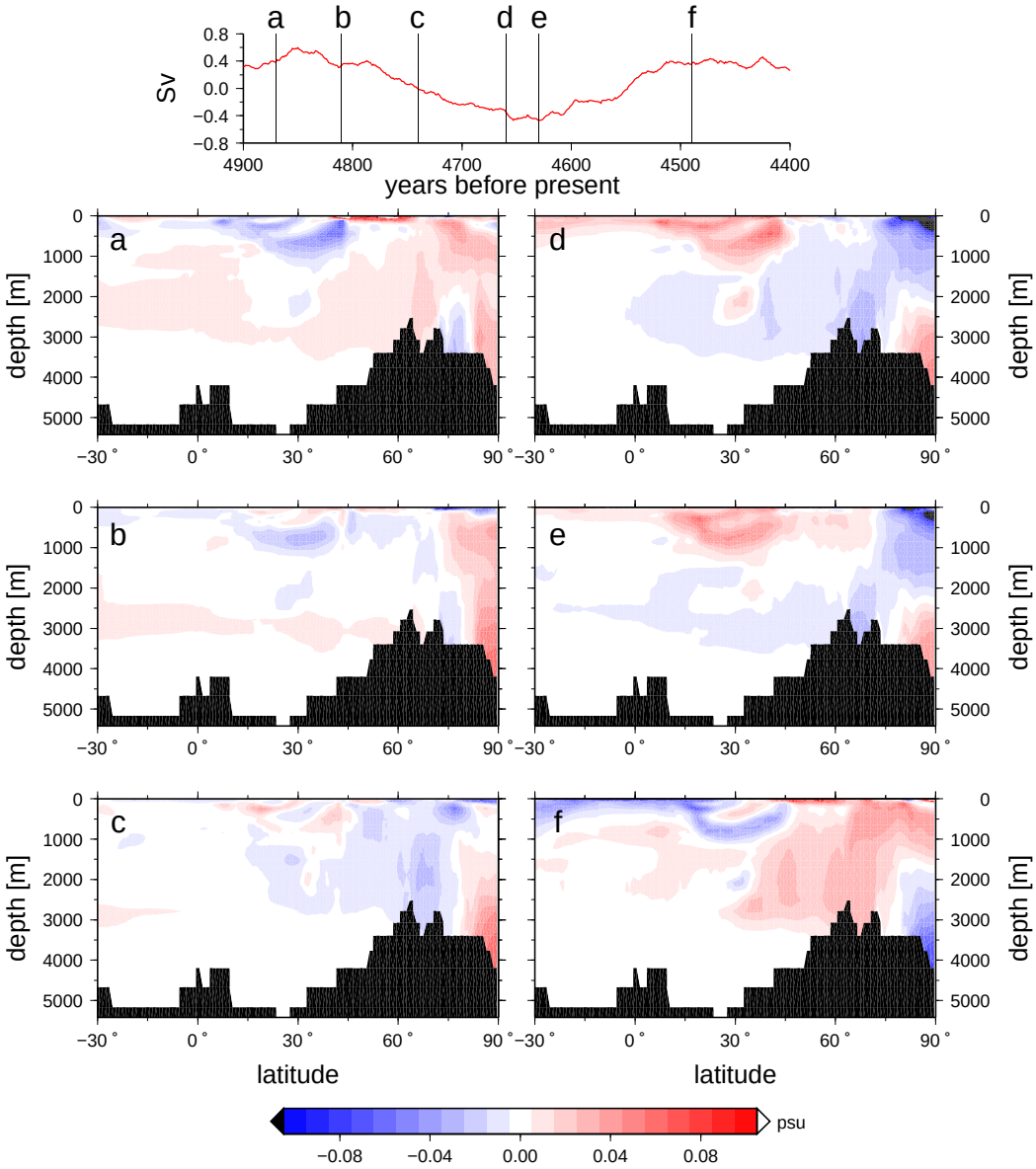

Figure 3.27: Snapshots of zonal mean salinity anomalies of the Atlantic Ocean of a single multi-centennial oscillation in the AMOC strength. The letters indicate the state of the AMOC in the upper time-series plot. Each of the lower graphs represents an average over 100 years of the salinity field which is detrended with respect to the whole simulation period.

masses from the southern latitudes and water mass influx from the Southern Ocean. These inputs are not directly coupled and depending on their phasing, differences occur in the length of the plateau-states when the AMOC is strong or weak and in the transitions from the weak state to the strong state.

The strong plateau-states tend to last longer than the weak ones, but are interrupted by smaller decreases in the AMOC strength (Fig. 3.23, e.g., in the intervals between 5,500 - 5,300 yBP, 5,000 - 4,850 yBP, and 3,250 - 3000 yBP). Also the transitions from the weak to the strong state exhibit interruptions (e.g., in the interval 2,250 - 2,000 years). These changes in the AMOC strength with small amplitude occur when the different contributions to STG salinity anomalies are out of phase, whereas in the case of large amplitude changes they all act in concert.

3.4 Discussion

Climate evolution from the mid-Holocene to today has been the subject of a recent comprehensive review by Wanner et al. (2008), which compiled results of various proxy- and modelling studies. The simulated mean climate evolution of our transient Holocene experiment shows agreement in most aspects: cooling in the northern high latitudes, decreased precipitation in the monsoon regions, and a trend toward lower NAO-indices. The southward ITCZ shift could not be established over the Caribbean, but over the African continent. Overall, we are confident that the simulated mean climate trends present our simulation capture the main aspects of the mid- to late Holocene climate and the analysis of ocean circulation changes and variability can be discussed in context with other Holocene climate proxy- and modelling studies.

Model simulations that investigate the response of the AMOC to Holocene orbital forcing are sparse. Our model simulation exhibits an increase in both deep water formation regions, and thus in the overall AMOC strength. In the study by Renssen et al. (2005) discussing ocean circulation changes in a transient simulation of Holocene climate with an Earth System Model of intermediate complexity, the overall AMOC strength remained constant. A reduction in deep water formation in the Nordic Seas was balanced by an increase in deep water formation in the Labrador Sea. The authors attributed weaker deep water formation in the Nordic Seas to increased sea-ice export from the Arctic that freshened the surface waters and thereby impaired convection.

The mechanism for the increase in the Labrador Sea proposed by Renssen et al. (2005) is similar to the advection mechanism we find. In the Nordic Seas, however, the effect of increased sea-ice export from the Arctic to the lower latitude oceans is outweighed by increasing salinity advected from the northeastern Atlantic and by the brine rejection effect in the Arctic Ocean where sea-ice volume increases. Ocean circulation in the Nordic Seas and the Arctic Ocean (Mauritzen 1996) accumulates both effects, which

lead to the formation of sub-surface water masses of higher density. These water mass property changes, in turn, intensify the strength of the overflows.

There is evidence for an increase in the AMOC in the course of the Holocene from paleo reconstructions of density gradients in the Florida Strait (Lynch-Stieglitz et al. 2009). The authors attribute the strengthening of the Florida Current to a southward migration of the intertropical convergence zone (ITCZ) leading to a decrease in precipitation (Haug et al. 2001) and enhanced wind driven currents. In our simulation, however, the latitudinal position of the ITCZ (calculated after Braconnot et al. 2007b) does not shift over the western tropical Atlantic. Nevertheless, freshwater influx into the tropical Atlantic decreases (Fig. 3.13 b) and increased easterly winds over the Caribbean (Fig. 3.14) strengthen the southern sub-tropical gyre, which is in agreement with a stronger Florida Current.

Variability in the AMOC and North Atlantic climate on interannual to multi-decadal time-scales has been studied far more extensively than the multi-millennial changes due to orbital forcing (e.g., Delworth et al. 1993; Timmermann et al. 1998; Jungclaus et al. 2005). Atmospheric conditions over the North Atlantic are thought to be the main contributor to variability from annual to interannual time-scales. Since the NAO is the dominant pattern of climate variability on these time-scales, its influence on ocean circulation has been the subject of many climate studies (see review by Visbeck et al. 2003). The NAO pattern in our model and its influence on ocean circulation on annual to interannual time-scales is consistent with this picture. On annual time-scales, the NAO induced changes in wind stress and surface temperatures affect the ocean circulation locally. But basin-wide responses take up to a decade to adjust to atmospheric conditions (e.g., Eden and Willebrand 2001) and also influence the AMOC on these time-scales (e.g., Böning et al. 2006). On time-scales less than seven years, the positive response of the SPG and the AMOC to NAO positive phases in our simulation is basically in agreement with regional Atlantic Ocean only model studies by Eden and Willebrand (2001) and Böning et al. (2006). After seven years however, the response to NAO positive phases of the Nordic Seas water masses, which are prescribed as constant in the two Atlantic Ocean only modelling studies, results in a reduction in the overflows and also decreases the deep water formation in the Labrador Sea via advection of relatively light water masses from the East Greenland Current. This causes a basin-wide negative NAO-response of the AMOC after 12 years. Similar responses of the convective activity in the Labrador Sea and the Nordic Seas to the NAO that we find have also been inferred from observations (Dickson et al. 1996; Curry et al. 1998). In a study investigating the AMOC response to global warming (Schweckendiek and Willebrand 2005), the properties of overflow water have also been found to be decisive.

Periods of long-term persistence of one NAO phase that exhibited by our Holocene simulation, have also been inferred from marine and continental proxy reconstructions (Sicre et al. 2008; Trouet et al. 2009). An NAO-index reconstruction from temperature

proxies in Scotland and precipitation proxies in Morocco for the last millennium (Trouet et al. 2009) shows a 300-year-long phase of positive NAO during the Medieval climate anomaly (MCA) and a shift towards a negative NAO during the Little Ice Age (LIA). Similarly long periods of 200 years of high surface ocean temperatures north of Iceland during the MCA and a decrease towards the LIA are found by Sicre et al. (2008). The authors also suggest that the long-term temperature changes reflect NAO-induced changes in ocean circulation. They propose a decrease in inflow from the North Atlantic through Denmark Strait and enhanced freshwater influence from Arctic sea-ice export during NAO negative phases in the transition from the MCA towards the LIA. This would be in agreement with our model results.

The annual surface temperature response to NAO over Europe in the model setup applied in the current study supports the hypothesis that for persisting NAO could have influenced the MCA and the LIA periods. The authors of the NAO reconstruction study propose special solar and volcanic conditions to explain the long-term persistence, whereas the model study we present comprises orbital forcing only which acts on much longer time-scales than centuries. In consequence, we propose that internal variability of the climate system is sufficient to allow for long periods of one NAO phase dominating so that these periods are not depending on external forcing.

The long-term trend in the NAO from dominating positive phases to more negative in the course of the experiment is supported by climate reconstructions (Nesje et al. 2001; Davis and Stevenson 2007). For AOGCMs, the response of the NAO to Holocene orbital forcing is ambiguous (Gladstone et al. 2005), but still supports the notion of an NAO-positive like shift during the Holocene. A decrease in NAO positive phases would support the cooling trend in the Nordic Seas and the long-term changes in water mass properties and the following increase in the AMOC disscussed above.

Variability on multi-centennial time-scales has been observed in high-resolution proxy data records from the Holocene (Stocker and Mysak 1992). The authors question the traditional interpretation that these long-term fluctuations are externally forced, e.g., by variations in solar activity. Indeed, multi-centennial variability in the AMOC has been detected in ocean general circulation models applying stochastic noise on top of climatological atmosphere forcing (Mikolajewicz and Maier-Reimer 1990) and latitudinal dependent freshwater fluxes (Winton and Sarachik 1993), suggesting that natural variability of the ocean circulation is responsible. Both studies find the oscillation to be a result of salinity anomaly advection by overturning circulation that can also be described in terms of a "loop" oscillation (Winton and Sarachik 1993) derived from a simple model of Welander (1982, 1986), that has also been found in a more recent modelling study with an idealized single-hemispheric ocean basin (te Raa and Dijkstra 2003). Also more recent studies with AOGCMs exhibit multi-centennial variability (Vellinga and Wu 2004; Park and Latif 2008). In both, a relatively strait-forward mechanism, involving the advection of salinity anomalies from the tropical Atlantic

and the Southern Ocean, respectively, to the deep water formation regions in the North Atlantic, could be established as the main driver of the variability.

In the present study, however, the mechanism is less clear. It seems to be a combination of advected salinity anomalies from the Southern Ocean, the tropical Atlantic, freshwater fluxes in the deep water formation regions, and sea-ice volume in the Arctic that influences the AMOC strength. Since the individual processes are not closely correlated, the phasing between them is decisive for the amplitude and the period of the variability. A difference between the multi-centennial variability found the other two AOGCM studies and the one presented here is that in the current study it is on top of a linear increase in the AMOC. It is possible that the long-term change in the AMOC induced by the applied orbital forcing leads to the more irregular behavior of the ocean circulation.

Some aspects of the mechanism present in the current study, however, can be related to mechanisms proposed in previous studies with idealized ocean models or even simple mechanical models. Weaver et al. (1991) described chaotic behavior with significant variability on multi-decadal time-scales of an idealized one-basin ocean model in the transition between two equilibrium states, triggered by switching from restoring to mixed boundary conditions. The mechanism they proposed involved an influence of the residence time of surface waters in a region of locally enhanced evaporation, in their case the Greenland Sea. In the present study, a similar mechanism could be proposed for the residence time of surface water masses in the tropical Atlantic: When the AMOC is weak, surface water masses pass the tropical and sub-tropical Atlantic more slowly, evaporating more water and becoming more saline and warm. Once these water masses reach the high northern latitude sinking regions, convection increases and enhances the AMOC. During such a strong AMOC phase, surface water masses pass the tropical Atlantic more rapidly, resulting in lower salinity and the mechanism is reversed. This mechanism has also been described in terms of a mechanical model of leaky water buckets on a tilted rotating wheel (Welander 1986). The net evaporation-precipitation ratio in the tropical Atlantic is subject to atmospheric processes that, although correlated to some degree to oceanic conditions, exhibit variability on shorter time-scales independent of the ocean and thus act as a stochastic forcing, which is not present in the two examples explained above. Since also these more simplified models show chaotic behavior it is not surprising to find irregular behavior in the present model setup. For this reason, it is quite possible that period and amplitude of the variability on centennial time-scales is dependent on the integration of short-term atmospheric fluctuations by internal ocean dynamics (Hasselmann 1976).

The absence of significant and continuous variability in the decadal frequency band between 10 and 70 years (Fig, 3.15) is maybe related to the relatively coarse resolution of the model. In a higher resolution version of the model used here, Jungclaus et al. (2005) show that multi-decadal variability occurs and is governed by freshwater exports

from the Arctic to the deep water formation region in the Labrador Sea. The mechanism involves a control on the freshwater export by geopotential height differences between the Nordic Seas and the Arctic Ocean that is probably not sufficiently represented in the coarse resolution version of the model.

In the last 2,000 years of the simulation, the amplitude of the multi-centennial variability of the AMOC decreases. This could be due to internal model variability or represent a different model regime. We speculate that these changes might be related to the long-term persisting phases of NAO in combination with the trend in the NAO-index towards more negative phases. As has been shown by Lohmann et al. (2009), the response of the SPG to persistent NAO positive and NAO negative forcing is asymmetric. Whereas the response to NAO positive forcing involves a stronger followed by a weaker SPG, the response to NAO negative forcing is merely a gradually weakening of the SPG. If this is considered as a decrease in short-term variability or fluctuation, it could lead to a weakening in the integration of short time-scale perturbations into long-term variabilities by ocean dynamics. Comparing the wavelet spectra of the time-slice simulations (2,000 years long) discussed in chapter 2 does not refute the argument, but also does not give a conclusive answer.

3.5 Conclusion

We have analyzed the evolution and variability of the Atlantic meridional overturning circulation (AMOC) in a transient simulation from the mid-Holocene to today with a coupled atmosphere-ocean general circulation model. The main results are:

- Orbital forcing induces a strengthening in the AMOC due to increased density of the North Atlantic deep water (NADW) produced in the Labrador Sea and the Nordic Seas.

- The increase in NADW density throughout the simulation is induced by advection of more saline water from the eastern North Atlantic by the sub-polar gyre in the Labrador Sea. In the Nordic Seas, increasing density enlarges the density contrast to the North Atlantic and leads to an increase in the hydraulic pressure and hence, overflow water from 3 to 5.5 Sv. Decreasing horizontal density gradients due to increased isopycnal uplift at the Nordic Seas margins, add to the hydraulic pressure effect.

- The AMOC exhibits significant variability on interannual and multi-centennial time-scales.

- The interannual AMOC variability is mainly driven by atmospheric forcing dominated by the North Atlantic Oscillation (NAO).

- Throughout the simulation, the NAO shows a trend from more positive phases to more negative phases. The NAO also exhibits periods of up to 300 years of one persisting phase, which could possibly be related to long-term climate anomalies in Europe.
- The multi-centennial AMOC variability is related to accumulating salinity anomalies in the sub-tropical gyre region that propagate into the sub-polar gyre region, after reaching a threshold, and trigger the oscillation.
- The amplitude and period of the oscillation is dependent on various processes in the tropical Atlantic, the Southern Ocean, the North Atlantic and the Arctic Ocean. This suggests that it is an accumulated response of the coupled system to small scale perturbations.

Chapter 4

Evolution of the Seasonal Temperature Cycle in a Transient Holocene Simulation: Orbital Forcing and Sea Ice

We quantify the influence of orbitally induced changes on the seasonal temperature cycle in a transient simulation of the last 6,000 years - from the mid-Holocene to today - using a coupled atmosphere-ocean general circulation model (ECHAM5/MPI-OM) including a land surface model (JSBACH).

The seasonal temperature cycle responds directly to the insolation changes almost everywhere. In the Northern Hemisphere, its amplitude decreases according to an increase in winter insolation and a decrease in summer insolation. In the Southern Hemisphere, the opposite is true.

Over the Arctic Ocean, however, decreasing summer insolation leads to an increase of sea-ice cover. The insulating effect of sea ice between the ocean and the atmosphere favors more continental conditions over the Arctic Ocean in winter, resulting in strongly decreasing temperatures. Consequently, there are two competing effects: the direct response to insolation changes and a sea-ice dynamics feedback. The sea-ice feedback is stronger, and thus an increase in the amplitude of the seasonal cycle over the Arctic Ocean occurs. This increase is strongest over the Barents Shelf and influences the temperature response over northern Europe.

We compare our modelled seasonal temperatures over Europe to paleo reconstructions. We find better agreements in winter temperatures than in summer temperatures and better agreements in northern Europe than in southern Europe, since the model does not reproduce the southern European Holocene summer cooling inferred from the paleo data. The temperature reconstructions for northern Europe support the notion of the influence of the sea-ice effect on the evolution of the seasonal temperature cycle.

4.1 Introduction

The amplitude of the seasonal temperature cycle depends on changes in the Earth's orbital parameters that alter the annual meridional distribution of insolation. The orbital forcing constitutes the dominant natural long-term climate forcing in the last 6,000 years, from the mid-Holocene to today (e.g., Wanner et al. 2008; Renssen et al. 2009). On millennial time-scales, the insolation changes are due to the precession of the Earth's elliptical orbit around the Sun and the changes in obliquity of the Earth's rotation axis with respect to the orbital plane. Since the obliquity was larger 6,000 years ago and at the same time summer solstice was closer to perihelion insolation in the Northern Hemisphere was higher in summer and lower in winter, resulting in increased seasonality. Although these changes in insolation were small in the annual mean ($< 4\,\mathrm{W/m^2}$), feedbacks between the different components of the Earth system amplify or dampen the insolation signal. This leads to changes in climate also on time-scales longer than seasonal as has been shown in several time-slice simulation studies (e.g. Braconnot et al. 2007a; Otto et al. 2009). The annual temperature change is caused by seasonal temperature changes that vary in their individual amplitudes. So the annual signal can be dominated by one particular season, and hence, by seasonality.

In a study by Denton et al. (2005), the role of seasonality in abrupt climate change events during the last 60,000 years has been discussed by means of temperature reconstructions from ice cores and glacier advances in Greenland. The authors found that during abrupt cold climate events the annual temperature anomalies in high northern latitudes are dominated by the winter temperature anomalies that are caused by increased winter sea-ice cover in the Northern Hemisphere. This leads to continental conditions over large parts of the northern high latitudes and thus to an increase in the amplitude of the seasonal temperature cycle.

In this study, we investigate how changes in seasonality affect the mean climate evolution from the mid-Holocene to today. Given the seasonal distribution of insolation in the Northern Hemisphere in the mid-Holocene, the expected direct respone is a decrease in the amplitude of the seasonal cycle in the course of the last 6,000 years. Nevertheless, sea-ice evolution over the Arctic Ocean and the interaction between atmosphere, ocean and sea ice, may alter this direct response. We present the evolution of the seasonal temperature cycle over the last 6,000 years in a coupled atmosphere-ocean model with an integrated dynamic land surface model and compare the results to Holocene temperature reconstructions obtained from pollen archives.

4.2 Model and Experimental Setup

We perform a 6,000-year-long transient simulation with the coupled atmosphere-ocean general circulation model ECHAM5/MPI-OM (Jungclaus et al. 2006) including the

land surface model JSBACH (Raddatz et al. 2007) with a dynamic vegetation module (Brovkin et al. 2009). The atmosphere component ECHAM5 (Roeckner et al. 2003) is run in resolution T31 (corresponding to 3.75°) and the ocean component MPI-OM (Marsland et al. 2003) is run in resolution GR30 (corresponding to ∼3°). The ocean model component includes a Hibler-type zero-layer dynamic-thermodynamic sea-ice model with viscous-plastic rheology (Semtner 1976; Hibler 1979).

Since we are mainly interested in the effects of orbital forcing on the evolution of the seasonal temperature cycle, we do not apply further external forcing such as solar, volcanic, or greenhouse gases and set greenhouse gases to pre-industrial values (CO_2 to 280 ppm, CH_4 to 700 ppb, N_2O to 265 ppb). Thus we do not expect the model results to perfectly match climate reconstructions. Rather, we are interested in finding mechanisms that determine the changes in the seasonal temperature cycle from the mid-Holocene to today. We apply orbital forcing on a yearly basis following VSOP87 (Bretagnon and Francou 1988) implemented in the radiation scheme of the atmosphere model component. In the simulation, we do not apply any acceleration technique. We initialize the transient experiment from a 3,500-year-long mid-Holocene (6,000 years before present) time-slice simulation with orbital forcing presented in chapter 2. For the following analysis we use monthly mean output from both the atmosphere and the ocean model.

4.3 Results and Discussion

4.3.1 Seasonal Insolation and Sea-Ice Effects

We define the amplitude of the seasonal temperature cycle (STCA) as the surface temperature difference between the coldest and the warmest month of the year. Similarly, we define the amplitude of the seasonal insolation cycle (SICA) as the difference between annual maximum and minimum incoming short wave radiation on a monthly mean basis. SICA depends on the external orbital forcing only. Fig. 4.1 a and c show zonally averaged Hovmoeller-type diagrams of SICA and STCA, respectively. Changes in STCA follow those in SICA qualitatively with the exception of the high northern latitudes where, despite decreasing SICA, STCA increases. The maximal STCA response in the low- and mid latitudes in the Northern Hemisphere (NH) is shifted northwards from 15° to 40°N for the maximum decrease in STCA and southwards from 15° to 30°S for the low- and mid latitudes increase in STCA in the Southern Hemisphere (SH). The difference between SICA and STCA in low- and mid latitudes can be attributed to planetary albedo effects. Fig. 4.1 b shows the evolution of the net incoming short wave radiation seasonal cycle amplitude (net SICA) that includes the planetary albedo effect and that corresponds more closely to STCA. The difference between SICA and net SICA in low- and mid latitudes occurs because of a southward shift of the intertrop-

ical convergence zone (ITCZ) over Africa (calculated after Braconnot et al. 2007b) and thus a decrease in cloud cover over the NH low latitudes and an increase in the SH ITCZ region. Nevertheless, the increase in STCA at high northern latitudes cannot be explained by net SICA which decreases at high northern latitudes. This is also true for the SH high latitudes, where the increase in STCA is disproportional to the increase in SICA and net SICA.

A spatially resolved plot of linear trends in STCA (Fig. 4.2) shows that the increase in STCA at high northern latitudes is confined to the Arctic Ocean, with the strongest signal over the Barents Shelf. This zonal mean increase outweighs the decrease in STCA over the continents at the same latitude bands. The expansion of sea ice is the most likely cause for the signal. Decreasing summer insolation in the high northern latitudes reduces summer sea-ice melt. In the Arctic Ocean, sea-ice cover increases from 90 to 95% in the annual mean (Fig. 4.3), mainly because of an increase in summer sea-ice cover. Because of the heat insulating effect of sea ice, the ocean cannot act as a reservoir gaining heat in the summer months and releasing it in the winter months, and thus, it dampens STCA. The annual mean atmosphere-ocean heat flux over the Arctic (positive values indicate heat flux directed from the atmosphere to the ocean), decreases in absolute values by 13% from -7.4 to -6.6 $\mathrm{W/m^2}$. The seasonal cycle of heat flux over the Arctic Ocean (Fig. 4.3) decreases by 22% with the summer heat flux decreasing from 70 to 52 $\mathrm{W/m^2}$ (24%) and the winter heat flux decreasing in absolute values from -36 to -28 $\mathrm{W/m^2}$ (22%).

The decrease in the amplitude of the seasonal cycle of sea-ice is due to an increase in summer sea-ice cover and the continental boundaries of the Arctic Ocean basin that limit winter sea-ice extent when the whole basin is sea-ice covered.

In the high southern latitudes, over the Southern Ocean and Antarctica, as opposed to the Arctic region, the sea-ice effect amplifies the changes in insolation. The increase in STCA over the Southern Ocean is stronger than the increase over Antarctica (Fig. 4.2). Austral summer insolation at high southern latitudes increases by only 5 $\mathrm{W/m^2}$ and insolation changes in austral autumn and winter are less than 2 $\mathrm{W/m^2}$ (Fig. 4.4). A strong decrease of 16 $\mathrm{W/m^2}$ occurs in austral spring, which leads to an increase in maximum sea-ice extent. The increased austral summer insolation leads to stronger ice melt and consequently, to an increase in the amplitude of the seasonal cycle of sea ice, despite the fact that the minimal sea-ice extent in the late Holocene is larger than in the mid-Holocene. The increase in the amplitude of the seasonal sea-ice cycle then amplifies the increase in STCA.

Over the NH continents and sub-Arctic oceans, STCA decreases according to the decrease in SICA, with the strongest decrease over North Africa, the northern part of the Arabian Peninsula and central Asia. In the SH, STCA increases over the oceans and Australia, but decreases over South America and southern Africa probably due to the southward shift of the ITCZ. Thus, we find two effects determining STCA in the

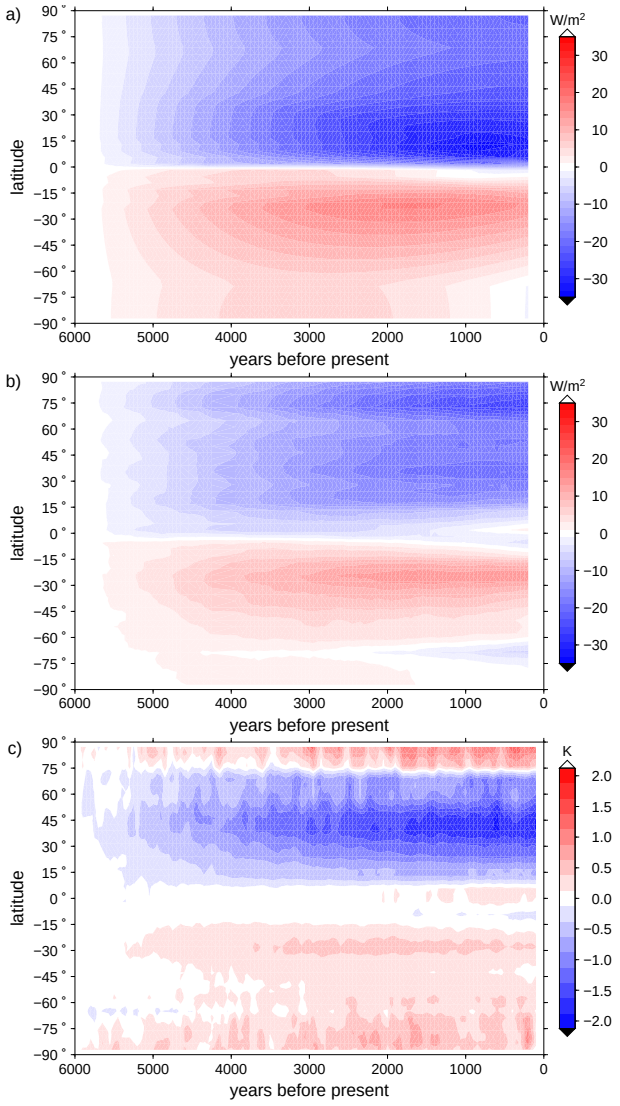

Figure 4.1: Zonal mean Hovmoeller type diagrams of **a)** the amplitude of the seasonal insolation cycle (the difference between yearly maximum and minimum insolation in W/m^2), **b)** the amplitude of the seasonal net insolation cycle (including planetary albedo), and **c)** the amplitude of the seasonal temperature cycle (the difference between annual maximum and minimum zonal mean temperature). The panels show anomalies with respect to conditions at the mid-Holocene (the mean of the first 100 years of the simulation).

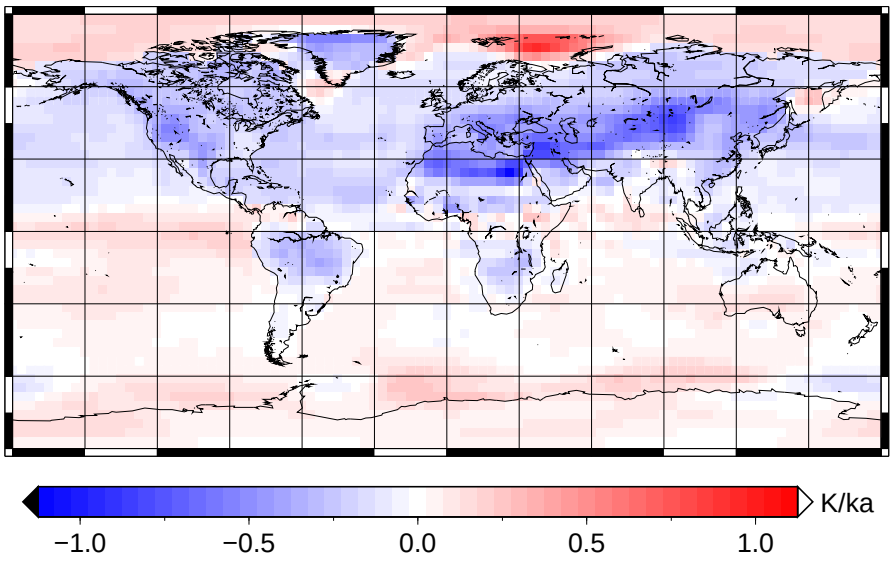

Figure 4.2: Linear trend in seasonal cycle amplitude (difference between warmest and coldest month) over the simulation period in K/ka - Kelvin per 1,000 years.

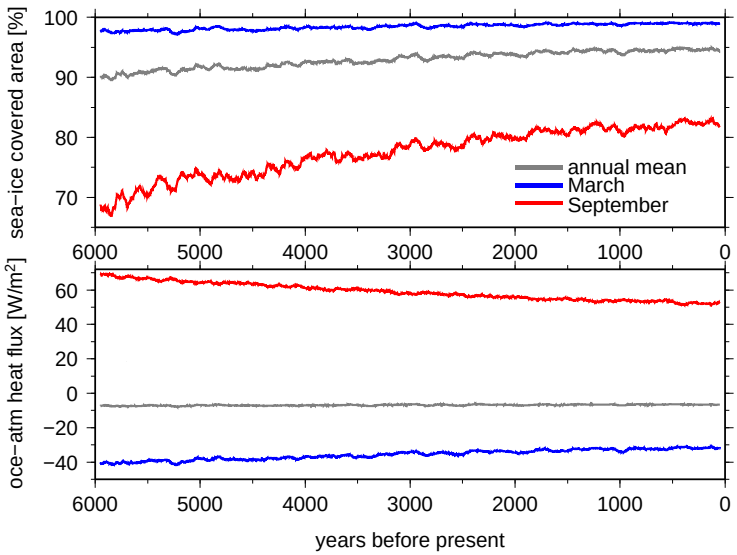

Figure 4.3: Upper panel: percentage of sea-ice covered area in the Arctic Ocean, lower panel: atmosphere-ocean heat flux in W/m^2 - positive values from the atmosphere to the ocean. Both panels show 100-year running means.

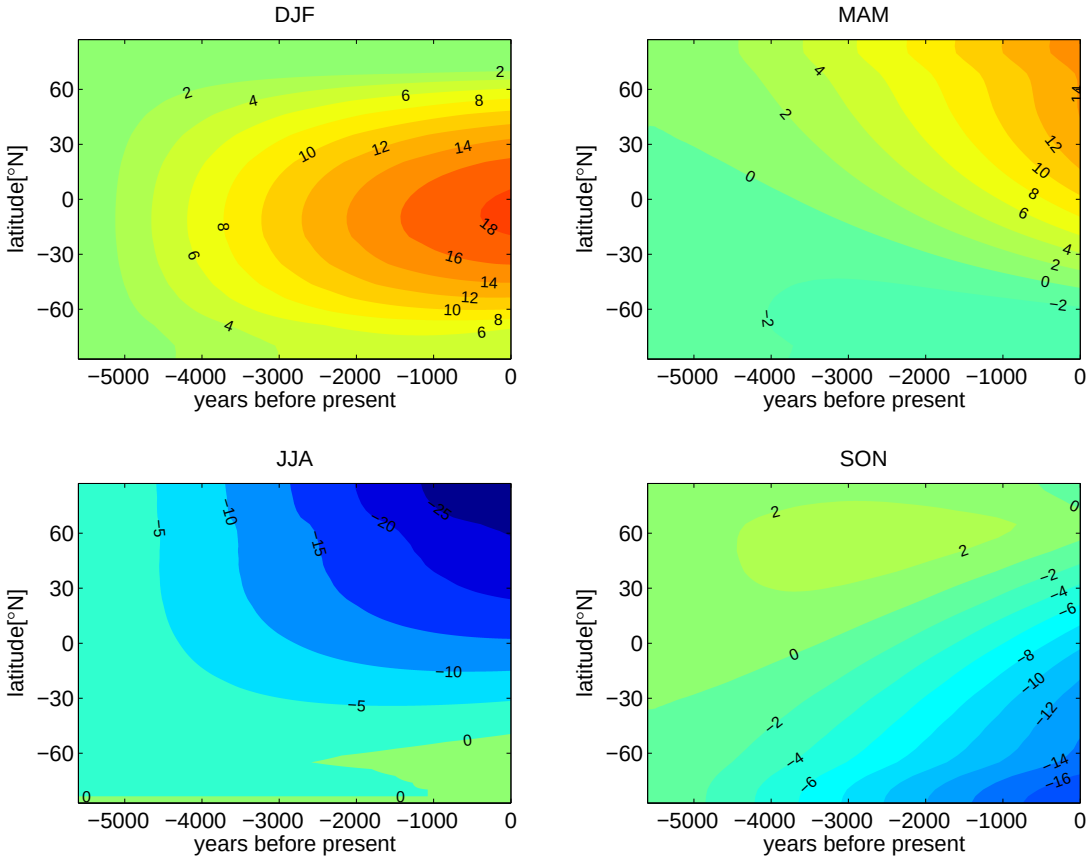

Figure 4.4: Changes in seasonal insolation from the mid-Holocene to today in W/m^2 (winter - DJF, spring - MAM, Summer - JJA, autumn - SON). The reference is 6,000 years before present.

mid- and late Holocene: seasonal insolation distribution and sea-ice cover.

To investigate what effect and also what season is dominating the changes in STCA we have a closer look at the annual mean temperature evolution. Zonal changes in surface temperature, an increase at low latitudes, and a decrease in high latitudes (Fig. 3.1), correspond to the changing insolation distribution with increasing insolation around the equator in boreal winter and decreasing insolation at high northern latitudes in boreal summer. In the low latitudes, the insolation induced warming in winter is accompanied by a southward migration of the ITCZ, which leads to a strong decrease in cloud cover and precipitation in the monsoon season from late summer to autumn both over the Indian sub-continent and the Sahel region. Due to these two effects the warming signal is present the whole year. The STCA decrease is strongest just north of these warming regions and is dominated by the insolation changes: an increase in summer insolation and thus temperature, and a decrease in both in winter.

In the Arctic Ocean, especially over the Barents Shelf and along the east coast of Greenland, cooling is enhanced where sea ice is expanding. The cooling signal is strongest in autumn and in winter, when - compared to the mid-Holocene conditions - sea-ice cover acts as an insulator and heat flux between the ocean and the atmosphere is inhibited. Thus, the autumn and winter temperatures sink, despite the fact that winter insolation is not changing significantly. So the sea-ice effect dominates the STCA. This is similar to the mechanism proposed to explain the abrupt climate changes in the last 60,000 years in Denton et al. (2005). Extensive winter sea-ice cover in the Arctic Ocean, leads to continental climate conditions over the Arctic region and cooler winters in the late Holocene compared to the mid-Holocene, when reduced sea-ice cover and thus open ocean in the Arctic region acts as a heat reservoir and thus leads to warmer winters. This affects not only the Arctic Ocean, but also influences the adjacent continents.

4.3.2 Comparison with Temperature Reconstructions for Europe

We compare the model results with the reconstruction of European winter and summer temperatures inferred from several pollen archives by Davis et al. (2003). In their paper, the authors sub-divide the European continent into six zones: northern, central, and southern Europe, with an eastern and western part each. Since the resolution of our model is quite coarse we discuss only changes for northern and southern Europe and the respective western and eastern parts, with 15°E being the boundary between east and west and 50°N being the boundary between northern and southern Europe.

The model results agree with the reconstructed data in trend and amplitude for northeastern European summer, and at least qualitatively in northwestern summer and southern winter temperatures. The largest discrepancy appears in southern European summer temperatures, where the model results exhibit a decrease and the reconstructed temperatures an increase. In a recent study, Davis and Brewer (2009) find the same

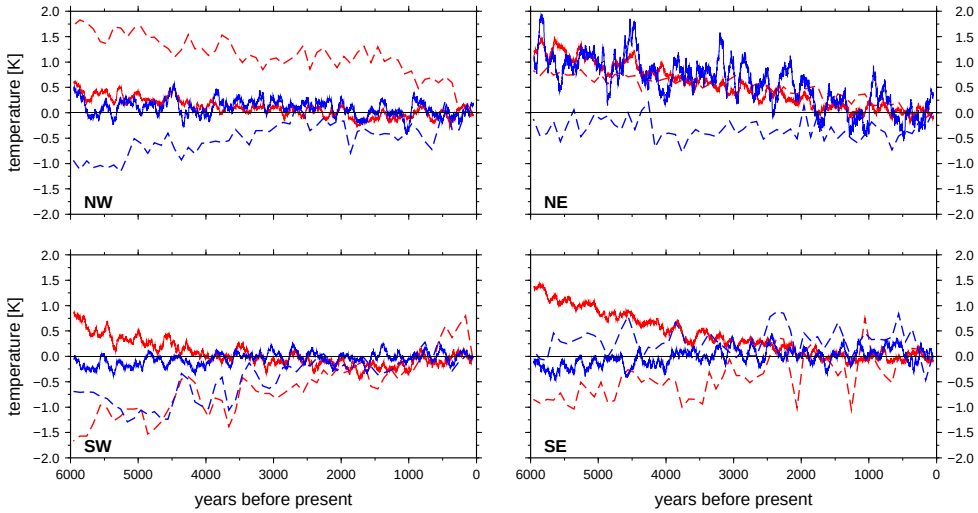

Figure 4.5: Comparison of seasonal temperature evolution between model results (solid lines) and reconstructions from pollen data (dashed lines) for northwestern (**NW**), northeastern (**NE**), southwestern (**SW**), and southeastern (**SE**) Europe - summer temperatures (red), winter temperatures (blue). Changes with respect to today's temperatures.

discrepancies when they compare their reconstructed data to Holocene time-slice model results from the PMIP2-exercise (Braconnot et al. 2007a). Davis and Brewer (2009) attribute the discrepancies to how climate models simulate the response of the latitudinal temperature gradient (LTG) between mid and high northern latitudes to a changing latitudinal insolation gradient (LIG) (Raymo and Nisancioglu 2003). Davis and Brewer (2009) define the LIG and the LTG as the difference between the latitude bands 30 - 45°N and 55 - 75°N in insolation and temperature, respectively, and show that reconstructed Holocene temperatures follow this seasonal LIG very closely (Fig. 4.6 a). For the modelled seasonal temperature gradients of the present study, however, this is only true for the winter, whereas the summer LTG is strongly divergent from the summer LIG (Fig. 4.6 b).

Summer LTG calculated from European temperature differences for late spring season (April to June), does resemble the LIG. But since other independent methods such as inverse modelling approaches to reconstructing mid-Holocene climate (Wu et al. 2007) and lake level reconstructions (Harrison and Digerfeldt 1993) indicate a Holocene summer cooling as well, this temporal shift is a rather improbable solution to the problem.

The modelled summer LTG follows the LIG if all continents are considered (Fig. 4.6 c). For the pollen-reconstructed temperatures, the argument of LTG sensitivity to LIG is

shown to be valid for all Northern Hemisphere continents as well (Davis et al. *in prep.*). It is possible that the discrepancy between reconstructed and modelled European temperatures is due to the coarse resolution of the model, that is not resolving changes in the atmospheric circulation induced by insolation changes correctly. The discrepancy could also result from a feedback or mechanism that is missing in the model. The missing summer cooling signal in southern Europe and the Mediterranean region is not specific for the model setup used in this study, but it is a common feature of coupled climate models (Braconnot et al. 2007b) in all of which mid-Holocene cooling is confined to the monsoon regions.

Nevertheless, because of the correspondence on the hemispheric scale between paleo reconstructions and model data and the qualitatively reasonable agreement between the two in northern latitudes, we argue that the effect of changing insolation and indirect effects, such as sea-ice cover have to be taken into account when interpreting reconstructed seasonal and also annual mean temperatures.

In addition, despite the discrepancies between the modelled and the reconstructed LTG, the reconstruction also indicates that STCA decreases more strongly in the northwestern part of Europe than in the northeastern part. This supports the notion of the influence of the sea-ice evolution in the Arctic Ocean and especially over the Barents Shelf on STCA. Still, since on these regional scales the model results diverge from the reconstructions, we cannot exclude the possibility that there are other reasons for this behavior in the proxy data that are not captured by the model.

The increase in the simulated southern European winter temperatures from the mid-Holocene to today, present in the reconstructions and the model, is likely related to a change in the North Alantic Oscillation (NAO, Fig. 3.21). The NAO-index shows a trend from dominating NAO positive states to prevailing NAO negative states. Climate reconstructions also indicate a more positive NAO-index during the mid-Holocene (Nesje et al. 2001; Davis and Stevenson 2007).

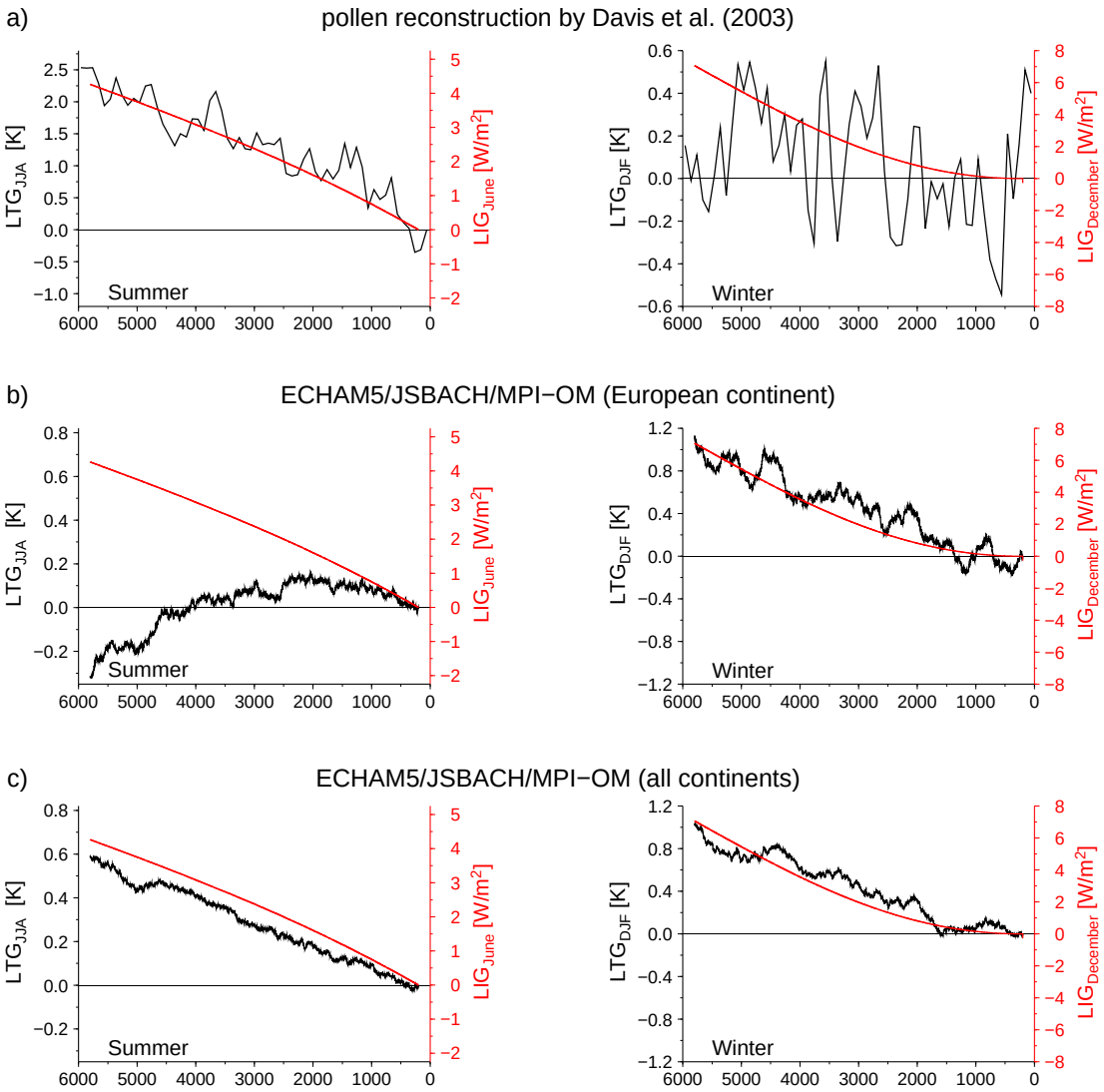

Figure 4.6: Seasonal latitudinal temperature gradients (in K, black lines, left y-axes) and June and December insolation gradients (in W/m^2, red lines, right y-axes). Both defined as the difference between the latitude bands 30 - 45°N and 55 - 75°N in temperature and insolation, respectively. **a)** temperature reconstruction from pollen (after Davis and Brewer (2009), subset of their figure 7), **b)** corresponding model results for the European continent, and **c)** model results for all continental land masses.

4.4 Conclusion

We investigated the response of the amplitude of the seasonal temperature cycle to orbitally induced changes in temporal and meridional insolation distribution. The main results are:

- The amplitude of the seasonal temperature cycle in the Holocene is determined by seasonal insolation distribution in the low- and mid latitudes and by sea-ice in the high latitudes.
- In the Northern Hemisphere, the sea-ice effect outweighs the insolation effect, in the Southern Hemisphere, the sea-ice effect amplifies the insolation effect.
- Despite the decrease in the amplitude of the seasonal insolation cycle, the amplitude of the seasonal temperature cycle increases in the Arctic Ocean. This, in turn, moderates the decrease of amplitude on the adjacent continents.
- Annual mean temperature changes in the high northern latitudes are dominated by a decrease in winter temperatures, whereas summer temperatures decrease to a lesser extent.
- A comparison of the model results to a temperature reconstruction from paleo archives also indicates an influence of sea-ice evolution on the amplitude of the seasonal temperature cycle.
- Discrepancies between the reconstruction and the model results appear in the southern European summer temperatures, where the model does not reproduce the mid-Holocene cooling inferred from the climate proxies.
- On the hemispheric scale, the modelled response in the latitudinal temperature gradient to the latitudinal insolation gradient matches the reconstructed response, suggesting that the coarse resolution version of the model might be responsible for the mismatch in southern Europe.

Chapter 5

Conclusion and Outlook

The aim of the present study was to assess the impact of orbital forcing on the mean state of the climate system during interglacial periods and to find out about the mechanisms in and between the different components of the climate system that communicate the differences in the boundary conditions. Furthermore, we investigated on what time-scales natural climate variability occurs in ocean circulation and what mechanisms govern this variability. We summarize the main results of the study by revisiting the research questions posed in the introduction and give the respective answers that emerged from the simulation results. Afterwards, we give an outlook by proposing possible directions of future research.

5.1 Summary

Analyzing the results of three time-slice experiments of the mid-Holocene, Eemian, and pre-industrial climates obtained from simulations with a coupled atmosphere-ocean general circulation model (AOGCM), we attempted to answer the following research questions (chapter 2):

(1) How do changes in orbital parameters alter the atmospheric and the oceanic circulation and the associated heat transports and how do these changes in circulation and heat transport influence regional climate?

Compared to pre-industrial climate, Eemian and Holocene annual mean temperatures show generally warmer conditions at higher latitudes and cooler conditions at lower latitudes. These changes in annual mean temperature - induced by the seasonal redistribution of solar radiation - are regionally enhanced through feedback mechanisms in the climate system, involving sea-ice cover, ocean heat transports, and atmospheric circulation patterns. The temperature increase in the Arctic results from increased oceanic heat transport to high northern latitudes and reduced sea-ice cover over the Nordic Seas and the Barents Sea, giving rise to enhanced ocean heat loss to the atmosphere. Changes in atmospheric circulation in the northern hemisphere also contribute

to the Arctic warming signal, since storm tracks over the northern North Atlantic over Iceland to the Arctic, northern and central Europe increase at the expense of a reduction of storm tracks over the Mediterranean region.

(2) Are there differences in the simulated climate under Eemian and Holocene boundary conditions disproportionate to the forcing that imply irregular responses to the induced insolation changes?

Changes in mean climate, atmospheric, and oceanic circulation are qualitatively similar in the Holocene and Eemian simulations. Larger eccentricity during the Eemian compared to Holocene and pre-industrial conditions enhances the precession signal and results in larger amplitudes of the response signals. We did not find an irregular response of the climate system to changing orbital parameters for interglacial periods. Thus, we argue that climate and climate variability in the Eemian and the Holocene evolve similarly, if the difference between the two is restricted to orbital forcing. Therefore, we focused on the Holocene period for the investigation of climate variability in the ocean component of the Earth system.

In chapter 3, we analyzed results obtained from a 6,000 year-long transient simulation of the mid- to late Holocene period run with orbital forcing. Focussing on changes in ocean circulation, we investigated the following research questions:

(3) How does the ocean circulation evolve in the long term under Holocene orbital forcing?

Orbital forcing induces a strengthening in the Atlantic meridional overturning circulation (AMOC) driven by changes in water mass properties in the deep water formation regions - the Labrador Sea and the Nordic Seas. In the Labrador Sea, a long-term increase in density in the produced North Atlantic deep water is induced by advection of more saline water from the eastern North Atlantic by the sub-polar gyre. In the Nordic Seas, increasing density enlarges the density contrast to the North Atlantic and leads to an increase in the hydraulic pressure and hence, overflows. Decreasing horizontal density gradients due to increased isopycnal uplift at the Nordic Seas margins, add to the hydraulic pressure effect.

(4) On what time-scales does the ocean circulation show variability and what are the responsible mechanisms?

The AMOC exhibits significant variability on interannual and multi-centennial timescales. The interannual variability is mainly driven by atmospheric forcing dominated by the North Atlantic Oscillation (NAO). During NAO positive phases cold conditions

over the Labrador Sea favor convection, whereas positive temperature and freshwater flux anomalies over the eastern North Atlantic and the Nordic Seas hamper the formation of overflows. After seven to twelve years, the warm and relatively fresh waters from the eastern North Atlantic reach the Labrador Sea, through advection by the sub-polar gyre, deep water formation in both formation regions is reduced and the AMOC gets weaker.

Throughout the simulation, the NAO shows a trend from more positive phases to more negative phases. Periods of up to 300 years of one persisting NAO phase may be related to long-term climate anomalies in Europe.

Multi-centennial variability is related to accumulating salinity anomalies in the subtropical gyre. After reaching a threshold, they propageate into the sub-polar gyre region and trigger an oscillation from the strong AMOC state to the weak AMOC state or vice versa. The amplitude and period of the oscillation is dependent on various processes in the tropical Atlantic, the Southern Ocean, the North Atlantic and the Arctic Ocean, suggesting that it is an accumulated response of the coupled system to small scale perturbations.

Using the results of the transient Holocene simulation, we investigated the direct and indirect influences of changing insolation forcing on the amplitude of the seasonal temperature cycle. The respective research questions in chapter 4 were:

(5) How does the seasonal temperature cycle in the Holocene evolve towards present day orbital conditions and what processes determine the amplitude of the seasonal temperature cycle?

The amplitude of the seasonal temperature cycle in the Holocene is determined by the seasonal distribution of insolation in the low- and mid latitudes and by sea-ice in the high latitudes. In the Northern Hemisphere, the sea-ice effect outweighs the insolation effect, in the Southern Hemisphere, the sea-ice effect amplifies the insolation effect. Despite the decrease in the seasonal insolation cycle amplitude, the amplitude of the seasonal temperature cycle increases in the Arctic Ocean and moderates the amplitude of the seasonal temperature cycle's increase on the adjacent continents. Annual mean temperature change in the high northern latitudes is dominated by a decrease in winter temperatures, whereas summer temperatures decrease to a lesser extent.

(6) How do the modelled seasonal temperatures compare to reconstructed temperatures from paleo-proxies?

The model results show the best agreement with the reconstructions in northern European summer. Discrepancies between the reconstruction and the model results are most obvious in the southern European summer temperatures, where the model

does not reproduce the mid-Holocene cooling inferred from climate proxies. On the hemispheric scale, the modelled response in the latitudinal temperature gradient to the latitudinal insolation gradient matches the reconstructed response, suggesting, that the coarse resolution version of the model might be responsible for the mismatch. A comparison of the model results to a temperature reconstruction from paleo archives indicates an influence of sea-ice evolution on the seasonal temperature cycle amplitude.

5.2 Possible Directions of Future Research

Our simulations of Holocene and Eemian time-slices reveal that orbital forcing does not differ qualitatively between the two periods. Proxy reconstructions, however, show differences the Holocene and the Eemian in timing of thermal maxima during the interglacial, as well as ocean properties at higher latitudes (e.g., Bauch and Erlenkeuser 2008). The introduction of an additional forcing mechanism besides orbital parameters could be able to shed light on this issue. The most obvious would be to test the influence of continental ice sheets on climate evolution for the Eemian period (e.g., Otto-Bliesner et al. 2006).

Climate model simulations under boundary conditions that are representative of a real climatic episode compared to models run under somewhat artificial idealized boundary conditions, offer the opportunity to evaluate the model results against reconstructions derived from paleo proxies. Our results on the evolution of the seasonal temperature cycle suggest that model results could also help in interpreting proxy data, as some assumptions made when translating the climate proxy to climate data may be not applicable. For example the sea-ice effect on the amplitude of the seasonal cycle could influence of the timing of the blooming season in marine proxy species, which is important when interprating seasonal temperatures (Lorenz et al. 2006).

The mechanisms determining the response of the climate system and climate variability presented in the current study are possibly also dependent on the specific model setup used. It has been shown by Jungclaus et al. (2005) that especially ocean variability on multi-decadal time-scales in the ECHAM5/MPI-OM coupled model setup is only resolved in a higher resolution version. The notion that the multi-centennial variability found in the spectrum of the ocean circulation may also be a mode of the real ocean is supported by variations on similar time-scales found in paleo reconstructions of ocean circulation Hall et al. (2004) and reconstructions of surface variables likely influenced by ocean circulation (Stocker and Mysak 1992).

To quantify the influence of model resolution on the variability spectrum, long-term integrations of Holocene climate with a higher resolution of the current model could be performed. This is becoming more feasible as limitations in computing resources are decreasing. Similarly, the question if persisting NAO phases influence centennial time-scale ocean circulation variability could be answered by performing an ensem-

ble of transient Holocene simulations. Comparison of the model results of this study with results of transient Holocene simulations obtained from studies with other coupled AOGCMs, will help to discriminate between features specific to the numerical representation of the climate system in the different models and physical processes present in the real world.

A combination of model- and also proxy intercomparison approaches would certainly be a promising route to take in the quest towards a better understanding of the climate system.

Bibliography

Antonsson, K., D. Chen, and H. Seppä, 2008: Anticyclonic atmospheric circulation as an analogue for the warm and dry mid-Holocene summer climate in central Scandinavia. *Climate of the Past*, **4**, 215–224.

Barnekow, L., 2000: Holocene regional and local vegetation history and lake-level changes in the Torneträsk area, northern Sweden. *Journal of Paleolimnology*, **23**, 343–456.

Bauch, H. A. and H. Erlenkeuser, 2008: A "critical" climatic evaluation of last interglacial (MIS 5e) records from the Norwegian Sea. *Polar Research*, **27**, 135–151.

Berger, A., 1978: Long-Term Variations Of Daily Insolation And Quaternary Climatic Changes. *Journal of the Atmospheric Sciences*, **35 (12)**, 2362–2367.

Bindoff, N., et al., 2007: Observations: Oceanic climate change and sea level. *Climate Change 2007: The Physical Science Basis. Contribution of Working Group I to the Fourth Assessment Report of the Intergovernmental Panel on Climate Change*, S. Solomon, D. Qin, M. Manning, Z. Chen, M. Marquis, K. Avery, M. Tignor, and H. Miller, Eds., Cambridge University Press, Cambridge, United Kingdom and New York, NY, USA.

Bitz, C., P. Gent, R. Woodgate, M. Holland, and R. Lindsay, 2006: The influence of sea ice on ocean heat uptake in response to increasing CO2. *Journal of Climate*, **19 (11)**, 2437–2450.

Blackmon, M., 1976: Climatological spectral study of 500 mb geopotential height of northern hemisphere. *Journal of the Atmospheric Sciences*, **33**, 1607–1623.

Böning, C. W., M. Scheinert, J. Dengg, A. Biastoch, and A. Funk, 2006: Decadal variability of subpolar gyre transport and its reverberation in the North Atlantic overturning. *Geophys. Res. Lett.*, **33 (21)**, L21S01.

Braconnot, P., S. Joussaume, O. Marti, and N. de Noblet, 1999: Synergetic feedbacks from ocean and vegetation on the African monsoon response to mid-Holocene insolation. *Geophysical Research Letters*, **26**, 2481–2484.

Braconnot, P., C. Marzin, L. Gregoire, E. Mosquet, and O. Marti, 2008: Monsoon response to changes in Earth's orbital parameters: comparisons between simulations of the Eemian and of the Holocene. *Climate of the Past*, **4 (4)**, 281–294.

Braconnot, P., et al., 2007a: Results of PMIP2 coupled simulations of the mid-Holocene and Last Glacial Maximum - Part 1: experiments and large-scale features. *Climate of the Past*, **3 (2)**, 261–277.

Braconnot, P., et al., 2007b: Results of PMIP2 coupled simulations of the Mid-Holocene and Last Glacial Maximum - Part 2: feedbacks with emphasis on the location of the ITCZ and mid- and high latitudes heat budget. *Climate of the Past*, **3 (2)**, 279–296.

Bretagnon, P. and G. Francou, 1988: Planetary theories in rectangular and spherical variables - VSOP 87 solutions. *Astronomy and Astrophysics*, **202**, 309–315.

Brovkin, V., T. Raddatz, C. H. Reick, M. Claussen, and V. Gayler, 2009: Global biogeophysical interactions between forest and climate. *Geophysical Research Letters*, **36 (L07405)**, L07 405.

Bryan, K., 1962: Measurements of Meridional Heat Transport by Ocean Currents. *Journal of Geophysical Research*, **67**, 3403–3414.

Cheddadi, R., G. Yu, J. Guiot, S. Harrison, and I. Prentice, 1996: The climate of Europe 6000 years ago. *Climate Dynamics*, **13(1)**, 1–9.

Claussen, M., C. Kubatzki, V. Brovkin, A. Ganopolski, P. Hoelzmann, and H.-J. Pachur, 1999: Simulation of an abrupt change in Saharan vegetation in the Mid-Holocene. *Geophys. Res. Lett.*, **26 (14)**, 2037–2040.

Curry, R. G., M. S. McCartney, and T. M. Joyce, 1998: Oceanic transport of subpolar climate signals to mid-depth subtropical waters. *Nature*, **391 (6667)**, 575–577.

Davis, B. and S. Brewer, 2009: Orbital forcing and role of the latitudinal insolation/temperature gradient. *Climate Dynamics*, **32 (2)**, 143–165.

Davis, B. A. and A. C. Stevenson, 2007: The 8.2 ka event and Early-Mid Holocene forests, fires and flooding in the Central Ebro Desert, NE Spain. *Quaternary Science Reviews*, **26 (13-14)**, 1695 – 1712.

Davis, B. A. S., S. Brewer, A. C. Stevenson, J. Guiot, and D. Contributors, 2003: The temperature of Europe during the Holocene reconstructed from pollen data. *Quaternary Science Reviews*, **22**, 1701–1716.

Delworth, T., S. Manabe, and R. J. Stouffer, 1993: Interdecadal variations of the thermohaline circulation in a coupled ocean-atmosphere model. *Journal of Climate*, **6 (11)**, 1993–2011.

Denton, G. H., R. B. Alley, G. C. Comer, and W. S. Broecker, 2005: The role of seasonality in abrupt climate change. *Quaternary Science Reviews*, **24 (10-11)**, 1159 – 1182.

Dickson, R., J. Lazier, J. Meincke, P. Rhines, and J. Swift, 1996: Long-term coordinated changes in the convective activity of the north atlantic. *Progress In Oceanography*, **38 (3)**, 241 – 295.

Duplessy, J.-C., E. Ivanova, I. Murdmaa, M. Paterne, and L. Labeyrie, 2001: Holocene paleoceanography of the northern Barents Sea and variations of the northward heat transport by the Atlantic Ocean. *Boreas*, **30**, 2–16.

Eden, C. and J. Willebrand, 2001: Mechanism of Interannual to Decadal Variability of the North Atlantic Circulation. *Journal of Climate*, **14 (10)**, 2266–2280.

Fairbanks, R. G., 1989: A 17,000-year glacio-eustatic sea level record: influence of glacial melting rates on the Younger Dryas event and deep-ocean circulation. *Nature*, **342 (6250)**, 637–642.

Furevik, T. and J. E. O. Nilsen, 2005: Large-scale atmospheric circulation variability and its impacts on the Nordic Seas ocean climate - A review. *Nordic Seas: An Integrated Pespective - Oceanography, Climatology, Biogeochemistry And Modeling*, **158**, 105–136.

Ganachaud, A. and C. Wunsch, 2000: Improved estimates of global ocean circulation, heat transport and mixing from hydrographic data. *Nature*, **408 (6811)**, 453–457.

Gladstone, R. M., et al., 2005: Mid-Holocene NAO: A PMIP2 model intercomparison. *Geophys. Res. Lett.*, **32 (16)**, L16 707.

Groll, N., M. Widmann, J. Jones, F. Kaspar, and S. Lorenz, 2005: Simulated relationships between regional temperatures and large-scale circulation: 125 kyr BP (Eemian) and the preindustrial period. *Journal of Climate*, **18 (19)**, 4032–4045.

Hagemann, S. and L. Dumenil, 1998: A parametrization of the lateral waterflow for the global scale. *Climate Dynamics*, **14 (1)**, 17–31.

Hagemann, S. and L. Gates, 2003: Improving a subgrid runoff parameterization scheme for climate models by the use of high resolution data derived from satellite observations. *Climate Dynamics*, **21 (3-4)**, 349–359.

Hald, M., et al., 2007: Variations in temperature and extent of Atlantic Water in the northern North Atlantic during the Holocene. *Quaternary Science Reviews*, **26**, 3423–3444.

Hall, I. R., G. G. Bianchi, and J. R. Evans, 2004: Centennial to millennial scale Holocene climate-deep water linkage in the North Atlantic. *Quaternary Science Reviews*, **23 (14-15)**, 1529 – 1536.

Hall, M. M. and H. L. Bryden, 1982: Direct estimates and mechanisms of ocean heat transport. *Deep Sea Research*, **29(3A)**, 339–359.

Harrison, S. P. and G. Digerfeldt, 1993: European lakes as palaeohydrological and palaeoclimatic indicators. *Quaternary Science Reviews*, **12 (4)**, 233 – 248.

Harvey, L. D. D., 1988: On The Role Of High-Latitude Ice, Snow, And Vegetation Feedbacks In The Climatic Response To External Forcing Changes. *Climatic Change*, **13 (2)**, 191–224.

Hasselmann, K., 1976: Stochastic climate models Part I. Theory. *Tellus*, **28 (6)**, 473–485.

Haug, G. H., K. A. Hughen, D. M. Sigman, L. C. Peterson, and U. Rohl, 2001: Southward Migration of the Intertropical Convergence Zone Through the Holocene. *Science*, **293 (5533)**, 1304–1308.

Hays, J., J. Imbrie, and N. Shackleton, 1976: Variations in the Earth's Orbit: Pacemaker of the Ice Ages. *Science*, **194**, 1121–1132.

Hegerl, G., et al., 2007: Understanding and attributing climate change. *Climate Change 2007: The Physical Science Basis. Contribution of Working Group I to the Fourth Assessment Report of the Intergovernmental Panel on Climate Change*, S. Solomon, D. Qin, M. Manning, Z. Chen, M. Marquis, K. Avery, M. Tignor, and H. Miller, Eds., Cambridge University Press, Cambridge, United Kingdom and New York, NY, USA.

Hibler, W., 1979: Dynamic thermodynamic sea ice model. *Journal of Pysical Oceanography*, **9 (4)**, 815–846.

Hurrell, J. W., 1995: Decadal Trends in the North Atlantic Oscillation: Regional Temperatures and Precipitation. *Science*, **269**, 676–679.

Imbrie, J., et al., 1992: On the Structure and origin of major glaciation cycles 1. Linear responses to Milankovich forcing. *Paleoceanography*, **Vol. 7, No. 6**, 701–738.

Jansen, E., et al., 2007: Palaeoclimate. *Climate Change 2007: The Physical Science Basis. Contribution of Working Group I to the Fourth Assessment Report of the Intergovernmental Panel on Climate Change*, S. Solomon, D. Qin, M. Manning, Z. Chen, M. Marquis, K. Avery, M. Tignor, and H. Miller, Eds., Cambridge University Press, Cambridge, United Kingdom and New York, NY, USA.

Joussaume, S. and K. E. Taylor, 1995: Status of the Paleoclimate Modeling Intercomparison Project (PMIP). *WCRP Report*, 425–430.

Jung, G., 1952: Note on the meridional transport of energy by the oceans. *Journal of Marine Research*, **11**, 139–146.

Jungclaus, J. H., H. Haak, M. Latif, and U. Mikolajewicz, 2005: Arctic-North Atlantic Interactions and Multidecadal Variability of the Meridional Overturning Circulation. *Journal of Climate*, **18 (19)**, 4013–4031.

Jungclaus, J. H., et al., 2006: Ocean circulation and tropical variability in the coupled model ECHAM5/MPI-OM. *Journal of Climate*, **19 (16)**, 3952–3972.

Kaspar, F., N. Kuhl, U. Cubasch, and T. Litt, 2005: A model-data comparison of European temperatures in the Eemian interglacial. *Geophysical Research Letters*, **32**, L11 703.

Kaspar, F., T. Spangehl, and U. Cubasch, 2007: Northern hemisphere winter storm tracks of the Eemian interglacial and the last glacial inception. *Climate of the Past*, **3 (2)**, 181–192.

Keith, D., 1995: Meridional energy transport: uncertainty in zonal means. *Tellus*, **47**, 30–44.

Kuhlbrodt, T., A. Griesel, M. Montoya, A. Levermann, M. Hofmann, and S. Rahmstorf, 2007: On the driving processes of the Atlantic meridional overturning circulation. *Rev. Geophys.*, **45 (2)**, RG2001.

Latif, M., et al., 2004: Reconstructing, monitoring, and predicting multidecadal-scale changes in the north atlantic thermohaline circulation with sea surface temperature. *Journal of Climate*, **17 (7)**, 1605–1614.

Levitus, S. and G. Isayev, 1992: Polynomial-approximation to the international equation of state for seawater. *Journal of Atmospheric and Oceanic Technology*, **9 (3)**, 705–708.

Liu, Z., E. Brady, and J. Lynch-Stieglitz, 2003: Global ocean response to orbital forcing in the Holocene. *Paleoceanography*, **18 (2)**, 1041.

Lohmann, K., H. Drange, and M. Bentsen, 2009: Response of the North Atlantic subpolar gyre to persistent North Atlantic Oscillation like forcing. *Climate Dynamics*, **32**, 273–285.

Lorenz, S. J., J. Kim, N. Rimbu, R. R. Schneider, and G. Lohmann, 2006: Orbitally driven insolation forcing on Holocene climate trends: Evidence from alkenone data and climate modeling. *Paleoceanography*, **Vol. 21**, PA1002.

Lynch-Stieglitz, J., W. B. Curry, and D. C. Lund, 2009: Florida Straits density structure and transport over the last 8000 years. *Paleoceanography*, **24 (3)**, PA3209.

Marshall, J., H. Johnson, and J. Goodman, 2001: A Study of the Interaction of the North Atlantic Oscillation with Ocean Circulation. *Journal of Climate*, **14 (7)**, 1399–1421.

Marsland, S. J., H. Haak, J. H. Jungclaus, M. Latif, and F. Roske, 2003: The Max-Planck-Institute global ocean/sea ice model with orthogonal curvilinear coordinates. *Ocean Modelling*, **5 (2)**, 91–127.

Mauritzen, C., 1996: Production of dense overflow waters feeding the North Atlantic across the Greenland-Scotland Ridge. Part 1: Evidence for a revised circulation scheme. *Deep Sea Research Part I: Oceanographic Research Papers*, **43 (6)**, 769 – 806.

Mikolajewicz, U. and E. Maier-Reimer, 1990: Internal secular variability in an ocean general circulation model. *Climate Dynamics*, **4**, 145–156.

Milankovic, M., 1941: Kanon der Erdbestrahlung und seine Anwendung auf das Eiszeitenproblem. *Special Publication, R. Serb. Acad. Belgrade*, **132**, 633 pp.

Miller, G., et al., 2006: Last interglacial arctic warmth confirms polar amplification of climate change. *Quaternary Science Reviews*, **25 (13-14)**, 1383 – 1400.

Mitchell, J. M., 1976: An overview of climatic variability and its causal mechanisms. *Quaternary Research*, **6 (4)**, 481 – 493.

Nesje, A., J. A. Matthews, S. O. Dahl, M. S. Berrisford, and C. Andersson, 2001: Holocene glacier fluctuations of Flatebreen and winter-precipitation changes in the Jostedalsbreen region, western norvay, based on glaciolacustrine sediment records. *The Holocene*, **11 (3)**, 267–280.

Otto, J., T. Raddatz, M. Claussen, V. Brovkin, and V. Gayler, 2009: Separation of atmosphere-ocean-vegetation feedbacks and synergies for mid-Holocene climate. *Geophysical Research Letters*, **36**, L09 701.

Otto-Bliesner, B. L., S. J. Marshall, J. T. Overpeck, G. H. Miller, A. Hu, and C. L. I. P. members, 2006: Simulating Arctic Climate Warmth and Icefield Retreat in the Last Interglaciation. *Science*, **311 (5768)**, 1751–1753.

Overpeck, J. T., B. L. Otto-Bliesner, G. H. Miller, D. R. Muhs, R. B. Alley, and J. T. Kiehl, 2006: Paleoclimatic evidence for future ice-sheet instability and rapid sea-level rise. *Science*, **311 (5768)**, 1747–1750.

Park, W. and M. Latif, 2008: Multidecadal and multicentennial variability of the meridional overturning circulation. *Geophys. Res. Lett.*, **35 (22)**, L22 703.

Raddatz, T. J., et al., 2007: Will the tropical land biosphere dominate the climate-carbon cycle feedback during the twenty-first century? *Climate Dynamics*, **29 (6)**, 565–574.

Raymo, M. E. and K. Nisancioglu, 2003: The 41 kyr world: Milankovitch's other unsolved mystery. *Paleoceanography*, **18 (1)**, 1011.

Renssen, H., H. Goosse, T. Fichefet, V. Brovkin, E. Driesschaert, and F. Wolk, 2005: Simulating the Holocene climate evolution at northern high latitudes using a coupled atmosphere-sea ice-ocean-vegetation model. *Climate Dynamics*, **24**, 23–43.

Renssen, H., H. Goosse, and R. Muscheler, 2006: Coupled climate model simulation of Holocene cooling events: oceanic feedback amplifies solar forcing. *Climate of the Past*, **2 (2)**, 79–90.

Renssen, H., H. Seppa, O. Heiri, D. M. Roche, H. Goosse, and T. Fichefet, 2009: The spatial and temporal complexity of the Holocene thermal maximum. *Nature Geoscience*, **2 (6)**, 411–414.

Rimbu, N., G. Lohmann, J.-H. Kim, H. W. Arz, and R. Schneider, 2003: Arctic/North Atlantic Oscillation signature in Holocene sea surface temperature trends as obtained from alkenone data. *Geophysical Research Letters*, **30**, 1280.

Rimbu, N., G. Lohmann, K. J. H. Lorenz, S. J. and, and R. R. Schneider, 2004: Holocene climate variability as derived from alkenone sea surface temperature and coupled ocean-atmosphere model experiments. *Climate Dynamics*, **23**, 215–227.

Roeckner, E., et al., 2003: The atmospheric general circulation model ECHAM5. Part I: Model description. Tech. Rep. Rep. 349, 127 pp., Max Planck Institute for Meteorology, available from MPI for Meteorology, Bundesstr. 53, 20146 Hamburg, Germany.

Schurgers, G., U. Mikolajewicz, M. Groeger, E. Maier-Reimer, M. Vizcaino, and A. Winguth, 2007: The effect of land surface changes on Eemian climate. *Climate Dynamics*, **29 (4)**, 357–373.

Schweckendiek, U. and J. Willebrand, 2005: Mechanisms Affecting the Overturning Response in Global Warming Simulations. *Journal of Climate*, **18 (23)**, 4925–4936.

Semtner, A. J., 1976: Model for thermodynamic growth of sea ice in numerical investigations of climate. *Journal of Physical Oceanography*, **6 (3)**, 379–389.

Sicre, M.-A., et al., 2008: Decadal variability of sea surface temperatures off north iceland over the last 2000 years. *Earth and Planetary Science Letters*, **268 (1-2)**, 137 – 142.

Stocker, T. F. and L. A. Mysak, 1992: Climatic fluctuations on the century time scale: A review of high-resolution proxy data and possible mechanisms. *Climatic Change*, **20**, 227–250, 10.1007/BF00139840.

te Raa, L. and H. Dijkstra, 2003: Modes of internal thermohaline variability in a single-hemispheric ocean basin. *Journal of Marine Research*, **61**, 491–516(26).

Timmermann, A., M. Latif, R. Voss, and A. Gruetzner, 1998: Northern Hemispheric Interdecadal Variability: A Coupled Air-Sea Model. *Journal of Climate*, **11 (8)**, 1906–1931.

Torrence, C. and G. Compo, 1998: A Practical Guide to Wavelet Analysis. *Bulletin of the American Meteorological Society*, **79**, 61–78.

Trenberth, K. E. and J. M. Caron, 2001: Estimates of meridional atmosphere and ocean heat transports. *Journal of Climate*, **14 (16)**, 3433–3443.

Trouet, V., J. Esper, N. E. Graham, A. Baker, J. D. Scourse, and D. C. Frank, 2009: Persistent Positive North Atlantic Oscillation Mode Dominated the Medieval Climate Anomaly. *Science*, **324 (5923)**, 78–80.

Valcke, S., A. Caubel, D. Declat, and L. Terray, 2003: Oasis ocean atmosphere sea ice soil user's guide. Tech. rep., CERFACS.

Vellinga, M. and P. Wu, 2004: Low-Latitude Freshwater Influence on Centennial Variability of the Atlantic Thermohaline Circulation. *Journal of Climate*, **17 (23)**, 4498–4511.

Visbeck, E. C. M., R. Curry, T. Delworth, B. Dickson, and G. Krahmann, 2003: The Ocean's Response to North Atlantic Oscillation Variability. *Geophysical Monograph Series*, **134**, 113–146.

Vonder Haar, T. H. and A. H. Oort, 1973: New estimate of annual poleward energy transport by northern hemisphere oceans. *Journal of Physical Oceanography*, **3 (2)**, 169–172.

Wanner, H., et al., 2008: Mid- to Late Holocene climate change: an overview. *Quaternary Science Reviews*, **27**, 1791–1828.

Weaver, A. J., E. S. Sarachik, and J. Marotze, 1991: Freshwater flux forcing of decadal and interdecadal oceanic variability. *Nature*, **353 (6347)**, 836–838.

Welander, P., 1982: A simple heat-salt oscillator. *Dynamics of Atmospheres and Oceans*, **6 (4)**, 233 – 242.

Welander, P., 1986: Thermohaline effects in the ocean circulation and related simple models. *Large-Scale Transport Preocesses in Oceans and Atmosphere*, J. Willebrand and D. Anderson, Eds., NATO ASI Series, 163–200.

Winton, M. and E. S. Sarachik, 1993: Thermohaline oscillations induced by strong steady salinity forcing of ocean general circulation models. *Journal of Physical Oceanography*, **23 (7)**, 1389–1410.

Wu, H., J. Guiot, S. Brewer, and Z. Guo, 2007: Climatic changes in Eurasia and Africa at the last glacial maximum and mid-Holocene: reconstruction from pollen data using inverse vegetation modelling. *Climate Dynamics*, **29**, 211–229.

Zhao, Y., et al., 2005: A multi-model analysis of the role of the ocean on the African and Indian monsoon during the mid-Holocene. *Climate Dynamics*, **25 (7-8)**, 777–800.

Acknowledgements

I wish to express my gratitude to my advisor Dr. Johann H. Jungclaus for his excellent supervision of my thesis. I am very grateful for his academic advice, his steady and patient support of my work, his confidence and encouragemet, and his ever open door when I had questions or felt I needed to discuss something. I especially thank Prof. Dr. Jochem Marotzke for his academic supervision, his reassuring support and sharing his expert knowledge that often helped me to see the broader perspective and to find the answers to problems encountered. I also would like to thank to Prof. Dr. Martin Claußen for chairing my advisory panel and his interest in my work.

I am grateful to Dr. Helga (Kikki) F. Kleiven and Prof. Ulysses Ninnemann for being wonderful hosts during my reseach stay at the Bjerknes Centre for Climate Reseach in Bergen, Norway and their excellent hands-on introduction to paleoceanography.

Spacial thanks to Dr. Basil Davis for providing his Holocene temperature data-set and interesting discussion on the model-data comparison.

I would like to thank all members of the ocean department for creating an inspiring working environment and for many interesting discussions, especially Dr. Helmuth Haak, Dr. Katja Lohmann, Dr. Stephan Lorenz, Dr. Daniela Matei, Dr. Uwe Mikolajewicz, Dr. Wolfgang Müller, and Dr. Davide Zanchettin. For their technical support and/or guiding my first steps in setting-up the model I would like to thank Michael Bozet, Dr. Veronika Gayer, Dr. Thomas Raddatz and Uwe Schulzweida. Thanks for ensuring invaluable administrative and organizational support to Dr. Antje Weitz and Cornelia Kampmann.

This thesis would not have been possible and not half the fun if it were not for the support and company of my fellow colleagues at the MPI and within IMRPS. Special thanks to my Bürokollege Florian Rauser, to Dr. Aiko Voigt, Mario Krapp, Dr. Malte Heinemann, Dr. Juliane Otto, Freja Vamborg, Steffen Tietsche, Fanny Adloff, Rosina Grimm, Dr. Julia Pongratz, Kevin Sieck, Laura Niederdrenk, Ronny Petrik and to everyone in the IMPRS. I would like to thank Dr. Zoltan Szuts and Freja Vamborg for proofreading the manuscript.

Financial support for this thesis was provided in the framework of the INTERDYNAMIK priority program of the German Reseach Foundation (DFG). The model in-

tegrations were perfomed on the Linux-cluster ot the German Climate Computation Centre (DKRZ) Hamburg.

Eidesstattliche Erklärung

Hiermit versichere ich, dass ich diese Arbeit selbständig verfasst habe und keine anderen als die angegebenen Quellen und Hilfsmittel benutzt habe.

Nils Fischer



ISSN 1614-1199